MULTI-MODAL IMAGING OF BRAIN OSCILLATIONS

By

JUE MO

A DISSERTATION PRESENTED TO THE GRADUATE SCHOOL
OF THE UNIVERSITY OF FLORIDA IN PARTIAL FULFILLMENT
OF THE REQUIREMENTS FOR THE DEGREE OF
DOCTOR OF PHILOSOPHY

UNIVERSITY OF FLORIDA

2012

To my Mom, Dad and my husband, for their love and support

ACKNOWLEDGMENTS

I am grateful to my mentor Dr. Mingzhou Ding for letting me participate in all these novel and interesting researches. Without his outstanding guidance and constant support, I would not be able to accomplish any of my research projects. What's more, I am most indebted to Dr. Ding for helping me improve my writing skills; he devoted a tremendous amount of time in reading and modifying my manuscripts.

I'd like to express my thanks to my undergraduate advisor Prof. Qinye Tong for guiding me to learn the complex system and encouraging me to study the neuronal system. Also, I cannot thank enough all the professors, students and staffs, who helped me throughout my study at the University of Florida. I owe a deep debt of gratitude to Dr. Ahn Andrew, Dr. Charles E Schroeder, Dr. Andreas Keil, Dr. Brandon Burtis, Dr. Brandi Ormerod, Dr. Thomas DeMarse, Dr. Hans van Oostrom, and Dr. Govindan Rangarajan for their cheerful enthusiasm and constant support. My interactions and collaborations with them have contributed immensely to my scientific development.

I'm thankful to all the colleagues and fellow students including Rajasimhan Rajagovindan, Yan Zhang, Kristopher Anderson, Anil Bollimunta, Sahng Min Han, Yuelu Liu, Xiaotong Wen, Chao Wang, Haiqing Huang, Amy Trongnetrpunya and Daesung Kang for all the delightful collaboration and inspiring discussions.

I owe a tremendous amount of gratitude to the past and present BME staff including Katherine Whitesides, Tifiny Dyer, Anide Pierre-Louis, Mary Wall, Danielle Wise, Valerie Anderson and Art Bautista-Hardman who handled all the financial, administrative, computing related resources.

Finally, I still want to dedicate my work to my father Anda Mo and mother Huiling Zhang; they are always supportive for any of my decision and happy for any of my accomplishments. I

am also grateful to my husband Yunpeng Li for cheering me up in times of depression and giving me advice in improving my weaknesses.

TABLE OF CONTENTS

page

LIST OF TABLES

LIST OF FIGURES

Abstract of Dissertation Presented to the Graduate School
of the University of Florida in Partial Fulfillment of the
Requirements for the Degree of Doctor of Philosophy

MULTI-MODAL IMAGING OF BRAIN OSCILLATIONS

By

Jue Mo

August 2012

Chair: Mingzhou Ding
Major: Biomedical Engineering

Oscillatory neural activity involves widespread neural ensembles in the central nervous system, and the oscillation in each frequency band is associated with specific functions, and can be used to trace the flow of information in the brain. Moreover, they are usually found as objective indices of cognitive dysfunction in the clinical conditions. By analyzing the multimodality imaging in animals and humans, we addressed the mechanisms and the functional roles of synchronized ongoing oscillatory activity in processes such as anticipatory attention and task control, and used the oscillatory activity to investigate the neuronal processes underlying pain.

First, by analyzing local field potentials and multiunit activities from the inferotemporal cortex of macaque monkeys during an intermodal selective attention task, we found an attention enhancement on ongoing alpha power and multiunit activities, and also found a positive relationship between ongoing alpha activity and subsequent visual stimulus processing. The functional role of alpha oscillation is suggested as maintaining stimulus template in the inferotemporal cortex. Second, we looked for a neuronal signature for the throbbing percept, a quality associates with many severe pain conditions. By combining the psychophysical recording and the EEG recording, we rejected the conventional vascular origin theory, and proposed that

the rhythmic throbbing percept does not originate from the peripheral sensory input but instead has a representation in the central neuronal system. Third, by applying a new measurement to assess the functional connectivity on BOLD signals, we expounded temporal relationship between cortical areas that was ignored by the conventional measurements, and showed that the new measurement advances the identification of functional networks. Fourth, our EEG-fMRI study revealed the positive correlation between the activity of introspective mental processing network and the visual alpha power under resting state, while prior studies failed to report the relationship between the two variables. Our result indicates that visual input influences the coupling.

CHAPTER 1
BACKGROUND

Neuronal networks in the human and animal cortex display oscillatory activity in several frequency bands from approximately 0.02 Hz to 500 Hz. Biophysical studies revealed that even single neurons are endowed with complex dynamics, possessing intrinsic abilities to resonate and oscillate at multiple frequencies. The pattern of neuronal oscillation was related to various cognitive states such as memory, attention and even consciousness. Hence, the synchronous activity of oscillating network is viewed as the "middle ground" linking single-neuron activity to behavior. Furthermore, neurological and psychiatric disorders are often accompanied by abnormal oscillations. Thus, the study of neuronal oscillations carries both basic and translational significance.

The electrophysiology activity of neuronal ensembles as measured by invasive electrodes or by non-invasive EEG or MEG, exhibits a broad range of oscillatory activity. The fluctuation of field potential was divided into several frequency bands, delta (1-3 Hz), theta (4-9 Hz), alpha (8-12 Hz), beta (13-25 Hz) and gamma (25-90 Hz). These oscillatory neural activities were observed both in humans and animals, and different frequency oscillations exhibit distinct task related modulation in their strength and synchrony. Oscillations in theta and alpha range have been long shown to reflect memory processes (Kahana et al., 1999; Klimesch, 1999; Weiss and Rappelsberger, 2000; Raghavachari et al., 2001; Jensen and Tesche, 2002; Vertes, 2005; Anderson et al, 2010). Alpha oscillations have been associated with alertness, arousal and attentional demands (Ray and Cole, 1985; LaBerge, 1997; Foxe et al., 1998; Bastiaansen and Brunia, 2001; Babiloni et al., 2006; Kelly et al., 2006; Thut et al., 2006; Klimesch et al., 2007, Rajagovindan and Ding 2011). The beta rhythm has been shown to be reduced in strength preceding movement and subsequently increase in strength after the movement is complete

(Pfurtscheller and da Silva, 1999; Zhang and Ding 2010). The gamma range oscillations are often found in early sensory areas and have been suggested to be involved in the binding of sensory information (Miltner et al., 1999; von Stein and Sarnthein, 2000; Herrmann et al., 2004; Palva et al., 2005; Womelsdorf et al., 2006; Doesburg et al., 2008). In particular, the neuronal oscillatory activity is considered the substrate for communication between functionally relevant cortical areas (Roelfsema et al., 1997; Miltner et al., 1999; Fries, 2005; Zanto et al., 2011; Anderson et al., 2010)

Recently, low-frequency oscillations observed in fMRI approaches and scalp EEG recordings have gained increased attention (Demanuele et al., 2007; Fox and Raichle, 2007; Zuo et al, 2010). Using these modalities, researchers consistently identified coherent spontaneous low-frequency fluctuations in the 0.01–0.1 Hz range during both resting and active-task conditions, which were considered as reflecting cyclic modulation of corresponding cortical excitability and long distance neuronal synchronization. Though lacking of strong experiment constraint, resting state fMRI was shown to generate robust results across datasets (Biswal et al, 2010). As one of the prominent results, assessing the temporal correlation between the resting state BOLD signals revealed "intrinsic networks", which coincide with functionally related areas (Biswal, 1996; Fox et al,. 2006; Wen et al., 2012). What's more, the task-free intrinsic connectivity network was able to predict task performance (Seeley et al., 2007).

Despite their relation to distinct cognitive conditions, the neuronal oscillations in different bands were found organized in a hierarchical way. Power of oscillation in high frequency band is modulated by the phase of the low frequency band, which appeared as the cyclical variations in the neuronal excitability (Lakatos et al., 2005). The impact of the ongoing brain state at the onset of an external stimulus on the effectiveness of the ensuing stimulus processing was shown since

the study of Arieli et al., (1996). In-vitro and in-vivo single unit recordings in addition to the computational modeling have explored mechanisms by which background synaptic activity can influence the responsiveness of cortical neurons to afferent input (Ho and Destexhe, 2000; Chance et al., 2002; McCormick et al., 2003; Wolfart et al., 2005; Haider et al., 2007). Similar effect was found in MRI study; the ongoing BOLD level preceding the stimuli showed significant impact on the subsequent event response (Fox et al., 2006). Contrary to some randomness assumptions, the trial-to-trial variability of stimulus response shows a temporal dynamic that oscillates in a low frequency (<0.1Hz, Kam et al., 2009), while the band limited power of ongoing oscillation in visual cortex displayed fluctuation in the same frequency range (Leopold et al., 2003). Hence, investigating the relationship between different frequency bands would improve our understanding of task performance variability.

The recent resurgence of interest in understanding the association between oscillatory activities under different temporal scales is owed to the development in multi-modal recording techniques. On the one hand, the efforts were made in understanding the neurophysiological basis of intrinsic activity (Tsodyks 1999, Arieli 1996). On the other hand, the limited spatial resolution in EEG/MEG required a complementary measurement in localizing the neuronal activity. An important clue that low-frequency BOLD coherence and neuronal activity may be related was the discovery that low-frequency fluctuations of the band-limited power of local field potential, recorded from cortical electrodes in the awake monkey, fluctuates approximately at the same frequency as the BOLD signal (Leopold 2003). Moreover, several studies in humans have reported significant correlations between alpha (Goldman 2002, Moosmann 2003, Laufs 2003a; Laufs 2006, Feige 2005) and beta (Laufs 2003b) power in the EEG, and simultaneously recorded BOLD signal fluctuations with different brain networks during rest. Yet, the significance of the

association depends on the experimental circumstance, and no biophysical model has been proposed to explain the previous observations consistently (Kilner et al., 2005).

In this dissertation, the characterization and functional significance of oscillations observed under different measuring scales and different experimental preparations is under investigation. First, local field potential and multiunit activity recorded from monkeys, scalp EEG and fMRI recorded from young students were analyzed separately, and then, simultaneous EEG-fMRI technique was used to link the activity under different temporal scales.

Aim 1: To identify how attention modulates ongoing alpha oscillations and how this internal modulation in advance of sensory stimulation improves signal processing in the high order visual region. It is well known from early studies that responses to stimuli at attended locations and attended sensory modalities are enhanced relative to unattended stimuli. It has also been shown in recent years that attention modulates baseline ongoing brain activity in advance of sensory input (Kastner et al., 1999; Dehaene and Changeux, 2005; Bestmann et al., 2007; Raj Rajagovindan & Ding, 2011; Anderson and Ding 2011). However, the mechanisms linking the pre- and post- stimulus attentional effects remain not well understood. An emerging consensus (Ray and Cole, 1985; Cooper et al., 2003, 2006) is that when a subject attends to external events, alpha power in scalp EEG decreases with attention (Worden et al., 2000; Sauseng et al., 2005; Rajagovindan & Ding, 2011; Anderson and Ding 2011). In contrast, when attention is directed internally, such as during visual imagery and retention of working memory, alpha power increases with attention (Bastiaansen et al., 2002; Jensen et al., 2002; Raghavachari et al., 2006) .

Through the analysis of the data recorded from monkeys selectively attending the auditory or visual stimulation, we expound the relationship between the magnitude of ongoing activity and the stimulus evoked response, and show that the relationship depends on the functional role

of the recorded regions. According to the earlier finding, primary alpha activity generators are located in the deep layers in V2 and V4, whereas in IT, such generators are located in the superficial layers (Bollimunta et al., 2008). This difference in laminar organization is hypothesized to be linked to the difference in function alpha might support. In particular, in V2 and V4, faster reaction time (RT) to auditory stimulus detection, considered an index of increased auditory attentiveness at the expense of lower visual attention, is associated with increased visual alpha power. In IT, however, faster auditory RT is associated with decreased alpha power, suggesting that visual attention increases alpha power in IT. In this study, we showed the relationship between the single trial response and its pre-stimuli oscillation depends on the function role of alpha in the particular region.

Aim 2: To identify the central representation of the throbbing percept associated with chronic pain. The subjective qualities of a patient's pain are essential, at times life-saving, features of the diagnostic evaluation. These clinically relevant pain qualities, or percepts, such as throbbing, crushing, lancinating, or aching pain, are critical details of the evaluation because they suggest invaluable, even pathognomonic, clues to the underlying disorder. Our present knowledge of these relationships holds that a family of receptors transduce touch, heat, cold, and chemical irritants into the activation of modality-specific sensory neurons, securing the fundamental basis for primary percepts (Basbaum, 2009). In turn, these sensory neurons engage pain-related circuits within the spinal cord and brain (Braz, 2005). However, there remains a substantial gap in knowledge between these "bottom up" molecular events (Ma, 2010) and the "top down" picture of how the brain represents experimental pain (Hashmi, 2008), and little knowledge of how this activity is related to clinically relevant pain qualities (Backonja, 2004).

Given the rhythmic nature of throbbing we wish to examine whether neuronal oscillation can serve as a neural signature of throbbing pulsatile pain, a clinically relevant pain quality associated with severe, disabling pain, and whose presence has well-established diagnostic, therapeutic, and prognostic significance. To accomplish this goal we combined a psychophysical approach with high-density scalp EEG recordings to characterize the cortical rhythms associated with this clinically relevant pain quality. We show that a modulation of the alpha rhythm (8-12 Hz) power correlates with throbbing percepts.

Aim 3: To examine whether total interdependence as a statistical connectivity measure would advance our understanding of resting state oscillatory functional networks. Resting-state fMRI has become a powerful tool for studying network mechanisms of normal brain functioning and its impairments by neurological and psychiatric disorders. The most common way to construct a connectivity map is based on the zero-lag correlation. Analytically, independent component analysis and seed-based cross correlation are the main methods for assessing the connectivity of resting-state fMRI time series. A feature common to both methods is that they exploit the covariation structures of contemporaneously (zero-lag) measured data but ignore temporal relations that extend beyond the zero-lag. To examine whether data covariations across different lags can contribute to our understanding of functional brain networks, a measure that can uncover the overall temporal relationship between two resting-state BOLD signals is needed.

In this dissertation we propose such a measurement referred to as total interdependence (TI). Comparing TI with zero-lag cross correlation (CC) we report three results. First, when combined with a random permutation procedure, TI can reveal the amount of temporal relationship between two resting-state BOLD time series that is not captured by CC. Second, comparing resting-state data with task-state data recorded in the same scanning session, we

demonstrate that the resting-state functional networks constructed with TI match more precisely the networks activated by the task. Third, TI is shown to be more statistically sensitive than CC and provides better feature vectors for network clustering analysis.

Aim 4: To identify the association between slow BOLD fluctuations and the amplitude modulation of the posterior alpha oscillation. It was suggested in 1932 (Bishop,1932) that cortical responsiveness fluctuate in a cyclic way, little is yet known about the neuronal basis and anatomical substrate of this temporal dynamic. Both fast and slow oscillation was found correlated to the behavior score. Lower score is associated with momentary attention lapse, during which the introspective process overcomes the extrospective process. This introspective process is thought to be mediated by the default mode network, which is comprised of regions as mPFC, PCC, bilateral IPL, and is anti-correlated with the task-positive network under either resting state or task state. Also, the attention lapse is accompanied by lower activation in visual area (Mason et al. 2007; Christoff et al. 2009; Gilbert et al. 2007; Weissman et al. 2006). The insufficient inhibition in DMN was shown to predict longer RT and higher error rate in detecting the upcoming target (Hayden et al. 2009; Jerbi et al. 2010). It is generally agreed that a critical functional role of ongoing alpha power is inhibiting the unattended sensory input and protecting internal information (S. Palva & J. M. Palva 2007; P Sauseng et al. 2005; Cooper et al. 2003). The moment-to-moment introspective judgment of attentional state, in which higher rating stands for better task engagement, is negatively correlated with the temporal dynamic of posterior alpha power (Macdonald et al. 2011). Therefore, expounding the relationship between the two neuronal indices will advance our understanding of the mechanism underlying involuntary attention lapse.

So far, no evidence suggests there is synchrony between the posterior alpha power and DMN activation. Based on the resting state studies with fMRI, the intrinsic connectivity map of the DMN is not disturbed under different resting-state conditions. Yet, the synchrony strength is enhanced within the network by eye-opening, and at the same time, stronger anticorrelation between the DMN and task positive network was observed (Yan et al. 2009). Both studies implied that DMN could be involved in activating mechanisms to repel external interruption under eye-open condition. In this dissertation, the relationship between the posterior alpha power and DMN was examined under both eyes-closed and eyes-open condition. Our result shows that the posterior alpha power and the activity of DMN are correlated only during the eyes-open condition, providing a view that, when the brain turns from an extrospective mode to an introspectively oriented mode (default mode), the posterior alpha increases to block out visual inference.

CHAPTER 2
GENERAL METHODS

The primary goals of this dissertation involve the investigation of spontaneously oscillating activities over a wide range frequency and under different imaging modality. Their functional role is examined by associating them with stimulus evoked responses and hence cognitive performance. The oscillatory nature of the signal necessitates the need for a spectral domain approach to study this problem. There is consensus that complex cognitive processes involve complex interaction between disparate regions of the brain. Synchrony (functional connectivity) analysis has emerged as a principled approach of identifying and quantifying inter-areal interaction and inferring causal influence among distributed networks. The spectrum and connectivity analysis were performed selectively with either parametric or nonparametric estimation method.

2.1 Parametric Multivariate Spectral Estimation

Multivariate autoregressive (MVAR) modeling is a parametric spectral analysis method in which time series models are extracted from datasets having either one long realization or a number of shorter realizations. In the latter case, the fundamental assumption of this algorithm is that the short-window time series can be treated as realizations of an underlying stationary stochastic process. As cognitive information processing involves transient changes in neural activity, MVAR can be used to investigate time series in short window size (<100 ms). The following is the procedure of MVAR proposed by Ding et al. (2000).

Let $X(t) = [X(1,t), X(2,t), \ldots, X(m,t)]^T$ be an *m*-dimensional jointly stationary random process. *T* denotes matrix transposition. In the case of neural recordings, *m* refers to the total number of recording channels to be analyzed. Assuming $X(t)$ is a zero mean stationary process, $X(t)$ can be modeled by the following p^{th} order autoregressive equations:

$$X(t) + A(1)X(t-1) + A(2)X(t-2) + \cdots + A(p)X(t-p) = E(t) \tag{2-1}$$

where *p* is the model order, and $A(i)$ are the unknown $m \times m$ coefficient matrices and $E(t)$ is the uncorrelated noise term with covariance matrix $\sum$. Multiplying $X^T(t-k)$ to Eq. 2-1 and taking expectation on both sides we arrive at the Yule-Walker equations.

$$R(-k) + A(1)R(-k+1) + \cdots + A(p)R(-k+p) = 0 \tag{2-2}$$

where $R(j)$ is covariance matrices of $X(t)X^T(t+j)$ with lag j. Also note that $< E(t) \bullet X^T(t-k) >= 0$, since $E(t)$ is an uncorrelated noise process. The unbiased estimator of the covariance matrix in Eq. 2-2 for a single realization of the *X* process is given by

$$R(n) = \frac{1}{N-n} \sum_{i=1}^{N-n} x(i)x^T(i+n)$$

In the case of multiple realizations of the process, as is usually the case, the covariance matrix is computed for each individual realization and then averaged across all the realizations to obtain the most robust estimate. In the case of short window of data, i.e. short sample length where *N* is small, it is apparent that the estimation from a single realization is poor. However, with increasing number of realizations this problem can be offset for short sample length time series. In the limiting case with number of realizations approaching infinity, the sample length of each realization may be as short as the model order plus one ($N = p+1$).

Coefficient matrices $A(i)$ and covariance matrix $\sum$ of noise term $E(t)$ is obtained by solving Eq. 2-2 through the Levinson, Wiggins and Robinson (LWR) algorithm. The noise covariance matrix $\sum$ is obtained as part of the LWR algorithm. One may also obtain $\sum$ as

$$\sum = R(0) + \sum_{i=1}^{p} A(i)R(i)$$

It is instructive to note that the Eq. 2-2 contain a total of pm^2 unknown model coefficients to be estimated from the same number of simultaneous linear equations.

Although the primary objective is to fit the best model to the data, which is to minimize the residual noise variance, this constraint alone may result in over-parameterization. The reason for this is because the variance of the residual term decreases monotonically with incorporating more and more past values of the process. Over-parameterization leads to inaccuracies in the estimation of the model coefficient besides the obvious increase in the computational complexity. Thus a penalization scheme to avoid over-parameterization is employed. Criterions that incorporate both minimization of the variance of the residual term and penalize excessive coefficients are the Akiake Information Criterion (AIC) and Bayesian Information Criterion (BIC) among several other similar criterions. The AIC is defined as

$$AIC(p) = -2\log\left[\det(\Sigma)\right] + \frac{2m^2 p}{N_{total}}$$

where N_{total} is the total number of data points from all the trials. The first term on the right hand side accounts for the variance minimization and the second term correspond to the cost associated with increasing parameters. Plotted as a function of p, the optimum model order corresponds to the minimum of this function. For typical neurobiological data N_{total} is very large and hence for practical ranges of p, the AIC function does not achieve a minimum due to inadequate penalization as the second term vanishes with large values of N_{total}. An alternative criterion is the Bayesian Information Criterion (BIC), which is defined as

$$BIC(p) = -2\log\left[\det(\Sigma)\right] + \frac{2m^2 p \log N_{total}}{N_{total}}$$

This criterion can compensate for the large number of data points and may perform better in neuroscientific applications. A final step and critical step necessary for determining whether the

autoregressive time series model is suited for a given data set, is to check whether the residual term is white. Here the residual term is obtained by computing the difference between the model's predicted values and the actually measured values.

Once an autoregressive model is adequately estimated, it becomes the basis for both time domain and spectral domain causality analysis. Spectral features are derived from MVAR models after acquiring $A(i)$ and $\sum$ estimates. Taking the Fourier transform, Eq. 2-1 can be rewritten in the spectral domain as

$$A(f)X(f) = E(f),$$

Defining $H(f) = \left(\sum_{i=0}^{m} A(i) e^{-ij2\pi f} \right)^{-1}$, then $X(f) = H(f)E(f)$

where $H(f)$ is the transfer function. The spectral matrix can be readily derived from

$$S(f) = \lim_{N\to\infty} \frac{1}{N} E[X(f)X^*(f)] = H(f)\sum H^*(f)$$

where * means both transpose and complex conjugate.

Spectral power is contained in the diagonal terms of the spectral matrix and the off-diagonal terms represent the cross spectra. Coherence spectra between two random process $X(i,t)$ and $X(j,t)$ is defined as:

$$C_{ij}(f) = \frac{\left|S_{ij}(f)\right|^2}{S_{ii}(f)S_{jj}(f)}$$

If the coherence value is equal to 1 or 0, the two processes are maximally interdependent or independent, respectively.

Once the transfer function, the noise covariance and the spectral matrix are estimated, Granger causality may be derived according to the procedures outlined in the following sections.

2.2 Multitaper Spectral Estimation

Multitaper spectral estimation (Thomson, 1982) refers to a set of nonparametric methods for estimating power spectra, coherences and related spectral quantities using an orthogonal set of data tapers, in specific, the discrete prolate spheroidal a.k.a Slepian sequences and their approximate minimum bias sine tapers.

Before proceeding to the mathematical formulation of the multitaper spectra estimation techniques it is worth noting the several favorable properties that motivated the use of this approach from among several other available estimation techniques. The problem of optimum spectral estimation is confronted with several key issues including that of minimizing the (a) bias of the estimators (b) variance of the estimators and (c) the spectral leakage among several other considerations. For further details on each of these considerations the readers may refer to (Lfeachor and Jarvis; Thomson, 1982; Mitra and Pesaran, 1999; Mitra and Bokil, 2007). For example consider one of the conventional nonparametric spectral analysis techniques, the Welch's method. In order to reduce the variance in the estimation, the approach involves splitting the data into overlapping segments followed by the estimation of the power or the cross spectrum for each segment and then averaging over all the segments. For data of short length, such approaches suffer from severe bias in the estimation. In comparison, the multitaper approach does not suffer from these limitations. Both reduction in bias and variance of the estimation is achieved since averaging the spectral estimates over different tapers enable reduction in the variance and since each taper is applied to the entire data instead of short segments of the data as in Welch's method the resulting bias in the estimation is smaller in comparison. Further the choice of the orthonormal Slepian tapers enables maximum sidelobe suppression hence offering the least spectral leakage in comparison to all other spectral estimation techniques. Thus multitaper approach offers the optimum spectral estimation in the

face of short sample length data or short sample length and limited realizations of data as often encountered in neuroscientific applications as is the case in this study. It is apparent from the aims set out to be addressed that it is crucial to be able to achieve single-trial estimation of the spectra. In light of this crucial requirement, this study utilizes the full advantage of this technique to enable single-trial estimation of spectral features during short prestimulus time periods which otherwise would not have been possible to estimate with sufficient accuracy using either the parametric framework based on autoregressive models presented earlier or through other common non parametric approaches.

A brief exposition of the mathematical formulation of the multitaper spectral estimation technique for univariate case is as follows. The extension to multivariate case is straightforward. Consider time series *x(t)* (t = 1,2…N) a zero mean second order stationary random process and let $w_k(t)$ denote the kth Slepian taper (window sequence) and k = 1,2…K.

Step 1: Let us define the time-bandwidth product given by $C = NW$, where N is the sample length and W the desired spectral bandwidth. If C is too small, the estimate will be unstable and may not have sufficient dynamic range and if C is too large, the estimate may not have adequate frequency resolution. For a given choice of C there are $K = 2C$ data taper sequences. Since the energy concentration of higher order tapers is poorer than the low order tapers, in practice it is common to choose $K = 2C-1$ or $K = 2C-2$.

Step 2: The Slepian tapers having the maximum energy concentration in the bandwidth W is determined by solving the following eigenvalue problem

$$\lambda_k w_k(t) = \sum_{j=0}^{N-1} \frac{\sin[2\pi W(t-j)]}{\pi(t-j)} w_k(j) \quad , \quad \text{for t = 1, 2…N.}$$

Step 3: The eigen coefficients of this problem reduces to the Fourier transform of the data sequence multiplied by the tapers (similar to periodogram). The windowed Fourier transform of the data *x(t)* is given by

$$\lambda_k = X_k(\omega) = \sum_{t=0}^{N-1} x(t) w_k(t) e^{-j\omega t}$$

Step 4: The spectrum then estimated as the average of the spectra obtained through each taper is given by

$$S(\omega) = \frac{1}{K} \sum_{k=0}^{K-1} X_k(\omega) X_k^*(\omega)$$

In the case of multiple realizations, the above estimate is further averaged across all realizations. For further treatment of this topic refer (Thomson, 1982; Thomson, 2007).

CHAPTER 3
ATTENTIONAL MODULATION OF ALPHA OSCILLATIONS IN MACAQUE INFEROTEMPORAL CORTEX

3.1 Introduction

Stimulus-evoked neural responses and their attentional modulation have been extensively studied (Gazzaniga et al. 2009). Whether and how attention modulates ongoing brain activity when it is deployed in advance of sensory stimulation has also attracted increased research interest (Kastner et al. 1999; Driver & Frith 2000; Pasternak & Greenlee 2005; Procyk & Goldman-Rakic 2006; Fuster 2008). This internally generated expectancy state improves behavioral performance by shortening reaction time and reducing the number of errors and is thought to be implemented by top-down control mechanisms (Knight et al. 1999; Hopfinger et al. 2000; Miller & Cohen 2000; Engel et al. 2001; LaBerge 2005; Buschman & Miller 2008; Rossi et al. 2007; Fuster 2008; Gregoriou et al. 2009).

In humans the relationship between field oscillations in the 8 to 12 Hz range, known as alpha oscillations, and attention has been the subject of extensive investigation (Pfurtscheller et al. 1997; Shaw 2003). An emerging consensus (Ray & Cole 1985; Cooper et al. 2003; 2006) is that when a subject attends to external events, alpha power in scalp EEG decreases with attention (Worden et al. 2000; Sauseng et al. 2005; Rangarajan & Ding 2010). In contrast, when attention is directed internally, such as during visual imagery and retention of working memory, alpha power increases with attention (Bastiaansen et al. 2002; Jensen et al. 2002; Raghavachari et al. 2006). Physiologically, whereas the decreased alpha power with external attention is thought to reflect increased excitability over sensory cortices to enhance stimulus processing (Jones et al., 2000; Thut et al., 2006; Klimesch et al., 2007; Romei et al., 2008; Rangarajan & Ding 2010), the significance of increased alpha power with internal attention remains debated. According to the alpha inhibition hypothesis (Jensen et al. 2002; Klimesch et al., 2007), the increased alpha power

reflects decreased excitability over sensory cortices, which in turn serves as a mechanism to protect the information maintained in working memory from external interference. On the other hand, the alpha representation hypothesis (Palva & Palva 2007) posits a direct role of alpha oscillations in representing the information maintained in working memory. Although recent studies lend support to the alpha inhibition hypothesis (van Dijk et al. 2010), the possibility that certain higher-order brain areas may utilize increased alpha oscillations to represent task-relevant information cannot be ruled out. The main reason is that noninvasive measures such as EEG/MEG have limited spatial resolution and lacks access to neuronal firing properties.

We have recently investigated spontaneous ongoing cortical alpha oscillations in behaving macaque monkeys. Our results showed that the laminar profile of the alpha generating mechanism in the inferotemporal (IT) cortex is different from that in V4 and V2 (Bollimunta et al. 2008). A natural question is whether this "structural" difference in alpha organization between higher-order versus lower-order visual areas can give rise to the difference in function supported by alpha oscillations. This study examined this issue at the level of IT by analyzing laminar profiles of local field potentials (LFPs) and multiunit activity (MUA) from two macaque monkeys performing an intermodal selective attention task, in which they received bimodal stimulation, but alternated attention between trial blocks to either visual or auditory stimuli.

3.2 Materials and Methods

3.2.1 Experiment Paradigm

Two male macaque monkeys, B and V, were trained to perform an intermodal selective attention task (Mehta et al. 2000a; 2000b; Lakatos et al. 2008). In this task (Figure 3-1A), interdigitated auditory and visual stimuli (beeps and flashes) were delivered with random stimulus onset asynchronies varying between 500 and 800 ms (Gaussian distribution), with a mean of 650 ms within each stream. Flashes were presented on a diffusing screen subtending 20

retinal degrees, at 1 meter in front of the monkey. To begin a trial block, the monkey had to depress a hand switch and fixate within a central 10 degree window centered on the visual stimulator. In alternating trial blocks, the monkey had to attend to either the visual, or the auditory stimulus stream, and make a manual response to an infrequently presented "oddball" stimulus (14% of trials) in the attended modality. Task difficulty, defined in terms of percent correct rate, was kept approximately the same between modalities to control the effects of arousal.

Data acquisition: Monkeys were surgically prepared for chronic awake recording as described before (Mehta et al. 2000a and 2000b). Briefly, the tissue overlying the calvarium was resected, and appropriate portions of the cranium were removed. The neocortex and overlying dura were left intact. Recording chambers incorporating parallel guide tube grids (Crist Instrument) were positioned normal to the brain surface for orthogonal penetration of foveal/parafoveal regions of IT cortex lying on the lower bank of the superior temporal sulcus. Implantation was guided by stereotaxic transformation of magnetic resonance imaging data, which delineated the cortical gyral pattern. Laminar profiles of local field potential (LFP) and multiunit activity (MUA) were sampled at 2k Hz using a linear array multielectrode with 14 equally spaced recording contacts (channels) schematically illustrated in Figure 3-1B (left). In each subject multiple penetrations were made in different visual cortical areas. Here, the data from a total of 9 penetrations from the inferotemporal cortex where the percent correct rates were all greater than 97% were analyzed, 6 in monkey B and 3 in monkey V.

3.2.2 Data Analysis

3.2.2.1 Preprocessing

Continuous LFP data were bandpass filtered between 3-100Hz and downsampled to 200 Hz. Both LFP and MUA data were epoched from -200 to 400 ms with 0 ms denoting the onset of

visual standard stimulus. For each penetration, following the rejection of trials with incorrect responses and trials with excessively large LFP and MUA magnitude, the number of trials available for analysis was roughly the same for the attend-visual and the ignore-visual (attend-auditory) conditions. Specifically, combining all nine penetrations, there are a total of 9762 attend-visual trials and 9846 ignore-visual trials.

3.2.2.2 Analysis of prestimulus ongoing activity

The prestimulus time period is defined to be -200 ms to 0 ms during which the monkey sustained attention to a given modality (Figure 3-1A). For a given channel and a given experimental condition, the trials of LFP data during the prestimulus time period were treated as realizations of a underlying stationary stochastic process and subjected to parametric autoregressive data modeling, where the model order was chosen to be 12 according to the Akaike Information Criterion (Ding et al. 2000). From the model coefficients the power spectrum was derived and the alpha band power was obtained by integrating the power spectrum from 8 to 12 Hz. Because the magnitude of alpha power varied significantly from channel to channel, to minimize the effect of this variability on population averaging, a normalization procedure was implemented in which the alpha power for a given condition is divided by the sum of the alpha power from both attention conditions. From the normalized alpha power of each recording channel, two types of averages were carried out: (1) across all penetrations to produce overall alpha power and (2) across channels in given layers to produce layer-specific alpha power. The MUA data from each trial were first averaged between -200 ms and 0 ms and then over all the trials in a given condition. The resulting quantity was subjected to the same analysis as that of alpha power. The statistical significance between conditions was assessed by a paired t-test.

3.2.2.3 From ongoing activity to evoked response

To investigate the impact of prestimulus alpha power on stimulus processing, a single-trial sorting and grouping procedure was used for the attend-visual condition. Step 1: For a given recording channel, LFP power in the alpha band during the prestimulus time period was estimated on a trial by trial basis by the multitaper method (Thomson 1982; Mitra and Pesaran 1999). Step 2: The alpha power was log-transformed to yield an approximately normally distributed variable and converted into a z-score. Step 3: The trials were rank-ordered according to prestimulus alpha power z-score and sorted in an ascending fashion into 50 nonoverlapping groups of equal size. Step 4: For each group, the efficacy of stimulus processing was assessed by two quantities: (a) power of stimulus-evoked LFP gamma oscillation (25 Hz to 50 Hz) and (b) magnitude of stimulus-evoked MUA, both during the time period of 50 ms to 150 ms. Each quantity, after log-transformation and z-scoring, was plotted as a function of the group mean alpha power z-score, from which a correlation coefficient was computed. Step 5: The above steps 1-4 were repeated for all recording channels across all 9 penetrations. The correlation coefficients were Fisher-transformed and tested for statistical significance. Step 6: The correlation coefficient between stimulus-evoked MUA magnitude and stimulus-evoked gamma power was also computed, Fisher-transformed, and tested for statistical significance.

3.3 Results

The percent correct rates for the attend-visual and ignore-visual conditions are 99.0% ± 0.31% and 98.3% ± 0.28%, respectively. LFP oscillations in the alpha band (8 to 12 Hz) were observed in all 9 penetrations during the prestimulus time period (-200 to 0 ms). An example is shown in Figure 3-1B (middle). Figure 3-2A is the power spectra from a representative channel where alpha peaks are readily identifiable and alpha power is higher for attend-visual than for ignore-visual conditions. Across nine penetrations, the average alpha peak frequency is 8.69 ±

0.88 Hz, and the average alpha power is significantly higher with visual attention ($p<0.001$), as seen in Figure 3-2B.

Bollimunta et al. (2008), analyzing data from a different condition of the same overall experiment in which the monkey discriminated auditory stimuli in the absence of visual input, found that the main alpha current generator of a source-sink-source configuration is located in the superficial layers of IT, and a weaker alpha current generator is located in the deep layers. This is illustrated in Figure 3-1B (right) for the attend-visual condition where the current source density profile was obtained using the phase realigned averaging technique (Bollimunta et al. 2008). Granger causality analysis further revealed that the superficial layer generator exerts unidirectional causal driving on the deep layer generator. Consistent with this overall picture, alpha power in the superficial layers is on average 19% higher for the attend-visual relative to the ignore-visual condition, and this contrasts with a 13% attentional increase of alpha power in the deep layers. Concomitant with increased alpha power in the LFP profile, MUA in the same prestimulus time period was also significantly elevated by visual attention (Figure 3-2C, $p<0.05$), suggesting that there is an attention-induced increase in excitability which is sufficient to cross the threshold for generating an increase in action potentials.

To investigate how prestimulus alpha activity impacted stimulus processing, prestimulus alpha power for each trial under the attend-visual condition from a given channel was log-transformed, z-scored, and sorted in an ascending fashion into 50 nonoverlapping groups. For each group, the average stimulus-evoked gamma power and stimulus-evoked MUA activity in the period of 50 ms to 150 ms was estimated, z-scored, and plotted as a function of the average alpha power z-score for that group. The results for a representative channel are shown in Figures 3-3A and 3-3B. For both evoked gamma and evoked MUA, a positive correlation is clearly seen,

suggesting that the stronger the prestimulus alpha oscillation, the stronger the stimulus-evoked activity. Across all recording channels, the average correlation coefficient is r=0.4 for evoked gamma and r=0.1 for evoked MUA, both significantly greater than zero at $p<0.0001$. Figure 3-3C plots the relation between evoked gamma and evoked MUA. Again a linear correlation is seen. Across all recording channels, the average correlation coefficient is r=0.2, which is significantly greater than zero at $p<0.0001$.

3.4 Discussion

Despite decades of investigation the physiological genesis and functional significance of alpha oscillations (8 to 12 Hz) are still debated (Andersen & Andersson 1968; Shaw 2003; Palva & Palva 2007). While data from animal models including rats, cats and dogs have contributed much to our understanding of the cellular basis of alpha (Lopes da Silva et al. 1973; Steriade et al. 1980; Hughes & Crunelli 2005), relatively little has been done in the behaving monkey, perhaps the most widely used animal model in cognitive neuroscience. Analyzing data from visual cortex of macaques performing auditory discrimination, we recently reported that in V2 and V4, primary alpha activity generators are located in the deep layers, whereas in the inferotemporal cortex (IT), such generators are located in the superficial layers (Bollimunta et al. 2008). This difference in laminar organization is hypothesized to be linked to the difference in function alpha might support. In particular, in V2 and V4, faster reaction time (RT) to auditory stimulus detection, considered an index of increased auditory attentiveness at the expense of visual attention, is associated with increased visual alpha power, consistent with the classical alpha reactivity in that visual attention reduces alpha power in sensory cortices. In IT, however, faster auditory RT is associated with decreased alpha power, suggesting that visual attention increases alpha power in IT.

In Bollimunta et al. (2008) the level of visual attention is indirectly inferred from the magnitude of auditory reaction time. In this study attention to visual and auditory stimuli is each explicitly manipulated. Three results are reported. First, prestimulus LFP alpha power is higher for the attend-visual condition relative to the ignore-visual (attend-auditory) condition. Second, prestimulus multiunit activity (MUA), reflecting the temporal envelope of local neuronal firing, is larger for the attend-visual than the ignore-visual condition. Third, on a trial by trial basis, stronger prestimulus alpha activity predicts stronger stimulus-evoked response, measured by evoked LFP gamma power and MUA magnitude. Taken together, these results suggest that alpha oscillations in the inferotemporal cortex are not only organized differently than lower level sensory cortices, they may also play a direct role in amplifying the representation of task-relevant information and facilitating sensory processing, which is in marked contrast to occipital alpha where its increase in power is often linked to functional inhibition.

In humans, when attention is directed externally to the environment (intake tasks), increased attention is associated with decreased alpha power (Worden et al. 2000; Sauseng et al. 2005; Rajagovindan and Ding 2010). In contrast, when attention is directed internally (rejection tasks), alpha oscillation increases with an increase in attentional demand (Bastiaansen et al. 2002; Jensen et al. 2002; Raghavachari et al. 2006). A common physiological interpretation is that decreased alpha power reflects increased cortical excitability for enhanced stimulus processing, whereas increased alpha power reflects reduced cortical excitability, providing an active inhibition mechanism for protecting the task-relevant information maintained in working memory from interference (Jones et al., 2000; Worden et al., 2000; Sauseng et al., 2005; Thut et al., 2006; Klimesch et al., 2007; Romei et al., 2008; Rangarajan & Ding 2010). Recently, in an

alternative explanation for the increase in alpha during internal attention tasks, alpha oscillations are given a direct role in representing task-relevant information (Palva and Palva 2007).

Many attention paradigms involve both a sensory intake component and an internal representation component. In the present experiment, monkeys discriminated either visual or auditory stimuli, while ignoring all stimuli in the unattended sensory modality. To perform the task effectively, the monkey must maintain a template of the stimulus attributes (representation) between successive stimulations in the working memory buffer (Knight and Nakada 1998), and at the same time direct attention externally to the environment for accurate detection and encoding of sensory input (intake). The inferotemporal cortex, as part of the working memory network, has been hypothesized as a higher-order area where task-relevant information is being maintained (Miller & Desimone, 1997). The observed increase in IT alpha with visual attention suggests that it may be part of the mechanism involved in representing such information. The concurrent increase of multiunit firing is consistent with this view. In addition, the positive correlation between prestimulus alpha power and stimulus-evoked response, particularly the gamma response, can be seen as providing further evidence of the alpha representation idea. Past work has suggested that stimulus-evoked gamma is a reflection of pattern matching between sensory input and working memory content (Herrmann et al. 2004); better representation (higher alpha) leads to more effective pattern matching (high gamma). These results, in conjunction with the previously reported decrease of alpha power in occipital areas of V2 and V4 with visual attention (Bollimunta et al. 2008), demonstrate that both increased and decreased alpha oscillations may be realized in the same experiment across diverse brain systems. It is worth noting that the experimental task used here is not a traditional internal attention task which in humans often involves visual imagery or manipulation of working memory load.

Attentional modulation of neuronal activity in the absence of sensory stimulation is thought to be implemented by top-down control mechanisms. Numerous studies employing a variety of techniques (Miller & Desimone 1994; Chao & Knight 1998; Knight et al. 1999; Naya et al. 2001; Moore & Armstrong 2003; Fuster 2008; Zhang & Ding 2010) have implicated the prefrontal cortex as a source of the top-down control signal. Because the projections from the prefrontal cortex terminate mostly in the superficially layers of IT (Rempel-Clower & Barbas 2000), the stronger attentional effect we observe in the superficial layers is consistent with this view. Functionally, given the interference of auditory stimuli on visual discrimination, the prefrontal cortex is especially important in resisting distraction and in maintaining stimulus representation necessary for task performance (Knight et al. 1999).

Besides alpha power, the phase of prestimulus alpha oscillations can also significantly affect stimulus processing (Jansen and Brandt, 1991; Makeig et al., 2002; Mathewson et al. 2009). However, the degree of interstimulus jitter is sufficiently large (hundreds of milliseconds) in the present experiment that the stimulus timing appears random at the time scale of alpha, which leaves alpha power as the main independent variable.

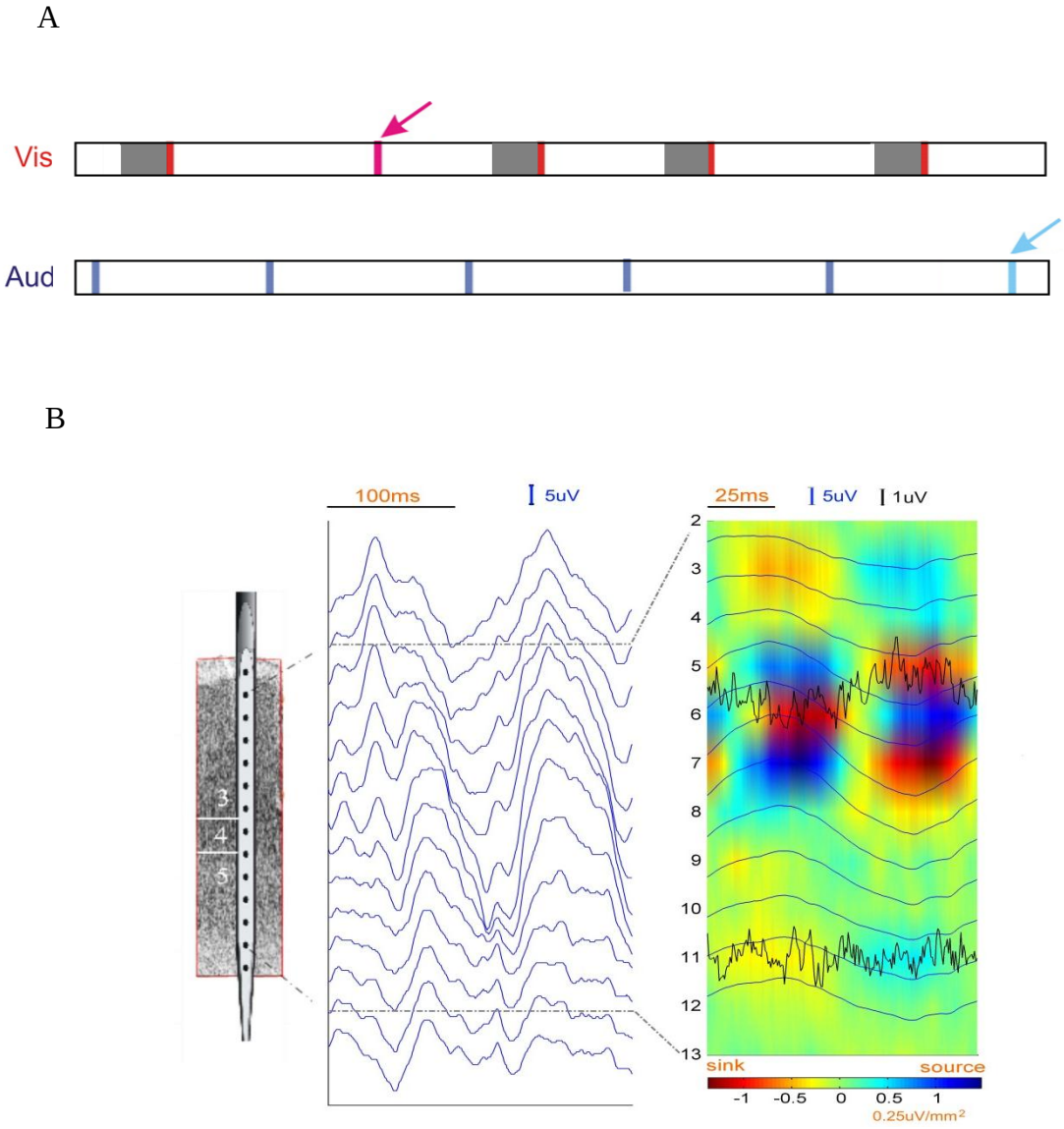

Figure 3-1. Protocol of attention experiment and the laminar distribution of alpha oscillation. (A) Time course of stimulus presentation in both the visual and auditory domains. The shaded interval prior to each standard visual stimulus defines the prestimulus time period. Vertical bars represent stimuli and the deviant stimuli are indicated by arrows. (B) Schematic of electrode (left), 200 ms of LFP data showing the presence of alpha oscillations (middle), and the current source density profile of alpha oscillations with MUA superimposed (right). Here the LFP data was bandpass filtered between 3 to 100 Hz.

A

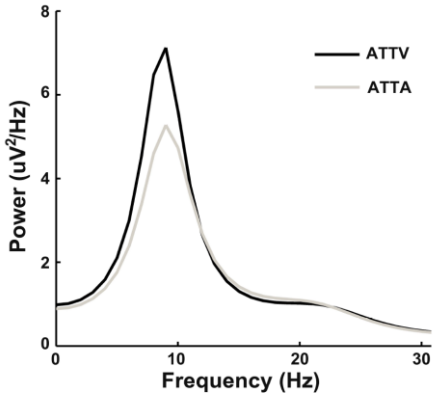

B

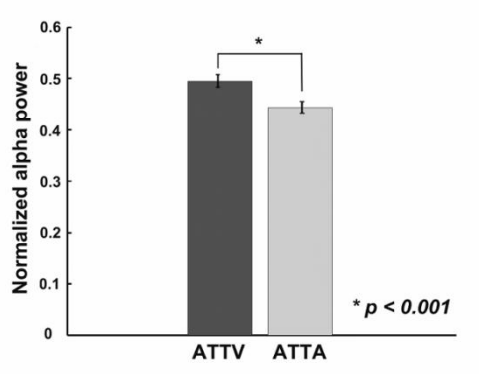

C

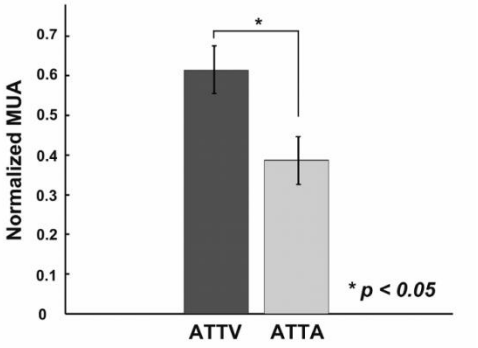

Figure 3-2. Attentional modulation of prestimulus neuronal activity. (A) LFP power spectra from a representative channel. (B) Comparison of averaged LFP alpha power. (C) Comparison of averaged MUA. For both LFP alpha power and MUA, a normalization procedure was carried out for each recording channel according to the formula: condition/(attend-visual+ignore-visual), before averaging. Error bar denotes the standard error of the mean. ATTV: attend-visual and ATTA: attend-auditory (ignore-visual).

A

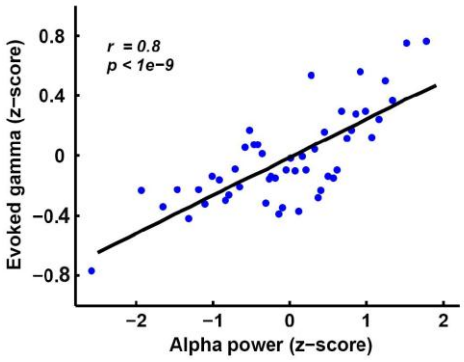

B

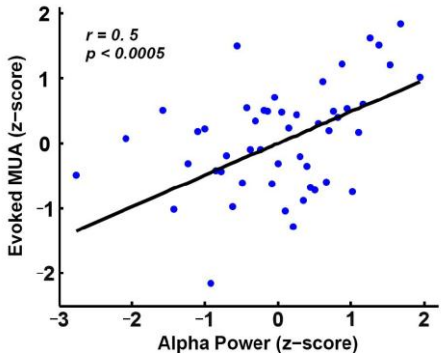

C

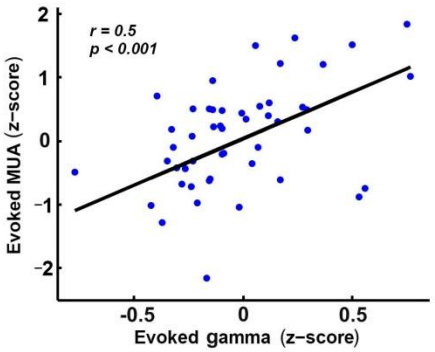

Figure 3-3. From prestimulus ongoing activity to stimulus-evoked response. (A) Stimulus-evoked gamma power (25 Hz to 50 Hz) and (B) stimulus-evoked MUA magnitude as a function of prestimulus alpha power for a representative recording channel. Here all quantities were converted into z-scores to facilitate comparison across different recording channels (see Methods). (C) Stimulus-evoked gamma power in Figure 3-3(A) versus stimulus-evoked MUA magnitude in Figure 3-3(B).

CHAPTER 4
CENTRAL REPRESENTATION OF THROBBING PAIN

4.1 Introduction

The subjective quality of pain is an essential part of the clinical evaluation. These clinically relevant pain qualities, such as throbbing, crushing, lancinating, or aching pain, are critical details of the evaluation because they suggest invaluable, at times life-saving, clues to the underlying disorder (Armstrong et al., 1998, Rosman et al., 1998, Kreiner et al., 2010). Many recent advances have propelled our understanding of the molecular mechanisms underlying the transduction of thermal and chemical stimuli by pain-responsive sensory neurons (Basbaum et al., 2009). However, very little is known about how these neurophysiologic responses initiate the great diversity of clinically relevant subjective qualities (Ma, 2010). A clearer understanding of the neurobiological basis of these clinically relevant pain qualities would not only improve our fundamental knowledge of pain pathophysiology but would also greatly enhance our ability to diagnose, measure, and design new therapies for clinical pain (Backonja and Stacey, 2004, Hansen et al., 2007, Victor et al., 2008, Jensen et al., 2010).

Among the many pain qualities, a throbbing or pulsatile quality is clinically relevant because it accompanies the most severe forms of acute pain (Aslan et al., 2009), correlates with disease severity (Ballard et al., 2010), and signals disease progression, such as the metastatic spread of cancer (Lam and Schmidt, 2011). The experience of throbbing pain also associates strongly with a lack of response to currently available therapies (Burstein et al., 2000, Walny et al., 2001), greater functional disability (Jensen et al., 2010, Blumenfeld et al., 2011), and comorbid depression (Kolotylo and Broome, 2000). Thus a delineation of the peripheral and central origins of the throbbing quality could provide important insights leading to the development of novel strategies for the relief of clinically significant pain.

The prevailing scientific view is that throbbing is a primary sensation caused by the rhythmic activation of pain-sensory neurons by closely apposed blood vessels. In dentistry, this model plays a key diagnostic role in inferring the viability of dental pulp from the presence of sensitized afferents and blood vessels (Seymour et al., 1983), though evidence for this view remains indirect (Grushka and Sessle, 1984, Hermanstyne et al., 2008, Kreiner et al., 2010). Recently, we questioned whether the throbbing quality in the case of migraine pain were related to heart rate (Ahn, 2010), challenging – if only indirectly - an important aspect of the long-held presumption that dilation of the cranial arteries underlies the throbbing quality of migraine pain (Graham and Wolff, 1938). However, because the pathophysiology of migraine pain is still controversial (Strassman and Levy, 2006, Olesen et al., 2009), the ability to generalize to other painful conditions is uncertain. The first study in Chapter 4 focused on the throbbing quality in dental pain, a condition where the peripheral origin of the pain is indisputable. In addition, by analyzing the simultaneously recorded throbbing pain rhythm and arterial pulse with advanced analytical methods, we were able to obtain greater insight into the mechanisms underlying these complex biological rhythms.

The throbbing quality is present in a great diversity of acute pain conditions associated with tissue injury and inflammation, such as acute post-surgical pain (Aslan et al., 2009), sickle-cell crisis (Ballas, 1993), acute bone fracture (Cottalorda, 2009), cervical artery dissection (Arnold, 2006), giant cell arteritis (Rozen, 2010), and acute dental pain (Seymour, 1983), is often cited as supporting evidence. However, the throbbing quality is also highly prevalent in a range of chronic pain conditions, many of which are associated with nerve injury alone, such as carpal tunnel syndrome (Jensen, 2010) and post-herpetic neuralgia (Niv, 1989), or conditions primarily affecting the central nervous system, such as chronic post-spinal cord injury pain (Cruz-Almeida,

2009), chronic post-traumatic brain injury pain (Ofek, 2007), and multiple sclerosis (Houtchens, 1997). Moreover, conditions involving isolated lesions of the central nervous system, in which throbbing pain is referred to the contralateral side of the body, such as in post-stroke central pain (Leijon, 1989) are fully inconsistent with the perception of hemodynamic events in the periphery. Isnard and colleagues also recently reported a patient whose episodic seizures were characterized by a throbbing pain sensation, and whose clinical and electrographic abnormalities resolved with the ablation of a focal area of cortical dysplasia within the right posterior insula (Isnard, 2011).

The broad clinical spectrum of throbbing pain thus suggests that the widely held view of the vascular origins of the throbbing rhythm could be examined more discerningly. Indeed our recent studies of the throbbing rhythm in patients with migraine (Ahn, 2010) and dental pain (Mirza & Mo, 2012) support the conclusion that subjective throbbing experiences do not correspond simply to hemodynamic events in the periphery. Here we report the psychophysical and neurophysiological characteristics of the throbbing rhythm in a patient with an unusual migrainous condition, whose isolated throbbing sensations, in the absence of pain or headache, presented the opportunity to gain further insights into the mechanisms underlying the experience of throbbing pulsations.

We chose the electroencephalogram (EEG) because of its established utility in capturing the neurophysiological representations of pain (Sarnthein et al. 2006; Stern et al. 2006), and because the high temporal resolution of the EEG was well suited to looking for a brain signature of the throbbing rhythm. A well-established neurophysiological correlate of pain is its modulation of the power of alpha oscillations (8-12 Hz) in clinical and experimental pain models (Backonja, 1991; Babiloni et al. 2006; Shao et al. 2012). Of particular interest to the neural

origin of throbbing pulsations was the observation that the frequency of the temporal variations of alpha power is in the range of 1Hz (M. J. Schroeder & Barr 2000; Montez et al. 2009), which is similar to the frequency of the throbbing sensations, and the relationship between the two rhythmic activities is thus a natural target of the present case investigation.

4.2 Methods

4.2.1 Experiment 1: Throbbing Quality in Dental Pain

4.2.1.1 Subjects

Subjects with acute dental pain were recruited from patients of the Student Oral & Maxillofacial Surgery Clinic at the University of Florida College of Dentistry, under a protocol approved by the Institutional Review Board. In the normal course of their evaluation clinic personnel identified patients with acute dental pain who additionally reported a sustained throbbing quality. Study personnel were on hand to obtain informed consent and perform the study in a manner so as to minimize interference with the usual course of treatment. The inclusion criteria were that subjects are 18 years or older, fluent in English, and have a recent onset of dental pain, within one week of the evaluation. A *post hoc* criterion was that analgesia was achieved after the injection of local anesthetic, which was satisfied in all cases.

4.2.1.2 Descriptors of dental pain.

Subjects rated the overall intensity of their dental pain on a 0-10 scale, with 0 representing no pain and 10 representing the worst imaginable pain. Subjects described the qualities of their pain and confirmed the presence of throbbing pain on a questionnaire containing a column of 21 pain descriptors (Table 4-1) with a 0-10 scale of relative intensity next to each descriptor. This questionnaire closely follows the short form McGill Pain Questionnaire (SF-MPQ) (Melzack, 1987) with minor modifications intended to more clearly define the temporal characteristics of the pain (items 7-10).

4.2.1.3 Recording of throbbing rhythm.

Simultaneous recording of the throbbing rhythm and arterial pulse were recorded on a BIOPAC MP-150 acquisition device (BIOPAC, Inc, Goleta, CA) at a sampling rate of 1000 Hz. Subjects indicated the rate and timing of the maximal point of pressure of the throbbing experience through the use of a sliding rheostat or push button. A pulse plethysmography probe attached to the earlobe simultaneously monitored the waveform of the subjects' extracranial arterial blood flow. The subjects provided 2-3 min of a simultaneous digital recording of their report of a throbbing rhythm and their arterial pulse. We obtained 48 recordings and analyzed 29 of these records more closely. There were 19 records that were excluded from some of the analysis because they were clearly too slow and/or too irregular to have a plausible relationship to arterial pulse.

4.2.1.4 Statistical analysis.

Arterial pulse and throbbing rates were obtained from representative portions of the record, excluding periods in the record containing interruptions of the task or artifacts in the arterial pulse, which were infrequent. The average rates are presented as the mean beats per minute (bpm) ± standard error of the mean (SEM). The average difference between throbbing and arterial pulse rates was tested versus a null of no difference with a paired Student's t-test, with $p<0.05$ set as the criteria of significance. The Pearson product moment correlation coefficient between the two measured rates was determined with the null hypothesis of unity. We present a 95% confidence interval, noting that the conventional view predicts a high correlation (such as $r>0.85$).

For the 19 rejected records, the average throbbing rate from these 19 records (17.2 bpm ± 2.6 SEM) was clearly much slower than their corresponding average heart rates (75.5 bpm ± 2.6 SEM. $P<0.0001$ unpaired t-test), and the standard deviation of the inter-event interval (3.7s ±

0.68) was much larger than those reported by the other subjects included in this study (0.29s ± 0.03, P<0.0001 paired t-test). In the post-recording debriefing, all of these subjects indicated a distinct lack of confidence in their report of the timing of their throbbing experiences. This proportion of people with difficulty reporting an internally perceived rhythm is consistent with our separate psychophysical control studies in which we asked normal healthy subjects to report their own arterial pulse, using the same recording apparatus; those who were unable to report their own arterial rhythm similarly recorded slow and non-rhythmic responses. The exclusion of these records from the present analysis did not affect the conclusions of this study. In fact, their inclusion would have further strengthened the numerical differences between the throbbing rhythm and arterial pulse.

4.2.1.5 Spectral analysis of heart rate variability and throbbing rate variability.

We investigated the temporal dynamics of throbbing and arterial pulse rhythms using spectral methods. The throbbing and arterial pulse records were filtered through a zero-phase filter set between 0.01 and 100 Hz and downsampled to 200 Hz. We used the midpoint of the rising phase in each cycle to represent discrete throbbing and arterial pulse events. The temporal sequence of discrete events was smoothed by using a Gaussian kernel at full width half maximum (FWHM, equal to the average inter-event interval) We calculated the power spectrum of each smoothed time series using Welch's method, normalized by dividing the total power, and then averaged across all subjects to yield the population power spectrum for throbbing and arterial pulse.

4.2.1.6 Determination of fractal scaling exponent.

We further analyzed the throbbing and heart rate variability by converting the discrete event sequence into an instantaneous rate time series where the instantaneous rate was defined as the inverse of the interval between two adjacent events (Berger et al., 1986, Potter and Kinsner,

2008). We calculated the power spectrum of each instantaneous rate time series, again using Welch's method. For the arterial pulse, this analysis is in agreement with previous fractal analyses of heart rate variability (Kobayashi & Musha T 1982),showing that the power spectra of the instantaneous heart rate time series are well described by a power law ($1/f^{\alpha}$ type), where the fractal scaling exponent α is defined by the slope of the log-log plot in the frequency range between 0.04 and 1Hz. Previous work on changes in heart rate variability after cardiac bypass surgery have hypothesized that changes in the value of α represent a change in the autonomic regulation of the heart (Komatsu et al., 1997). To our knowledge the present work is the first study to apply an analogous fractal analysis to the rhythm of throbbing pain. The significance of the difference in α between heart and throbbing rate variability, assessed by a paired t-test, was taken as evidence of distinct mechanisms underlying these two rhythms.

4.2.1.7 Phase coupling analysis.

To address the temporal relationship between the two rhythms, we analyzed the phase synchronization between the heart rate and throbbing rate waveforms. Because the throbbing and heart rates were usually different ($f_{HR} \neq f_{throbbing}$), we applied a method that can examine phase relationships between two non-identical oscillators synchronized at a m:n frequency ratio (Tass et al., 1998). Let the relative phase between the two oscillators be, $\psi_{n,m}(t) = n\phi_1(t) - m\phi_2(t)$, where ϕ_1 is the phase for heart rate, and ϕ_2 is the phase for throbbing rate at time t determined by the Hilbert transform. Here *m* and *n* are integers so that *m/n* is close to $f_{HR} / f_{throbbing}$. For example, if the total event number of heart beat and throbbing is 75 and 65, then we used both 7/6 and 8/7 as *m/n* for the tests. If the two oscillatory activities are independent then the distribution of $\psi_{n,m}(t)$ is uniform. A departure from uniform distribution gives evidence for

coupling between the two oscillators. We assessed the uniformity of the relative phase distribution using Kuiper's test (Fisher 1995). If the Kuiper statistic V is larger than 1.62 ($p<0.1$) then the distribution is considered non-uniform. Setting even this lenient criterion none of the subject records (including the 19 records that were set aside from the main analysis) showed evidence of phase coupling.

4.2.2 Experiment 2: EEG Signature of the Persistent Throbbing Pain

4.2.2.1 Case history.

Subject was a 56 year old clinical psychologist with a prior adult headache history consistent with the diagnosis of migraine, consisting of episodic throbbing frontal head pain accompanied by nausea, photophobia and phonophobia, whose usual triggers included stress, lack of sleep, wine, and skipped meals, and who obtained consistent relief from oral sumatriptan. Her present clinical history began at the age of 49 when she was disabled by chronic low back pain due to multi-level degenerative disc disease, obtaining only partial pain relief with a daily regimen of oxycodone. However, concurrent with this chronic back pain and opiate use, the subject developed a chronic daily headache, consisting of dull holocephalic pressure, from which she no longer obtained complete relief from sumatriptan, NSAIDS, and caffeine containing combination analgesics.

At age 53, she underwent a multi-level laminectomy and stabilization of the L2-3, L3-4, and L4-5 intervertebral spaces, which together with continued physical therapy, resulted in a successful resolution of her chronic back pain. However the patient's headache and continued opioid use continued until age 54, when the presumptive diagnosis of analgesic overuse headache prompted the withdrawal from all abortive medications, including opioids, triptans, NSAIDs, and caffeine. Patient also discontinued estrogen replacement therapy. The chronic daily headache gradually remitted over several months, and by age 55 she returned to a stable

baseline of episodic migraine attacks at less than one per month, with full or near-complete relief from oral sumatriptan.

However, despite the remission of her chronic daily headache, the subject became aware of a chronic throbbing, pulsatile, or wooshing sensation located in the frontal and bitemporal regions of the head. Subject was aware of this sensation at all times, though the sensation became more intense towards the end of the afternoon, during which times she found them intrusive and disruptive to concentrating on her work. There were no other provocative maneuvers, such as bending, coughing, valsalva, or physical exertion, though the throbbing sensation was aggravated by agitation and strong emotions. The throbbing sensation also became much more intense leading up to and during her episodic migraine attacks. The only known palliative technique was distraction, such as with vigorous physical activity.

An extensive imaging workup failed to reveal evidence for an arteriovenous fistula, cerebral sinus thrombosis, or other abnormality that could account for a pulsatile tinnitus. Medications that had no effect on the throbbing sensation included naproxen, sumatriptan, atenolol, verapamil, topiramate, valproic acid, and gabapentin. It was notable that atenolol produced a symptomatic bradycardia without any effect on the rate or quality of the throbbing sensation. At one year follow up from the time of evaluation and two years from the onset of symptoms, the subject continues to experience a daily throbbing sensation.

4.2.2.2 Experiment protocol.

The subject refrained from using pain medications for 72 hours prior to the evaluation. As was customary for the subject, the throbbing intensity increased gradually throughout the day. She recorded the psychophysical properties of the throbbing quality at the beginning and end of the day, while we simultaneously recorded the arterial pulse. High-density EEG was recorded in two sessions each lasing 5 minutes. Each recording session consisted of a brief resting state

during which she fixed gaze at a fixation target, followed by a psychophysical task in which she was asked to indicate the throbbing rhythm by pressing an instrument key in synchrony with the timing of the throbbing pulsations. Based on the subjective rating of the throbbing intensity, the two EEG recording sessions were referred to as weak and strong throbbing conditions, respectively. The throbbing rate obtained from averaging the response interval in the weak throbbing condition is 50 bpm, which is slower to the 68 bpm in the stronger throbbing condition.

4.2.2.3 EEG recordings and data preprocessing.

The electroencephalogram (EEG) data was recorded with a 128-channel BioSemi Active System at a sampling rate of 1024Hz. The stimulus and the response was delivered and registered by E-Prime and by a Berisoft EXKEY microprocessor logic pad. Raw EEG signals were bandpass filtered with cutoffs set at 0.53 and 50Hz and downsampled to a sampling frequency of 250Hz. Data from each channel were re-referenced against the average reference. Independent component analysis (ICA) (EEGLAB tutorial) implemented in EEGLAB 7.2 was used to remove muscle artifacts, movement artifacts and excessive eye blinks. To mitigate the impact of volume conduction, BESA 5.2 was used to transform voltage time series into current source density (CSD) time series.

4.2.2.4 Estimation of alpha power time series.

The CSD time series was divided into nonoverlapping windows of 500 ms in duration. The power spectrum for each window was estimated using a multitaper approach (Mitra & Pesaran 1999) and the alpha power was obtained by integrating the power spectral density between 8 to 12Hz. Alpha power as a function of time was referred to as the alpha power time series or alpha power oscillation.

4.2.2.5 Analysis of alpha power time series.

To assess the relation between alpha power and throbbing sensation, the sequence of throbbing reports was transformed into a continuous waveform by convoluting the sequence of discrete key presses with a Gaussian kernel, and synchrony between the alpha power time series and the continuous events was measured by coherence. Here the window length was 10 s and the overlap was half the window length. Further smoothing was achieved by the multitaper method (Mitra & Pesaran 1999).

To test the statistical significance of the coherence between the throbbing rhythm and the alpha power oscillation, we created a baseline condition by pairing the throbbing record with randomly chosen epochs of alpha power time series from the resting state record. The distribution of coherence estimated in this fashion constituted the null hypothesis distribution where no relationship between the throbbing record and the alpha power oscillation existed.

The dynamics of the neuronal networks during strong and weak throbbing sessions was evaluated by computing and averaging coherence of alpha power time series for all pairwise combination of posterior channels. The window length used was 25 s (50% overlapping).

4.3 Results

4.3.1 Experiment 1: Throbbing Quality in Dental Pain

At a university-based student oral surgery clinic, in the normal course of 512 evaluations, clinic staff identified 48 subjects who reported a strong and distinct sense of throbbing pain. Of these, 29 subjects were able to record a throbbing pain whose rhythm could possibly be related to their arterial pulse (see Methods).

4.3.1.1 Overall pain characteristics.

Subjects were on average 36 years old ± 2 SEM, and were 66% women. They reported moderately high pain intensity, averaging 7.7 ± 0.4 SEM on a scale from 0 to 10 (see Methods).

In addition, the subjective qualities of their dental pain, described by ratings of words from a questionnaire with 21 pain descriptors (Table 4-1; Figure 4-1A), had characteristic features. The qualities of throbbing (descriptor #8), aching (descriptor #1) and tender (descriptor #16) were prominent, and were similar to the responses from an unselected sample of 51 consecutive patients obtained on alternate clinic days. This unselected sample also resembled the overall characteristics of the subject group, being on average 37 years old ± 2 SEM, 55% women, and also reported moderate to high pain intensity levels (7.2 ± 0.3 SEM).

4.3.1.2 Throbbing rate and arterial pulse rate.

To obtain a psychophysical record, subjects signaled the rhythm and timing of their throbbing experience by pressing a button connected to a digital recording device, while simultaneously recording their arterial pulse for 2-3 min. Overall temporal characteristics of the throbbing rhythms included an average throbbing rate (44 bpm ± 3 SEM) that was distinctly slower than the average heart rate (73 bpm ± 2 SEM, $p<0.001$). On an individual basis, the paired throbbing and arterial pulse rates (Figure 4-1B) were numerically independent (best fit in blue; Pearson r=0.10 with 95% CI from -0.28 to 0.45) and inconsistent with the values that would have been predicted by the traditional view (the identity line in red - Figure 4-1B). Whereas arterial pulse rates respected the usual physiological range, throbbing rates ranged widely, with the most highly represented throbbing rates at 31-40 bpm (Figure 4-1C).

4.3.1.3 Spectral analysis of throbbing rhythms.

Next we compared the spectral characteristics of each rhythm. Figure 4-2 shows representative segments of the analyzed waveforms of arterial pulse and the throbbing rhythm from two subjects, one in whom the two rates match closely (Figure 4-2A) and one in whom the arterial pulse rate and throbbing rate ratio was approximately 3:2 (Figure 4-2B). The averaged

power spectra for all 29 subjects for the arterial blood flow and throbbing experience (Figure 4-2C) demonstrated the incongruous relationship between these two rhythmic events.

4.3.1.4 Heart rate and throbbing rate variability observe distinct power laws.

We previously noted that for migraine pain the physiologic variation in heart rate (related to respiration) allowed us to observe a clear mismatch between the two rhythms (Ahn, 2010). To address this relationship more systematically, we compared the variability in the arterial and throbbing records, through a spectral analysis of heart rate and throbbing rate variability. To analyze beat-to-beat variability, we first converted the smoothed waveforms of each record into an instantaneous rate time series (Figures 4-3A and B), and plotted the averaged power spectra for the instantaneous rate time series for all subjects on a log-log scale, for arterial pulse (HRV) and throbbing rhythm(TRV), respectively (Figures 4-3C and D). The linear region over the low frequency range indicated the presence of a $1/f^{\alpha}$ power law relationship, as has been previously reported for heart rate variability (Kobayashi & Musha T 1982; Komatsu et al., 1997). As was the case for heart rate variability, the power spectra of the throbbing rate time series were also well described by a power law. However, the fractal-scaling exponent α, which correspond to the average slopes of the log-log plots, are significantly different (1.06 ± 0.10 SEM for heart rate variability and 1.59 ± 0.09 SEM and for throbbing rate variability, paired t-test $p<0.0001$), providing strong evidence that the variability in these rhythms arise from distinct physiological mechanisms.

4.3.1.5 Phase coupling analysis.

Another independent way to appreciate a relationship between two rhythms is to treat each as an oscillator and determine whether there is a relationship (synchrony) between the two oscillators. For a given pair of heart rate and throbbing rate oscillators whose rates had a ratio of

m:n the relative phase can be calculated as , $\psi_{n,m}(t) = n\phi_1(t) - m\phi_2(t)$, where ϕ_1 is the phase for heart rate, and ϕ_2 is the phase for throbbing at time t. Figure 4-4A shows the relative phase distribution for a typical subject where the Kuiper statistic V=0.27 (p>0.1), falls far short of a minimal threshold value of V=1.62 (p=0.1) indicating that the distribution is uniform and that the two oscillators are not coupled. Figure 4-4B shows the Kuiper's statistic (V) for all subjects, which demonstrates that none of the individual records showed evidence for coupling between the two rhythms.

4.3.2 Experiment 2: EEG Signature of the Persistent Throbbing Pain

4.3.2.1 Psychophysical recording.

The subject recorded her subjective perception of the throbbing rhythm into a digital recording device while we simultaneously recorded her cranial arterial pulsations with a pulse oximeter attached to her earlobe (see Methods). The subjective throbbing rate of 48 ± 1.7 bpm was significantly slower than the subject's regular heart rate of 68 ± 2 bpm ($p < 0.005$, paired t-test).

4.3.2.2 Throbbing intensity influences alpha power.

We compared the overall EEG spectral power between weak and strong throbbing conditions. Figure 4-5A shows the power spectra from a representative parietal-occipital channel, which indicates that the overall alpha power (8-12Hz) was higher in the session associated with the stronger throbbing pulsations. When represented topographically as the percent change of alpha power over the whole scalp, the change in alpha power was most prominent over the posterior channels (Figure 4-5B).

4.3.2.3 Throbbing rate synchronizes with the dominating oscillation in the alpha power time course.

The magnitude or power of alpha oscillations fluctuates over time. The alpha power oscillation was found to be in synchrony with the reported instances of throbbing pulsations (Figure 4-6A and Figure 4-6B). The coherence between the smoothed button press time course and the simultaneous alpha power time series from the parietal-occipital site (PO_3) has a significantly higher value in the strong throbbing session (0.35), compared to that in the weak throbbing session (0.25), and both are significantly higher than that of the baseline null hypothesis dataset created using a random permutation approach ($p<0.05$). Critically, when the same analysis was applied to the alpha power time course from the somatosensory/premotor region (electrodes C3/C5), a coherence value of 0.08 was found, which was not significantly higher than the baseline null hypothesis value ($p>0.3$), providing evidence that the EEG-behavior coupling is not induced by movement.

To further examine the synchrony between alpha power time series and the concurrently recorded instances of throbbing, we measured the variability of the lag between each throbbing instance and the nearest peak of the alpha power time series, and found that it was smaller during the strong throbbing session (~0.24 second) compared to the weak session (~ 0.43 second). The decrease in variance is significant (two sample F-test, $p<0.1$). In the strong throbbing session, the average interval between adjacent throbbing events is around 1.25 ± 0.05 second, which is close to the average interval between adjacent peaks in the alpha power time series (1.20 ± 0.49 second), whereas in the weak throbbing session, the average interval between adjacent throbbing events is around 1.44 ± 0.11 second, which is larger compared to the average interval between adjacent alpha power peaks of 1.18 ± 0.45 second.

4.3.2.4 Throbbing intensity modulates the power and coherence of alpha power time course in posterior channels.

Increased alpha power is observed consistent among the posterior channels exhibiting throbbing modulated alpha power in Figure 4-5B. Among the same group of channels, the enhancement in coherence of alpha power time course is observed in the strong throbbing session across wide frequency band (Figure 4-6C). The inter-channels coherence is significant different between the weak and throbbing session under paired t-test ($p<0.01$).

4.4 Discussion

The experience of throbbing pain is prevalent and clinically relevant but poorly understood. Its pulsatile character compels the common presumption that it is in some way linked to heart rate. Some clinical conditions that involve vascular pathology, such as cerebral sinus thrombosis (Wasay et al., 2010), sickle cell crisis (Ballas and Delengowski, 1993), giant cell arteritis (Rozen, 2010), and spontaneous cervical artery dissection (Arnold et al., 2006), have characteristic throbbing qualities that would appear to implicate the experience of vascular dilation, though only indirectly.

Vascular sensations are also a key feature of the current view of migraine (Olesen et al., 2009), a highly prevalent headache disorder whose throbbing quality (Scher et al., 1998, Kelman, 2006) is a diagnostic hallmark (IHS, 2004) and is associated with high severity, frequency, and disability (Blumenfeld et al., 2011). Early studies of migraine focused on the amplitude of cranial artery pulsations, leading to the so-called vascular theory, which hypothesized that the pain of migraine is a primary disorder of cranial artery dilation (Graham and Wolff, 1938). However, several important inconsistencies with the clinical condition draw strong criticism against this theory (Goadsby, 2009). Moreover, data showing a direct relationship between vascular pulsations and the subjects' perception of throbbing remain elusive. More recent

electrophysiological evidence for this traditional view, which in physiological terms predicts that pain-sensory neurons are activated by the dilation of blood vessels by normal arterial pulsations, suggest otherwise (Malliani and Pagani, 1976, Goder et al., 1993, Strassman et al., 1996, Levy et al., 2005, Strassman and Levy, 2006).

The finding in Experiment 1, that the throbbing rhythm exhibits a fractal power law, lays a novel framework for further studies aimed at determining how throbbing pain engages brain regions involved in other important cognitive functions, such as the awareness of pain (Craig, 2009, Lee et al., 2009), or the perception of rhythm and timing (Meck et al., 2008). In addition, because the throbbing quality is associated with a broad range of disabling pain conditions that are refractory to presently available therapies, such as cancer pain (Lam and Schmidt, 2011), traumatic brain injury (Ofek and Defrin, 2007), sickle cell crisis (Ballas and Delengowski, 1993), pelvic pain (Ballard et al., 2010) and migraine (Blumenfeld et al., 2011), the perception of throbbing pain could possibly serve as a functional target in the development of novel therapeutic approaches for severe and disabling pain.

In addition to the limitations that are inherent to the cross-sectional study conducted in Experiment 1, the lack of additional historical detail about the dental patients could have adversely affected the results of this study. For example, neuropathic conditions unrelated to dental pulp involvement, such as trigeminal neuralgia, would misrepresent the subject population. However, this clinic by and large provides primary care for patients with dental pain resulting from dental caries, periodontal disease, and trauma. Accordingly, subjects had substantial relief of their pain after the injection of local anesthesia, which assisted in relating the pain to the pulp or associated periodontal tissue. The inclusion of a subject with one of these

other conditions would thus be uncommon, and their very infrequent inclusion would not significantly affect the overall conclusions of this study.

Non-invasive electrophysiological approaches such as EEG represent an important opportunity to understand pain processing (Hauck et al., 2008) and the insights generated may suggest novel neuromodulatory approaches for the treatment of chronic pain (Jensen et al., 2008). Among the most prominent and consistent changes in the EEG pattern with pain is the increase in overall power in the alpha (8-12Hz) range (Sarnthein et al. 2006; Stern et al. 2006; J. G. van Dijk et al. 1991). By combining the EEG recording with the psychophysical property of throbbing in the Experiment 2, we showed that alpha power is significantly higher in strong throbbing relative to weak throbbing is consistent with this line of evidence. Functionally, given alpha relationship to attention (Steriade et al. 1990; Bollimunta et al. 2011), the increase in alpha power in pain has been thought to represent a change in selective attention to nociceptive stimulation (Dehghani et al. 2003), possibly representing a reduction in attention to visual stimuli (Cao et al. 1999; Sanchez del Rio et al. 1999; Jonkman & Lelieveld 1981), and whose hemispheric asymmetry may explain certain aspects of the migraine attack (de Tommaso et al. 1998; Jonkman & Lelieveld 1981). A modulation of the alpha rhythm is also appreciated in experimental models of pain (Backonja, 1991; Babiloni et al. 2006; Shao et al. 2012), where it may also represent a gating of nociceptive input and sensory processing (Hauck, 2008) .

Close inspection of EEG data reveals that the magnitude or power of alpha oscillations fluctuates over time. These fluctuations observe characteristic temporal behavior known as power-law long-range correlation, which exhibits 1/f dynamics as a function of frequency (Linkenkaer-Hansen et al. 2001; Nikulin & Brismar 2004). This feature was thought to be the basis for effective communication in the brain and is also known to be affected by pain

processing (Linkenkaer-Hansen et al. 2001; Linkenkaer-Hansen et al. 2004; Leopold et al. 2003) Recent simultaneous fMRI-EEG studies demonstrate that alpha power can be modulated by various large-scale brain networks (Laufs et al. 2003a 2003b; Mantini et al. 2007) and suggest its potential as a biomarker for some clinical conditions (Montez et al. 2009; Smit et al. 2011). Our finding that alpha power fluctuations are synchronized with the reported throbbing events and the degree of synchrony is modulated by throbbing intensity, provides not only a neuronal signature of the experience of throbbing pain, but also a direct pathway toward uncovering the large scale network activities underlying the perception of throbbing pain.

What underlies the modulation of alpha power? A recent theory proposes that the power of a higher frequency oscillatory activity may be rhythmically modulated by the phase of a lower frequency oscillation (Canolty & Knight 2010). Although we found evidence that alpha power is modulated the phase of the delta rhythm (0 to 3 Hz) (Lakatos et al. 2008; Gomez-Ramirez et al. 2011), the delta rhythm itself is not synchronized with the throbbing reports.

Two comments are in order for the EEG results. First, the subject reported rhythmic throbbing events by pressing an instrument key, raising the possibility of motor contamination. This is unlikely as the synchrony between the sensorimotor channels and throbbing percept is not significant and is not modulated by throbbing intensity. Second, due to EEG's limited spatial resolution, it's hard to distinguish the contribution from different brain regions. Future work with improved technology is necessary to over this problem and to further reveal the activation of deep brain structures in pain perception.

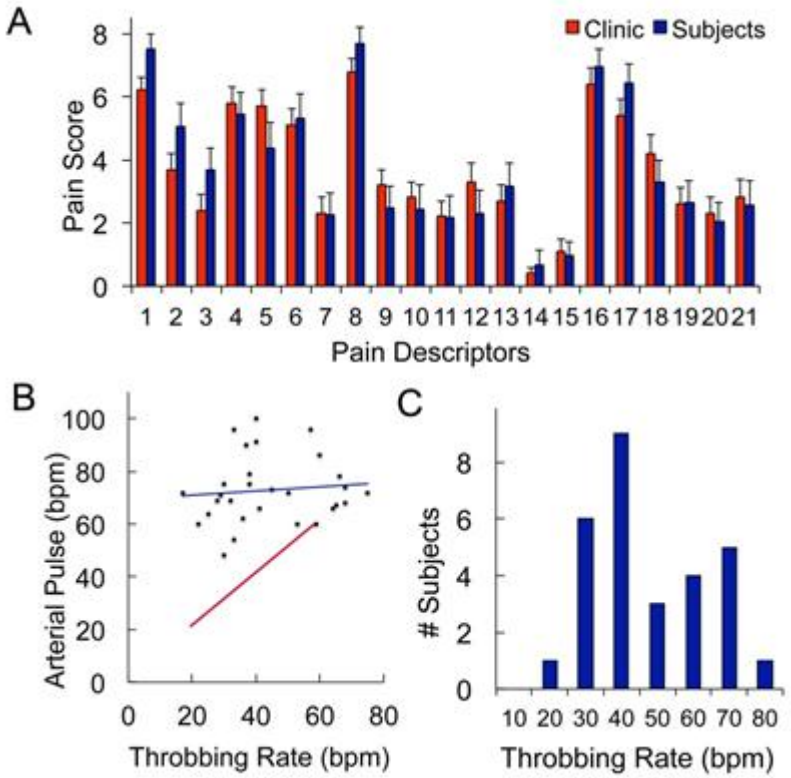

Figure 4-1. Throbbing is a characteristic feature of dental pain, and its rate is distinctly slower than heart rate. (A) Subjects (n=29) and an unselected sampling of the general clinic population (Clinic, n=51) confirmed the prevalence of the throbbing quality in dental pain, and demonstrated that the overall pain characteristics of the study sample are similar to the general clinic population. (B) The individual throbbing and arterial pulse rates were unrelated (in blue; Pearson r=0.10 with 95% CI -0.28 to 0.45), and clearly distinct from the prediction by the prevailing view (in red). Overall, the average throbbing rate (44 bpm ± 3 SEM) was distinctly slower than the average arterial pulse rate (73 bpm ± 2 SEM, $p<0.001$). (C) Throbbing rates ranged widely, but the most common rates were in the range of 31-40 bpm.

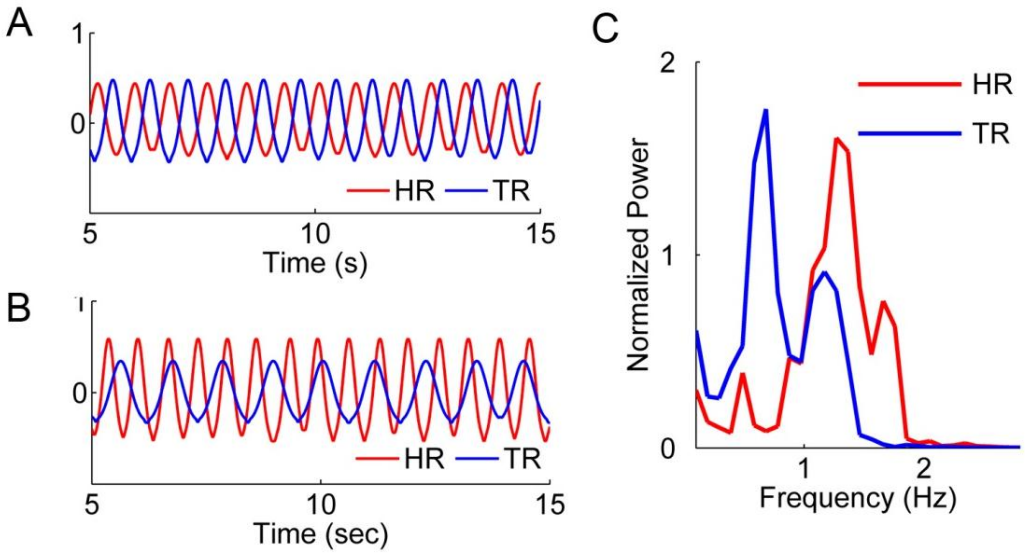

Figure 4-2. Spectral analysis of the throbbing rate and the arterial pulse rate reveals their distinct temporal characteristics. The superimposed and smoothed waveforms of the recorded arterial pulse (HR) and throbbing rhythm (TR) from two representative patients (A) a subject whose frequency ratio $f_{HR} / f_{throbbing}$ is 1:1 (B) another subject whose frequency ratio $f_{HR} / f_{throbbing}$ is 3:2. (C) The average normalized power spectra from all subjects reveals the distinct frequency characteristics of the HR and TR waveforms.

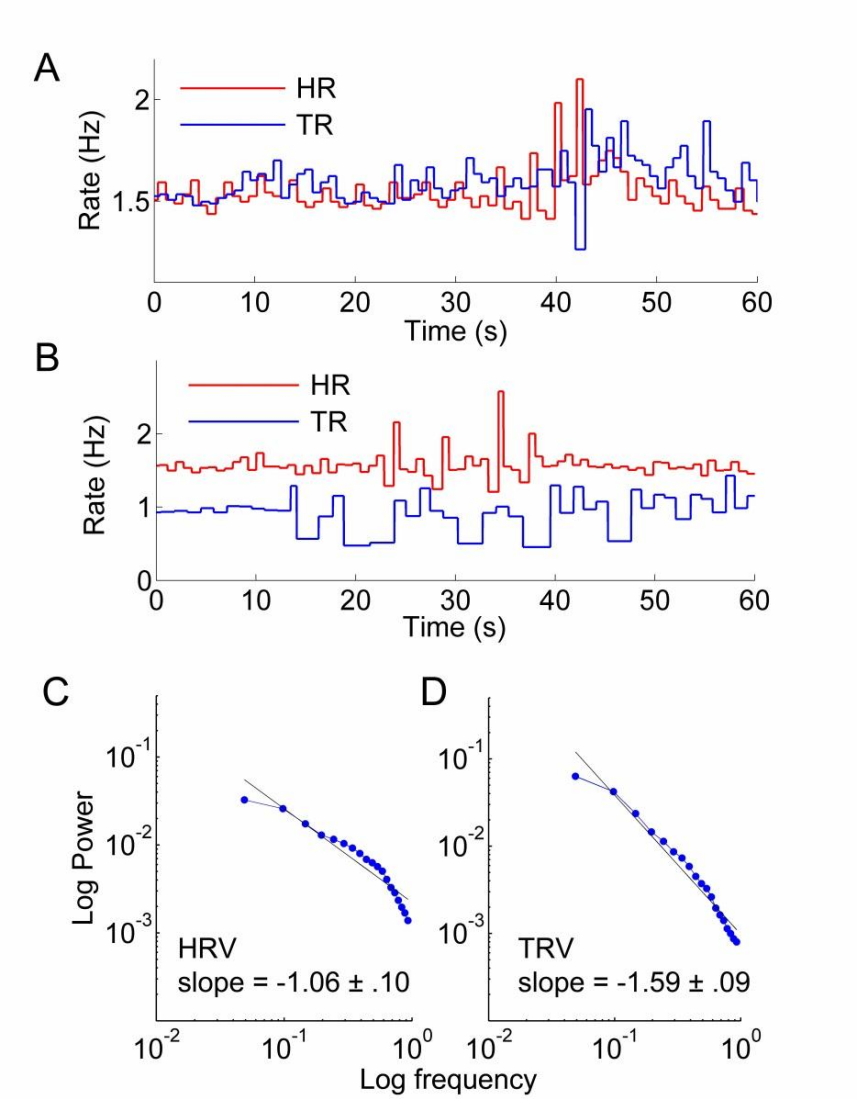

Figure 4-3. Fractal analysis of heart rate (HRV) and throbbing rate variability (TRV) shows that the two rhythms observe distinct power laws. Representative instantaneous heart rate and throbbing rate series are shown in (A) and (B) from the same subjects in Figure 4-2A and 4-2B. The instantaneous rate was determined by 1/interval between adjacent two events (see Methods). The log-log plots of averaged power spectra of the instantaneous rate series are shown in (C) for heart rate and in (D) for throbbing rate. The black line is the best linear fit. The spectral scaling exponents, defined by the respective slopes (HRV 1.06 ± 0.10; TRV 1.59 ± 0.09), are significantly different (Student's paired t-test $p<0.0001$).

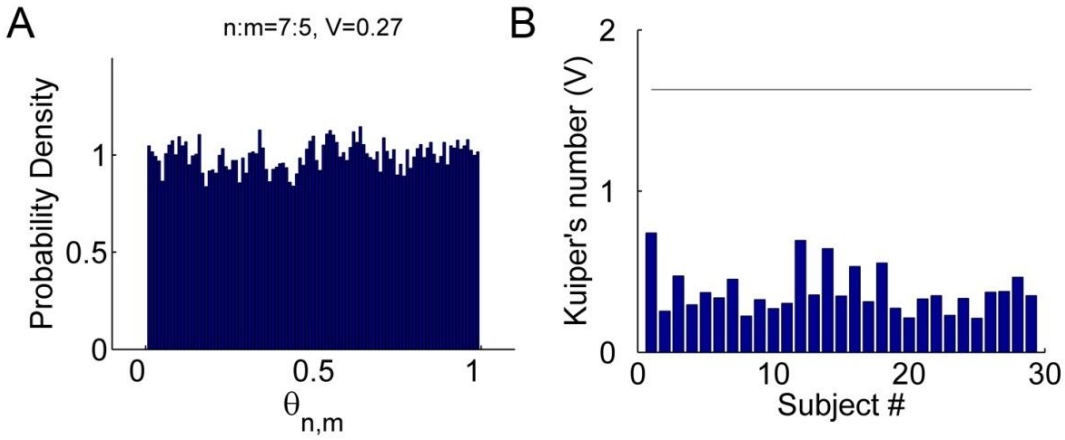

Figure 4-4. An analysis of synchrony between arterial pulse and throbbing rhythm shows no relationship. (A) The distribution of the relative phase in the record from a single subject is approximately uniform, indicating a lack of synchrony. (B) Using a quantitative measure of the uniformity of distribution, the Kuiper's statistic V is below the level of significance for all subjects ($p>0.1$), where the horizontal line signifies $V=1.62$ ($p=0.1$), a minimal threshold for a non-uniform distribution.

Table 4-1. Pain descriptors used to identify pain qualities

Descriptor Number	Pain quality
1	Aching*
2	Heavy
3	Squeezing
4	Sharp
5	Stabbing
6	Shooting
7	Electric shock
8	Throbbing, pulsing*
9	Jack-hammering
10	Exploding
11	Hot/Burning
12	Cold/Freezing
13	Tingling or “Pins and Needles”
14	Itching
15	Numbness
16	Tender*
17	Pain caused by light touch
18	Tiring/Exhausting
19	Sickening
20	Fearful
21	Punishing/Cruel

Descriptors marked with asterisk (*) are those found to be most prominent in this study.

A B

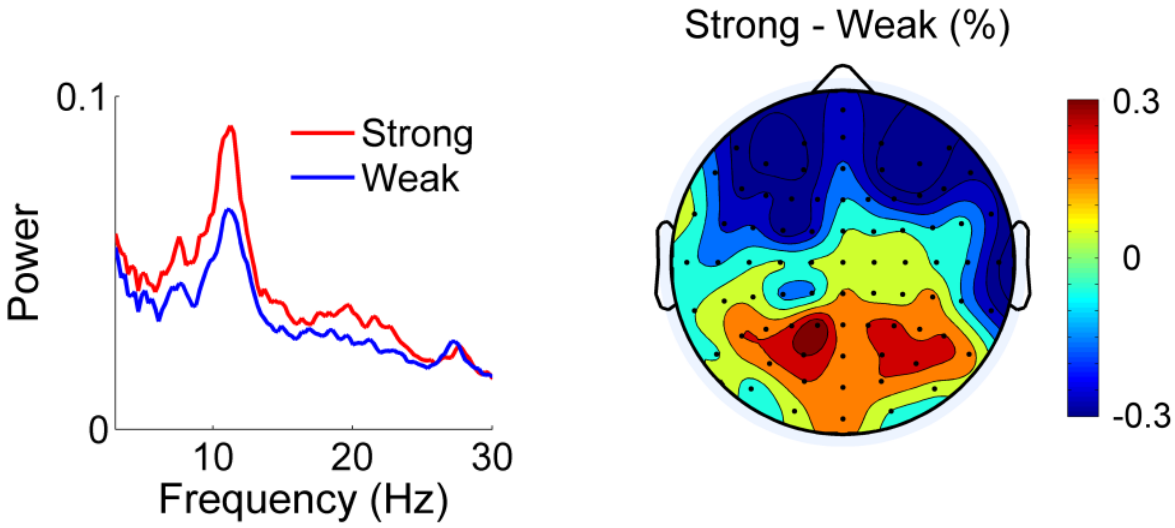

Figure 4-5. Spontaneous alpha power (power between 8-12Hz) is modulated by the intensity of the throbbing sensation. (A) Power spectra from one of the parietal-occipital channel. (B) Topography of the percentage change in alpha power, in which each channel is calculated by $(A_{strong}- A_{weak})/A_{weak,}$ A stands for alpha power.

A

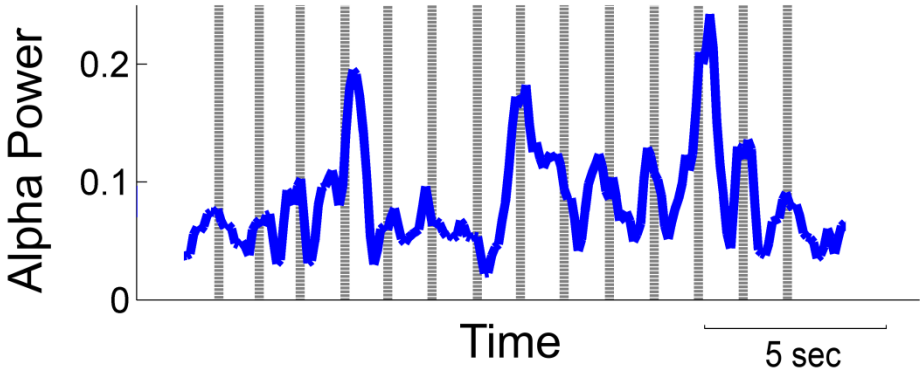

B

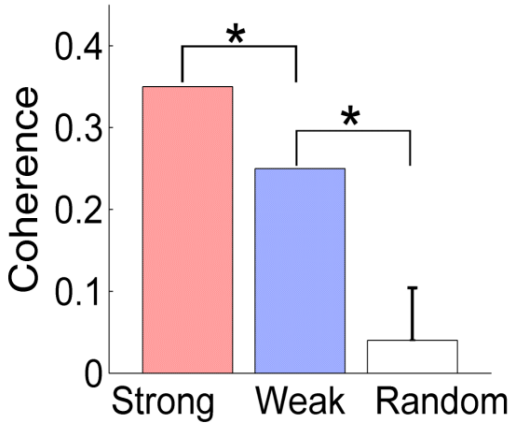

C

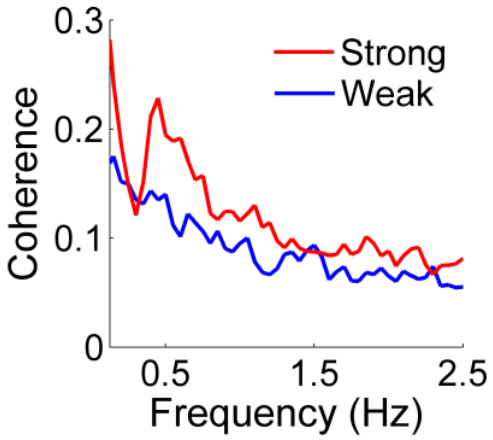

Figure 4-6. The point process of reported throbbing onset (vertical dash line) is plotted over alpha power time series from parietal-occipital channel during (A) the strong throbbing session. (B)The throbbing movement is more synchronized with the alpha power from parietal-occipital in the strong throbbing session than the weak throbbing session, though in the synchrony is significant under either condition ($p < 0.05$ under random permutation). (C) Coherence of amplitude envelop of alpha oscillation was calculated between pairwise posterior channels, and then averaged. The temporal dynamic of alpha powers is more synchrony when stronger throbbing sensation was reported. The difference between two conditions is significant under paired t-test across channels ($p<0.01$).

CHAPTER 5
EXPLORING RESTING-STATE FUNCTIONAL CONNECTIVITY WITH TOTAL INTERDEPENDENCE

5.1 Introduction

The brain is comprised of many anatomically and functionally distinct networks. These networks are spontaneously active even in the absence of sensory input or motor output (Biswal et al., 1995; Fox and Raichle 2007; Kenet et al. 2003; Raichle and Mintun 2006). Progress over the past 15 years has firmly established that functional magnetic resonance imaging (fMRI) data recorded during rest is an important tool to reveal the spatial organization and temporal dynamics of these networks (Lowe et al. 2000; Yan et al. 2009; van den Heuvel and Hulshoff Pol 2010). When two distinct brain regions are said to belong to the same functional network the main criterion is that the intrinsic blood oxygen level dependence (BOLD) fluctuations from the two regions significantly co-vary with one another (Dosenbach et al., 2007; Fox et al., 2006). Remarkably, functional networks identified in such a statistical manner match the brain networks activated by various cognitive tasks (Biswal et al., 1995; Fox, et al., 2006), correlate with behavior during development and aging (Beason-Held et al., 2009; Church et al., 2009; Jolles et al. 2011; Kelly et al., 2009), and predict brain pathology (He B.J. et al., 2007a; He Y. et al., 2007b; Lynall et al., 2010; Supekar et al., 2008).

There are two classes of methods for mapping resting-state functional brain networks: independent component analysis (ICA) (Beckmann et al., 2005; Damoiseaux et al., 2006) and seed-based correlation analysis (Biswal et al., 1995; Fox et al., 2005). Whereas ICA has the advantage of being model-free and entirely data-driven, seed-based correlation is more convenient for examining the connectivity between a given region of interest and the rest of the brain. Statistically, both methods exploit the contemporaneous covariation structures in the data. Among time series models, such characterization is only sufficient for the white noise process,

which, by definition, may only exhibit contemporaneous correlations. It is well-established that resting-state fMRI are not white noise; they are time series exhibiting rich temporal patterns such as rhythmic activities in the low frequencies (Chang and Glover, 2010). Physiological factors that can contribute to temporal relations across scans include intrinsic temporal structures in neuronal signals such as local field potentials, neuronal transmission delays (Nishitani and Hari, 2002; Schmolesky et al., 1998; Van Essen et al., 1992), and variable latency in the hemodynamic response function (Handwerker et al., 2004). How much temporal dependence between BOLD signals was ignored by the prevailing statistical approaches? To what extent the ignored temporal structure may have contributed to our understanding of cognitive brain networks? These questions remain to be answered. In addition, the ignored temporal dependence may help explain the discrepancy between spatial structures identified by resting-state analysis and that by task activation.

In Chapter 5, we introduce a novel method called total interdependence (TI) to measure the overall temporal relationship between two resting-state fMRI time series. Although this measure has been considered in past neurophysiological (Rajagovindan and Ding 2008; de Pasquale et al., 2010) and task-state fMRI studies (Roebroeck et al., 2005), it has not been applied to resting-state fMRI data. The mathematical theory behind the method was first developed by Gelfand and Yaglom in the context of assessing mutual information between two Gaussian stochastic processes (Gelfand and Yaglom, 1959). Geweke (1982) further showed that for two time series this quantity is the sum of three possible contributors towards their overall temporal interdependence: the influence the first time series exerts upon the second, the influence the second time series exerts upon the first, and co-varying common input (Rajagovindan and Ding, 2008). This observation forms the basis of the term total interdependence. In this work,

analyzing resting-state fMRI data, we compared the performance of TI to that of the conventional cross correlation (CC) method. In addition, task-state fMRI data recorded immediately following the resting-state period in the same scanning session were used to further validate the TI method, and to establish the functional significance of the resting-state networks identified by TI.

5.2 Methods

5.2.1 Experimental Design and Data Acquisition

Twelve healthy subjects gave informed consent and participated in the study. The experimental protocol was approved by the Institutional Review Board of Beijing Normal University. Both resting-state data and task-state data were recorded in the same scanning session. During resting-state recording, the subject was instructed to relax with their eyes closed for 10 minutes. After a 5 minute break, the subject performed a trial-by-trial cued visual spatial attention task (Wen et al., in press). There were 12 attention blocks (A blocks) and 12 passive view blocks (B blocks). Each attention block lasted 1 minute. The passive view block was of the same duration in which the same stimuli as the attention block were presented but no attention was required. There were 15 trials in each attention block. Each trial started with a cue directing the subject's covert attention to either the left or the right visual field. Imperative stimuli were presented following a delay period. The subjects were instructed to respond to the target stimuli in the attended hemifield (Rajagovindan and Ding, 2011; Wen et al., in press) by pushing a button with their right hand. Fixation was maintained toward the center of the presentation screen throughout the experiment. Attention blocks and passive view blocks were divided into 6 runs with each run containing 4 blocks organized in an ABBA and a BAAB fashion across runs. Brain activations and deactivations obtained by contrasting attention blocks against passive view blocks provide regions of interest to be used to initiate and validate the resting-state analysis.

Functional MRI data were recorded on a 3-Tesla Siemens whole-body MRI system at the Beijing Normal University MRI center using a T2*-weighed echoplanar imaging (EPI) sequence (echo time (TE), 30ms; repetition time (TR), 2000ms). Each whole-brain volume consisted of 33 axial slices (field of view, 200 mm; matrix, 64×64; slice thickness, 3.60mm, flip Angle=90°, voxel size=3.13×3.13×3.60mm). For high-resolution anatomic images a T1-weighted 128-slice MPRAGE sequence was used (TR, 2530 ms; TE, 3.39 ms; flip angle, 7°; inversion time, 1100 ms voxel size=1 ×1.33 ×1mm).

5.2.2 Definition of Seed Regions

Both cross correlation (CC) and total interdependence (TI) are seed-based methods. We combined task-state data and resting-state data to define seed regions. For task-state data, the first 5 time points (10 seconds) of each run were discarded to eliminate transient effects, and the remaining data were preprocessed using SPM2 (http://www.fil.ion.ucl.ac.uk/spm/). Preprocessing steps included slice timing, motion correction, coregistration to individual anatomical image, normalization to the Montreal Neurological Institute (MNI) template (Friston et al., 1995), and re-sampling of the functional images into a 3×3×3 mm^3 per voxel resolution. Normalized images were spatial-smoothed using an 8mm FWHM (Full Width at Half Maximum) Gaussian core. Global scaling was then applied to remove the global signal before GLM analysis. We note that although the removal of global signal is a debated issue (Zarahn et al. 1997; Aguirre et a., 1998; Glover et al., 2000; Gavrilescu et al., 2002; Junghöfer et al., 2005; Macey et al. 2004; Wise et al., 2004; Birn et al. 2006; Lund et al., 2006; Fox et al., 2009), for our data, global scaling appeared to give more precisely defined regions of task activation, which was crucial for providing a template to compare with resting-state data. In the random-effects analysis, for each subject, from the fitted GLM model, the attend condition and the passive view condition were compared to produce the contrast image. These contrast images were fed into a

GLM that implemented a one-sample t-test to yield group-level activation regions ($t>5.20$, FDR corrected, $p<0.002$) and deactivation regions ($t<-5.20$, FDR corrected, $p<0.002$). Among regions activated by the attention task, we selected bilateral intraparietal sulcus (IPS) and bilateral frontal eyefield (FEF*)* of the dorsal attention network (DAN) (Corbetta and Shulman 2002; Corbetta et al., 2008), and dorsal anterior cingulate cortex (dACC) and bilateral anterior insular cortex (AI) of the task control network (TCN) (Dosenbach et al., 2006), to aid and to validate the resting-state analysis. Voxels with local maximum t-values in these regions were chosen as the seed voxels. Their coordinates were given in Table 5-1.

The resting-state time series was preprocessed using similar steps and filtered between 0.01-0.1Hz with a zero-phase bandpass FIR filter (Fox et al., 2006; Lowe et al. 2000). Because the regions deactivated by the attention task are rather diffuse, to more precisely define the default mode network, an ICA analysis was applied where the resting-state time series from all subjects were concatenated for each voxel. Twenty five aggregate independent components (ICs) were identified using the GIFT toolbox (http://icatb.sourceforge.net/) where the number of components was determined by the Minimum Description Length (MDL) criterion provided by the toolbox. All aggregate ICs were visually inspected, and the IC representing the default mode network (DMN) was selected (Buckner et al., 2008). Among the DMN regions, we selected the posterior cingulate cortex (PCC), the medial prefrontal cortex (mPFC), and the bilateral inferior parietal lobe (IPL) for the resting-state analysis. The seed voxel in each region was chosen to be the voxel that attained the local maximum t-value in the group ICA map ($t>4.75$, FDR corrected, $p<0.005$). The coordinates of these voxels were given in Table 5-2. Importantly, seed voxels identified in this manner also fell in the task-deactivated regions, and the DMN network identified with ICA exhibited substantial overlap with the task-deactivation map.

5.2.3 Cross Correlation and Total Interdependence

We compared two connectivity methods: cross correlation (CC) (Fox et al., 2005) and total interdependence (TI). For a pair of simultaneously acquired time series: (x_1,y_1), (x_2,y_2), (x_3,y_3),…(x_n,y_n), CC was computed according to

$$CC_{x,y} = (\sum_{i=1}^{n} x_i y_i) / \sqrt{(\sum_{i=1}^{n} x_i x_i)} \sqrt{(\sum_{i=1}^{n} y_i y_i)} \,. \quad (5\text{-}1)$$

From the definition, it is clear that CC only measures the contemporaneous (zero-lag) linear relationship between x time series and y time series, and does not account for the possible relations existing across different lags (e.g. between x_i and y_{i+2}). In contrast, TI, as defined by Gelfand and Yaglom (1959), was computed according to:

$$TI_{x,y} = -\frac{1}{2\pi} \int_{-\pi}^{\pi} \ln(1 - C_{xy}{}^2(\lambda)) d\lambda \,, \quad (5\text{-}2)$$

where $C_{xy}(\lambda)$ is the coherence between the two random processes, *x* and *y*, at frequency $f = \lambda / 2\pi$. For two Gaussian processes this formula was shown to measure the total amount of mutual information between them. Geweke (1982) further demonstrated that TI captures the total linear relationship between x and y time series. Numerically, for a given sampling frequency f_s, Eq. 5-2 can be recast into an implementable form:

$$TI_{x,y} = -\frac{2}{f_s} \sum_{i=1}^{N-1} \ln(1 - C_{xy}{}^2(i\Delta f)) \Delta f \,, \quad (5\text{-}3)$$

where $\Delta f = \frac{f_s}{2(N-1)}$ is the frequency resolution and *N* is the number of desired frequency points in the interval between 0 and the Nyquist frequency $f_s / 2$.

In this study CC was calculated directly from data using standard procedures. TI was estimated by fitting bivariate autoregressive (AR) models to pairs of BOLD signals (Bressler and Seth, 2011; Ding et al., 2000; 2006). Coherence was derived from the model coefficients and integrated over frequency according to Eq. 5-3. Applying Akaike information criterion (AIC)

and Lagrange multiplier whiteness test (Lütkepohl, 2005) the optimal model order was determined to be 2.

5.2.4 Functional Connectivity Maps

For a given seed region X, the CC values with respect to the rest of the brain were normalized by Fisher's transformation for each subject before group analysis. The TI values were z-transformed for each subject according to, $t_i = (TI_i\text{-mean}(\{TI_i\}))/\text{std}(\{TI_i\}))$, where TI_i is the value of TI between the seed voxel and the ith voxel, and $\{TI_i\}$ denotes the collection of such values from all voxels. For both CC and TI, group level one-sample t-test was applied to yield the X-seeded CC map and the X-seeded TI map.

5.2.5 Comparison of Methods

Several tests were performed to compare the performance of TI and CC. First, for a pair of time series: (x_1,y_1), (x_2,y_2), $(x_3,y_3),\ldots(x_n,y_n)$, we randomly but synchronously shuffled the time indices to generate a pair of surrogate time series, (x_{k1},y_{k1}), (x_{k2},y_{k2}), $(x_{k3}, y_{k3}),\ldots(x_{kn},y_{kn})$, where $(k1, k2, k3\ldots, kn)$ were a random permutation of $(1,2,3,\ldots n)$. CC would remain the same for the shuffled time series according to Eq. 5-1. TI, however, would be reduced because the shuffling procedure destroyed the temporal relations across lags. By computing the percentage reduction of TI, we can demonstrate intuitively and quantitatively the degree of total interdependence between the two time series that is not captured by CC. For this test, time series from voxels in a spherical region of 5 mm in diameter surrounding the seed voxel of a region of interest were extracted to represent that region of interest. Between two regions of interest we considered all pairwise combinations of voxels within two similarly constructed spheres. For each pair of time series, random shuffling was carried out 50 times, and the 50 values of TI were averaged and compared with the TI from the original time series to calculate percentage reduction.

Second, the spatial patterns of CC and TI maps were compared. To assess the functional significance of these patterns, we further compared them with well-established network models. Two quantities were used for these comparisons: spatial correlation and spatial overlap. For a given brain, we generated a binary version of the map by assigning to its suprathreshold voxels the value of 1 and other voxels the value of 0, and treated the binary map as a vector in a space whose dimension equals to the total number of voxels. Spatial correlation between two maps is the normalized dot-product of the two corresponding vectors. Spatial overlap was used to compare the similarity between CC and TI maps in a given brain region. Letting $\{V_{CC}\}$ denote the collection of the suprathreshold voxels (t>5.20) in the CC map and $\{V_{TI}\}$ the collection of suprathreshold voxels (t>5.20) in the TI map, and letting $|\{x\}|$ denote the number of elements in the set $\{x\}$, the spatial overlap between the two maps for the region is $\left|\{V_{CC}\}\cap\{V_{TI}\}\right| / \left|\{V_{CC}\}\cup\{V_{TI}\}\right| \times 100\%$.

Third, for visualization purposes, brain maps were projected onto a 3-dimensional brain template from the MRIcroN software package (http://www.cabiatl.com/mricro), as well as onto a flattened 3-dimensional brain surface template from the CARET software packages (http://brainmap.wustl.edu/caret.html).

Fourth, receiver operator characteristic (ROC) curve was applied to compare the statistical sensitivity of CC and TI in deciding the network membership of predefined voxels. The ROC curve is a graphical plot of true positive rate (TPR) against false positive rate (FPR) of making a binary decision when the discrimination threshold is varied (Lasko et al., 2005). For the dACC-seeded map, suprathreshold voxels in AI, or $\{AI_{t>thres}\}$, known from prior work as part of TCN (Dosenbach et al., 2006; Seeley et al., 2007), were defined as true positive detections, whereas suprathreshold voxels in FEF, $\{FEF_{t>thres}\}$, known from prior work as part of DAN (Corbetta and

Shulman, 2002; Corbetta et a al., 2008), were defined as false positive detections. TPR and FPR were computed according to $TPR = |\{AI_{t>thres}\}| / |\{AI\}|$ and $FPR = |\{FEF_{t>thres}\}| / |\{FEF\}|$. Here $\{AI\}$ and $\{FEF\}$ were predefined according to the task activation map (t>5.20, FDR corrected, p<0.002). Similarly, for the rIPS-seeded maps, $\{FEF_{t>thres}\}$ were defined as true positive detections, and $\{AI_{t>thres}\}$ as false positive detections. The ROC curve was constructed by plotting $TPR = |\{FEF_{t>thres}\}| / |\{FEF\}|$ versus $FPR = |\{AI_{t>thres}\}| / |\{AI\}|$ as threshold was varied. Between CC and TI, if the ROC curve for one measure is more biased toward the TPR axis, this measure is said to perform better in discriminating between the true and false populations. The diagonal line on the TPR-FPR plane is equivalent to random guesses.

Fifth, a clustering analysis was applied to maps generated from 7 seed regions, including dACC, bilateral AIs, bilateral FEF, and bilateral IPS. The purpose was to examine whether TCN and DAN, two functional networks known to be comprised of these regions, could be correctly segregated by CC and TI. Each map, generated by either CC or TI, was treated as a vector in a high dimensional feature space (Cohen et al., 2008). The Euclidean distance between two feature vectors was calculated to determine the similarity of the two spatial maps. If two regions belonged to the same functional network, the connectivity maps seeded in these two regions should be more similar (shorter Euclidean distance) than the connectivity maps generated by two seed regions belonging to different functional networks (longer Euclidean distance). K-means algorithm (k=2) (MacQueen, 1967) was used to segregate feature vectors. Similar approach has been applied in previous functional mapping studies (Fox et al., 2006).

5.3 Results

5.3.1 Random Permutation and Total Interdependence

We start by assessing the degree of temporal relationship between two BOLD signals that is not captured by cross correlation (CC). Resting-state recordings from a typical voxel in the dorsal anterior cingulate cortex (dACC) and a typical voxel in the right anterior insula (rAI) were displayed in Figure 5-1A. Surrogate data, created by randomly but synchronously shuffling the time indices of both time series, were shown in Figure 1B. Despite the qualitative difference in appearance between the original data and the shuffled data, CC was not changed (see Eq. (1)), equaling to r=0.63 for both cases. However, total interdependence (TI) was reduced from 0.64 (Figure 5-1A) to 0.51 (Figure 5-1B), a reduction of (0.51-0.64)/0.64=-20%. This percentage change reflected the amount of temporal relationship occurring across non-zero lags that were unaccounted for by CC. In Figure 5-2, for select pairs of regions in the default mode network, the percentage change averaged across subjects was -4% for PCC-PCC (posterior cingulate cortex), -9% for PCC-mPFC (medial prefrontal cortex), -14% for PCC-lIPL (left inferior parietal lobe), and -28% for PCC-rIPL (right inferior parietal lobe). For select pairs of regions in the task control network, the percentage change averaged across subjects was -6% for dACC-dACC, -19% for dACC-rAI, and -22% for dACC-lAI (left anterior insula).

5.3.2 Default Mode Network

The connectivity between the seed voxel in PCC and all other voxels in the brain was evaluated using CC and TI. Figure 5-3 showed the resultant maps after taking $t>5.20$ (FDR corrected, $p<0.002$) as the threshold for both measures; voxels that were in anti-phase relationship with the seed voxel were excluded. Both CC and TI maps resembled the known spatial structure of the DMN, and the spatial correlation between the two maps was 0.83, indicating that they were similar. Closer examination of Figure 5-3 revealed that CC and TI maps

overlapped differently in different DMN regions. For PCC, mPFC, and lIPL, where the two maps were more similar, the spatial overlap between the two maps, which was the ratio between the number of overlapping voxels and the number of voxels in the union of CC and TI maps, was 77% for PCC, 65% for mPFC, and 35% for lIPL. For rIPL, where the two maps were least similar, the spatial overlap was 20%. These findings were in agreement with Figure 5-2, which showed that for PCC-PCC, PCC-mPFC, and PCC-lIPL, the temporal relationship that was not captured by CC was relatively small, at -4%, -9%, and -14%, respectively, whereas for PCC-rIPL, the amount of temporal relationship missed by CC was larger, at -28%.

5.3.3 Task Control Network

The connectivity between the seed voxel in dACC and all other voxels in the brain was evaluated using CC and TI. The CC map in Figure 5-4 ($t=5.20$, FDR corrected, $p<0.002$) included dACC and bilateral AIs, the three established regions of TCN (Dosenbach et al., 2006), as well as right frontal eyefield (rFEF) and right middle frontal gyrus (rMFG), two areas of the frontal-parietal attention system (Corbetta and Shulman, 2002; Corbetta et al., 2008). In contrast, using the same threshold, the TI map included only dACC and bilateral AIs, suggesting that TI was able to identify TCN more precisely, without having to contend with the intrusion from areas belonging to other networks. The spatial correlation between the CC map and the TI map was 0.48, suggesting that relative to DMN where the spatial correlation between CC and TI maps was 0.83, the two maps for TCN were more discrepant.

The dACC-seeded CC and TI maps were examined further by comparing them with the task-defined TCN (Figure 5-5A). By not selecting an *a priori* threshold, dACC-seeded maps in the right hemisphere were represented as color-coded t-values ($t>0$) in Figures 5-5B and 5-5C. For TI (Figure 5-5C), the three regions of the TCN network were clearly delineated with sharp and clearly defined boundaries, whereas for CC (Figure 6-5B), dACC and AI clusters were more

diffuse and the map included other regions not belonging to TCN, including FEF, MFG, intraparietal sulcus (IPS), and temporal parietal junction (TPJ). Similar effects were found in the left hemisphere. In Figure 5-5D, the spatial correlation between the task-defined TCN and the dACC-seeded TI and CC maps revealed that over a broad range of threshold values, the TI map has larger overlap with the task-defined TCN than the CC map. The number of suprathreshold voxels in TI and CC maps that did not belong to the task-defined TCN, plotted as a function of threshold in Figure 5-5E, demonstrated that the TI contained fewer false-positive detections than CC.

5.3.4 ROC Analysis of Statistical Sensitivity

The statistical sensitivity of TI and CC was tested using the receiver operator characteristic (ROC) curve method. Between two measures, the measure whose ROC curve is more biased toward the true positive rate (TPR) axis is said to perform better in discriminating between a true and a false population. For dACC-seeded maps, voxels in task-activated AI formed the true population, and voxels in task-activated FEF formed the false population. In contrast, for rIPS-seeded maps, true and false populations were reversed. The ROC curves obtained from TI for both cases indicated that it exhibited superior statistical sensitivity in correctly deciding the network membership of predefined voxels.

5.3.5 Clustering Analysis

Past work has used resting-state connectivity maps as feature vectors to divide brain regions into distinct functional networks through clustering analysis (Church et al., 2009; Hlinka et al., 2011). As shown in Figure 5-7A, for TI, the dACC-seeded spatial map and bilateral AI-seeded spatial maps were clustered together to form one network, in agreement with prior knowledge that these areas belong to TCN (Dosenbach et al., 2006). Bilateral FEF-seeded and bilateral IPS-seeded maps, on the other hand, were clustered together to form another network,

again in agreement with prior knowledge that these areas belong to DAN (Corbetta and Shulman 2002; Seeley et al., 2007). In contrast, for CC (Figure 5-7B), bilateral FEF-seeded, dACC-seeded and bilateral AI-seeded maps were incorrectly clustered together to form one network, and the bilateral IPS-seeded maps were clustered together to form another.

5.4 Discussion

Prevailing methods for resting-state functional connectivity analysis do not take into account the time series structure in resting-state fMRI data. We propose to address this problem by introducing a method called total interdependence (TI). It was shown that, when combined with a random permutation approach, TI can reveal the degree of temporal dependence between BOLD signals that were not captured by the traditional zero-lag cross correlation (CC) method. Functionally, TI was able to more precisely identify the three constituent regions of the task control network, which were further validated by the task-state data recorded during the same experiment. Finally, we showed that TI performed better in a clustering analysis of network segregation and exhibited superior statistical sensitivity.

5.4.1 Measures of Temporal Relationship

Seed-based connectivity analysis can reveal brain regions whose activities co-vary with that of the seed region. Such covariations have been taken to indicate shared functionality and are the basis for defining functional networks (Biswal et al., 1995; Buckner et al., 2008; Fox et al., 2006; Vincent et al., 2007). Which statistical measure is chosen to perform functional connectivity mapping, however, could significantly influence the outcome. Zero-lag cross correlation coefficient, by far the most widely practiced, is a linear method and does not take into account the temporal dependence beyond the contemporaneously acquired data points. Past work has pointed out its weaknesses (Garofalo et al., 2009). A recent study by Hlinka et al. (2011) adopted mutual information to measure both linear and nonlinear portions of the interaction

between fMRI time series. They found that the nonlinear portion is negligible for the reason that fMRI time series are well-approximated by Gaussian stationary processes. Recognizing the presence of temporal relationship across different scans, Curtis et al. (2005) introduced spectral coherence to measure functional connectivity between different brain regions, disclosing modulated frontal-parietal interactions in a working memory task. To what extent the temporal relationship across different scans may impact resting-state connectivity analysis remains to be clarified. This is the main objective of the present study.

Our starting point is the introduction of total interdependence in Eq. 5-2. Although TI is defined in terms of spectral coherence, the formula in Eq. 5-2 allows it to be interpreted as the total amount of mutual information between two Gaussian stationary processes (Gelfand and Yaglom 1959). Geweke (1982) further demonstrated that the quantity in Eq. 5-2 can be decomposed into 3 components, namely,

$$TI_{x,y} = F_{x\to y} + F_{y\to x} + F_{xy}, \tag{5-4}$$

where $F_{x\to y}$ is the causal influence from x to y, $F_{y\to x}$ is the causal influence from y to x, and F_{xy} is the instantaneous causality between x and y, reflecting possible common input (Brovelli et al., 2004; Ding et al., 2006; Goebel et al., 2003; Granger, 1967; Jiao et al., 2011; Rajagovindan and Ding, 2011; Roebrock et al., 2005). In light of the fact that these three components represent the only ways two time series can interact with one another, we thus term the quantity in Eq. 5-2 total interdependence.

5.4.2 Temporal Structures in Resting-State fMRI Data

A bivariate white noise process, whose power spectra are flat, exhibits only contemporaneous correlation. CC captures the entire temporal dependence for such processes. However, neurobiological time series, including BOLD signals, are usually not white noise

processes. Being able to assess the amount of temporal relationship missed by CC is thus a key step towards understanding its limitations. We proposed to accomplish this by randomly but synchronously shuffling the time indices of two fMRI time series and comparing TI before and after this randomization. The result showed that CC stayed unchanged while TI was reduced after temporal order randomization. Because for white noise there should be no reduction in TI, the percentage of the reduction following the temporal randomization procedure can thus be viewed as the amount of temporal relationship not captured by CC.

For the voxel pairs in the default mode network (DMN), the amount of uncaptured temporal relationship varied from quite substantial (PCC-rIPL at 28%) to less substantial (PCC-PCC at 4%, PCC-lIPL at 9%, and PCC-mPFC at 14%); see Figure 5-2. In agreement with this, the PCC-seeded CC map and TI map were more overlapped in PCC, mPFC, and lIPL, but less overlapped around rIPL; see Figure 5-3. Past work has shown that DMN is functionally more lateralized to the left hemisphere (Buckner et al., 2008, 2009). This means that PCC-rIPL may not be as strongly coupled as PCC-lIPL. The CC approach, measuring only part of the total interdependence, may work even less effectively in this case when connectivity is relatively weak to begin with. For the voxel pairs in the task control network (TCN), similar patterns of TI reduction were observed, as seen in Figure 5-2.

Physiologically, besides temporal correlations inherent in various rhythmic neural activities, neural transmission and processing delays (Nishitani and Hari, 2002; Schmolesky et al. 1998; Van Essen et al., 1992) between different nodes of a large-scale network, and variations in the hemodynamic response functions (Aguirre et al., 1998; Handwerker et al., 2004; Kruggel and von Cramon, 1999) are other contributing factors to the presence of temporal dependence beyond the zero-lag. Our observation that uncaptured temporal dependence by CC is more

substantial for voxel pairs between far-separated regions than for voxel pairs within a region can be seen as a manifestation of these factors. On the other hand, while TI is reduced for dACC-dACC and PCC-PCC following random shuffling, the reduction is much less severe relative to that of interregional TI, indicating that the temporal relationship between functionally similar voxels in the same brain region is dominated by contemporaneous dependence.

5.4.3 Functional Significance of TI

As shown in Figure 5-2, the degree of temporal relationship not captured by CC can vary from ROI pair to ROI pair, and from network to network, causing differences in spatial maps established by CC and TI. How to evaluate the functional significance of these differences? We addressed this by combining task-state data with resting-state data and by focusing on the three core regions in the task control network. Temporal randomization test revealed that for dACC-rAI and dACC-lAI, about 20% of the temporal relationship was not captured by CC. The dACC-seeded CC map included FEF, an area of the dorsal attention network, in addition to more diffusely defined dACC and bilateral AIs, members of the task control network. In contrast, the dACC-seeded TI map was free from the confounding influences from other networks and contained sharply-defined dACC and bilateral AIs, which were further shown to be highly consistent with the three core regions defined by our attention task; see Figures 5-4 and 5-5.

Functional imaging studies have firmly established the role of dACC and bilateral AI in exerting control over behavioral performance at the task level in a variety of experimental contexts (Botvinick et al., 2004; Dosenbach et al., 2006; Kerns et al., 2004; Nelson et al., 2010; Sridharan et al., 2008). Resting-state connectivity analysis based on cross correlation, however, has to date often not been able to unequivocally establish dACC and bilateral AI as forming a distinct resting-state functional network (Seeley et al., 2007). The consistent inclusion of areas such as FEF and lateral prefrontal regions in CC maps has led to the debate of whether these

additional areas should be considered part of the task control network (Church et al., 2009; Dosenbach et al., 2006; Fox et al., 2005; 2006; Mennes et al., 2010; MacDonald et al., 2000). Whereas independent component analysis (ICA) can sometimes identify the three core regions of TCN, it is often the case that the ICA components containing this network often contain additional regions such as dorsal lateral prefrontal cortex, anterior frontal lobe, supplementary motor areas, or temporal lobe (Beckmann et al., 2005; De Luca et al. 2006). There were even reports where dACC is missing from the ICA component (Damoiseaux et al. 2006; 2008). In light of the foregoing, TI, with its ability to clearly establish dACC and bilateral AI as forming a distinct functional network at rest, provides results more in line with task-based imaging studies, and thus represents an improvement over previous methods.

Analogous to the task control network, the FEF-seeded map constructed with CC (not shown) always includes dACC and AI regions (Fox et al., 2006), in addition to the other dorsal attention network areas. This is again inconsistent with the task-based imaging studies where the different functional roles played by the two networks have been carefully delineated. The application of connectivity measures such as TI, which takes into consideration of the overall temporal interdependence between BOLD signals, can help resolve these inconsistencies. Although by applying a more stringent threshold CC can generate maps that better resemble the TCN activation map the match remains not as precise as the TI map. Figures 5-5D and 5-5E address this point. Over a broad range of threshold values the spatial correlation between the CC map and the task-defined TCN is lower than that between the TI map and the task-defined TCN. As the threshold increases, the regions included in the CC map begin to shrink rapidly, whereas the regions included in the TI map stay relatively constant. The ROC curve analysis and the

clustering analysis (Figures 5-6 and 5-7) further demonstrate TI as exhibiting better statistical characteristics than CC.

5.4.4 Estimation of TI

TI is defined in terms of spectral coherence (Eq. 5-2). There are two ways to compute spectral coherence from time series data: nonparametric Fourier-based methods and parametric AR-based methods. For long and relatively noise-free time series, Fourier based spectral analysis and AR-based spectral analysis produce similar results (Dhamala et al., 2008). Functional fMRI data, whether recorded during resting-state or during task-state, are often short and noisy. Nonparametric spectral analysis is not optimal for this type of data. Parametric spectral analysis based on AR model fitting is known to be more robust and can provide smooth and accurate spectral estimates (Ding et al., 2000; Jiao et al., 2011; Wen et al., in press). This is the reason behind our adoption of the parametric AR method to assess the performance of TI. It should be note that filtering can impact the value of TI. In this study resting-state fMRI data were band-pass filtered between 0.01-0.1 Hz (Lowe et al., 2000; Fox et al., 2005, 2006). This commonly applied filter allowed us to compare our results with the results of other resting-state studies.

A

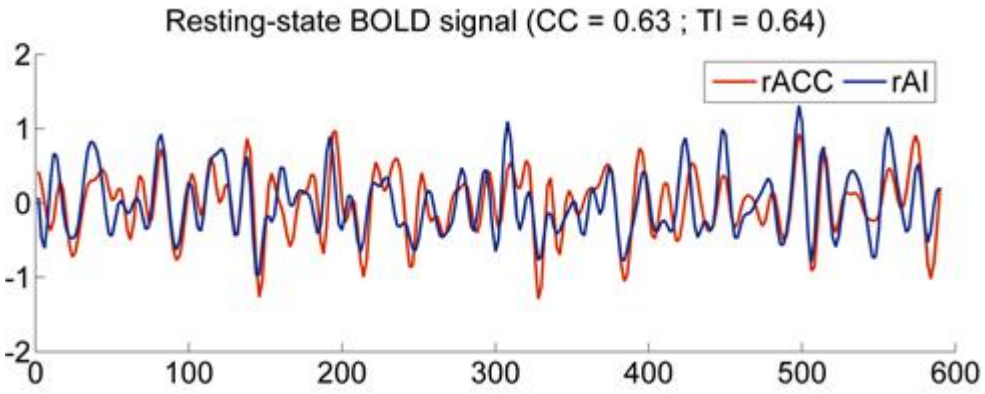

B

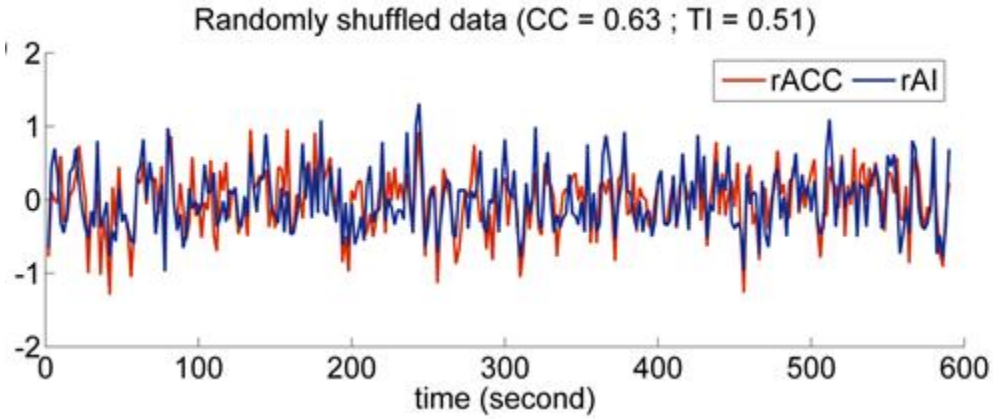

Figure 5-1. Original and randomly shuffled BOLD signals. A: Resting-state fMRI data from dorsal anterior cingulate cortex (dACC) and right anterior insula cortex (rAI). Bandpass filtering between 0.01 and 0.1 Hz was applied. B: Surrogate data where the time indices for the two BOLD signals in Figure 5-1A were randomly but synchronously shuffled. Cross correlation (CC) remained the same for both Figure 5-1A and 5-1B. The reduction in total interdependence (TI) was indicative of the amount of temporal relationship between the two signals in Figure 1A not captured by CC.

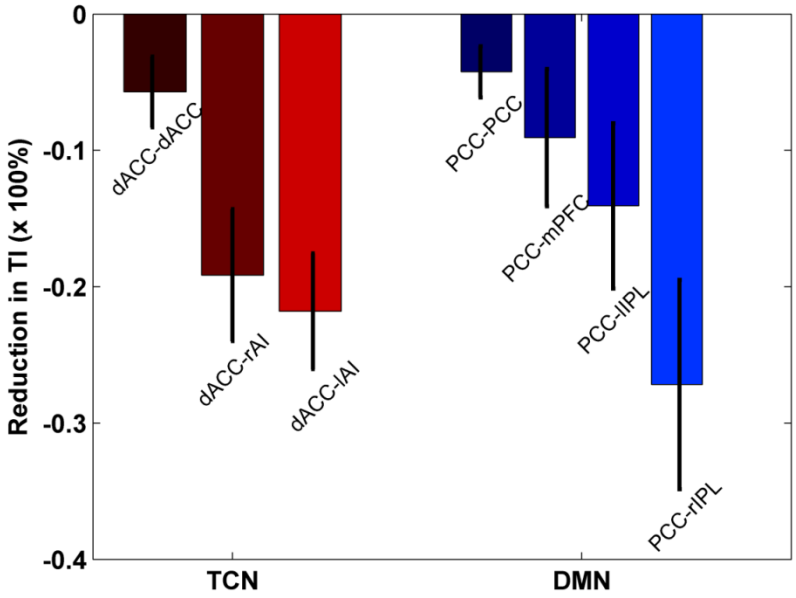

Figure 5-2. Reduction in total interdependence (TI) after temporal randomization. dACC and posterior cingulate cortex (PCC) were chosen as seed regions for the task control network (TCN) and the default mode network (DMN), respectively. mPFC: medial prefrontal cortex; lIPL: left inferior parietal lobe; rIPL: right inferior parietal lobe; rAI: right anterior insular; lAI: left anterior insular.

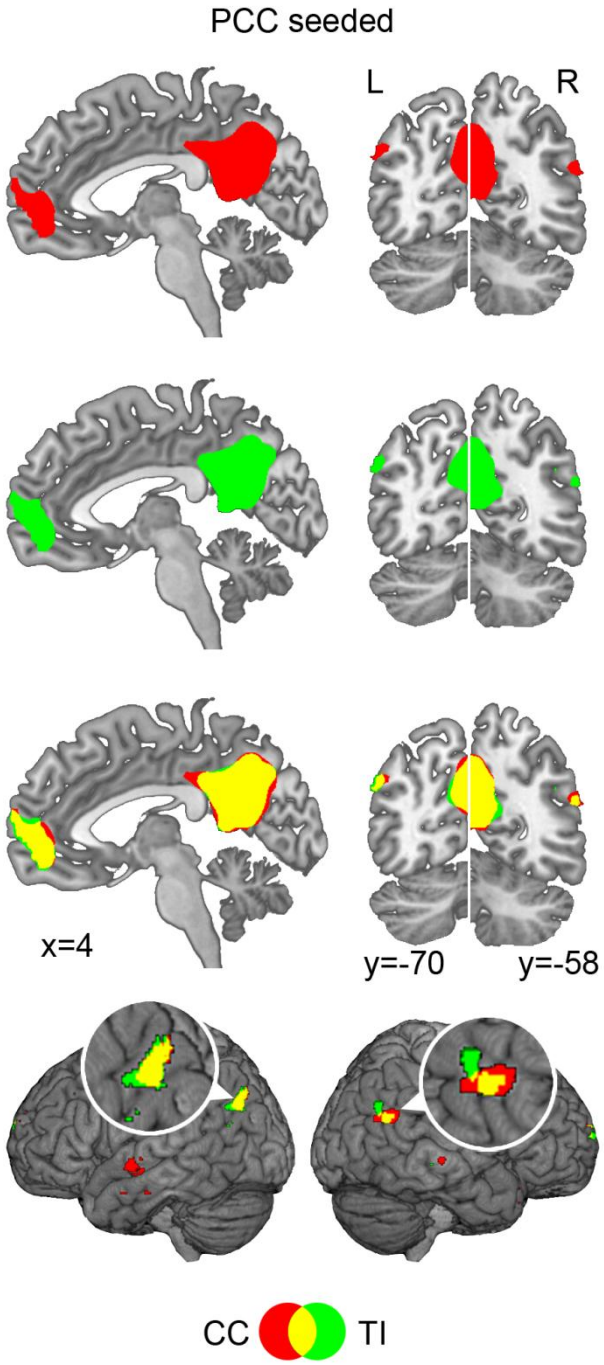

Figure 5-3. PCC-seeded connectivity maps. Both the CC map (red) and the TI (green) map contained the major nodes in the default note network (DMN) ($t=5.20$, $p<0.002$, FDR corrected for both CC and TI). The overlap (yellow) between the two maps was higher in mPFC, lIPL, and PCC than in rIPL. rIPL and lIPL regions were magnified to facilitate visual comparison.

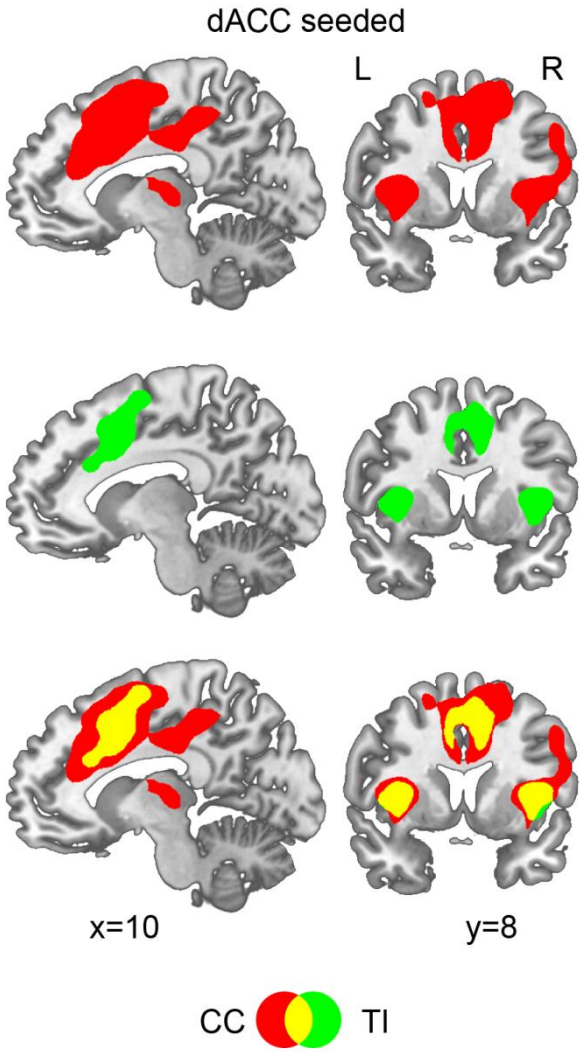

Figure 5-4. dACC-seeded connectivity maps. Although both the CC map (red) and the TI map (green) contained dACC, rAI, and lAI, the three nodes in TCN ($t=5.20$, $p<0.002$, FDR corrected for both CC and TI), the CC map also contained regions beyond TCN, including frontal eyefield (FEF), middle frontal gyrus (MFG), and middle cingulate gyrus (MCG).

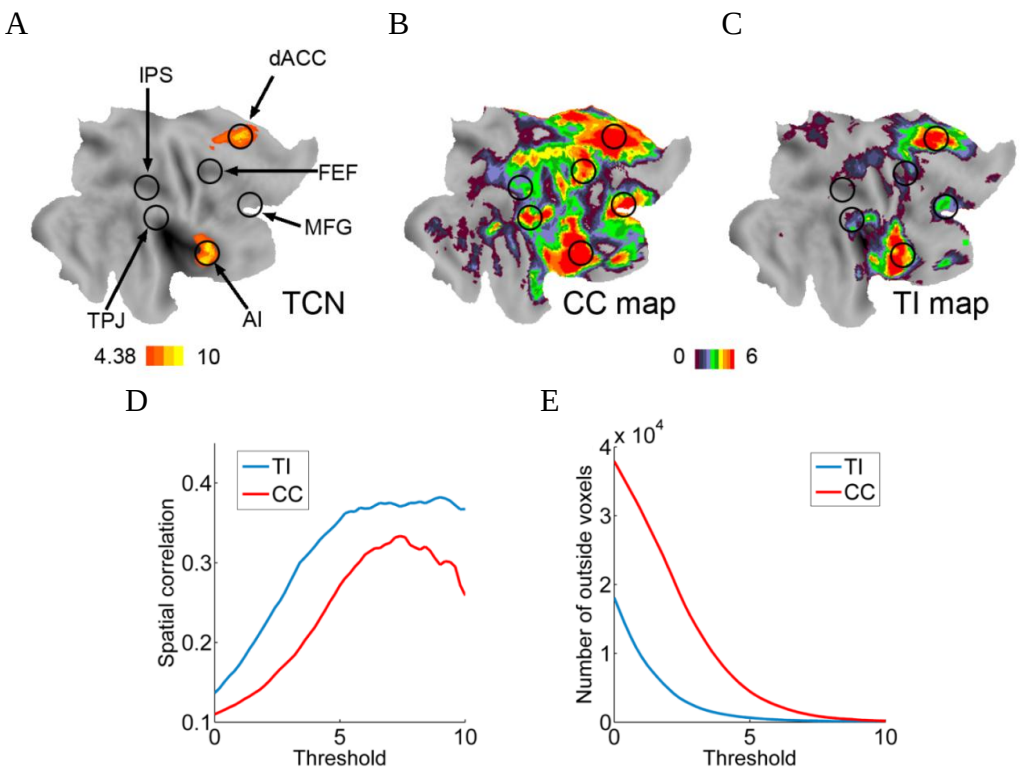

Figure 5-5. Comparison between task-state and resting-state data. A: Regions activated by the attention task were marked by circles. TCN was highlighted. B: dACC-seeded CC map from resting-state data. C: dACC-seeded TI map from resting-state data. Group level t-values were color-coded and projected on a flattened brain surface template of the right hemisphere. The CC map (B) was more diffuse and contained many regions not belonging to TCN. In contrast, the TI map (C) was more localized and matched more precisely the TCN activated by the attention task. D: Spatial correlation between the task-activated TCN and suprathreshold resting-state CC and TI maps. E: Number of voxels in suprathreshold TI and CC maps that do not belong to the task-activated TCN. IPS: intraparietal sulcus; TPJ: temporoparietal junction.

A B

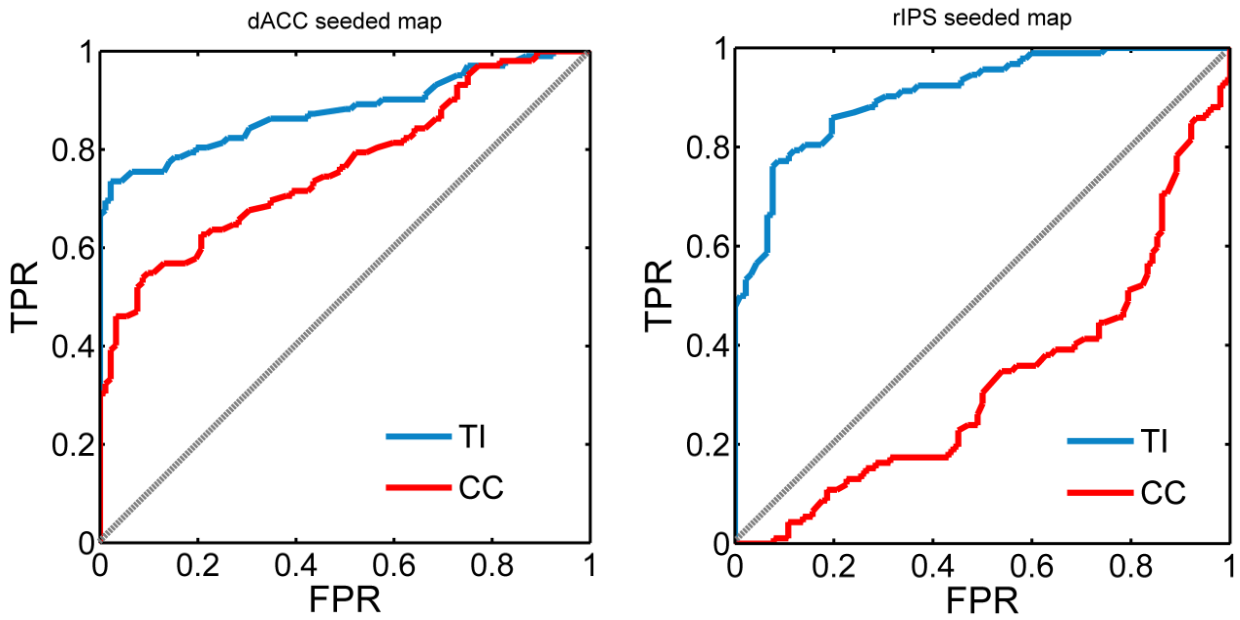

Figure 5-6. ROC analysis of statistical sensitivity. A: True positive rate (TPR) versus false positive rate (FPR) as function of discrimination threshold when deciding whether a predefined voxel belonged to TCN in the dACC-seeded resting-state maps. Task-activated voxels in rAI and rFEF were defined as the true and false populations. B: TPR versus FPR when deciding whether a predefined voxel belonged to DAN in the rIPS-seeded resting-state maps. Task-activated voxels in rFEF and rAI were defined as the true and false populations. In both cases TI achieved superior statistical sensitivity over CC.

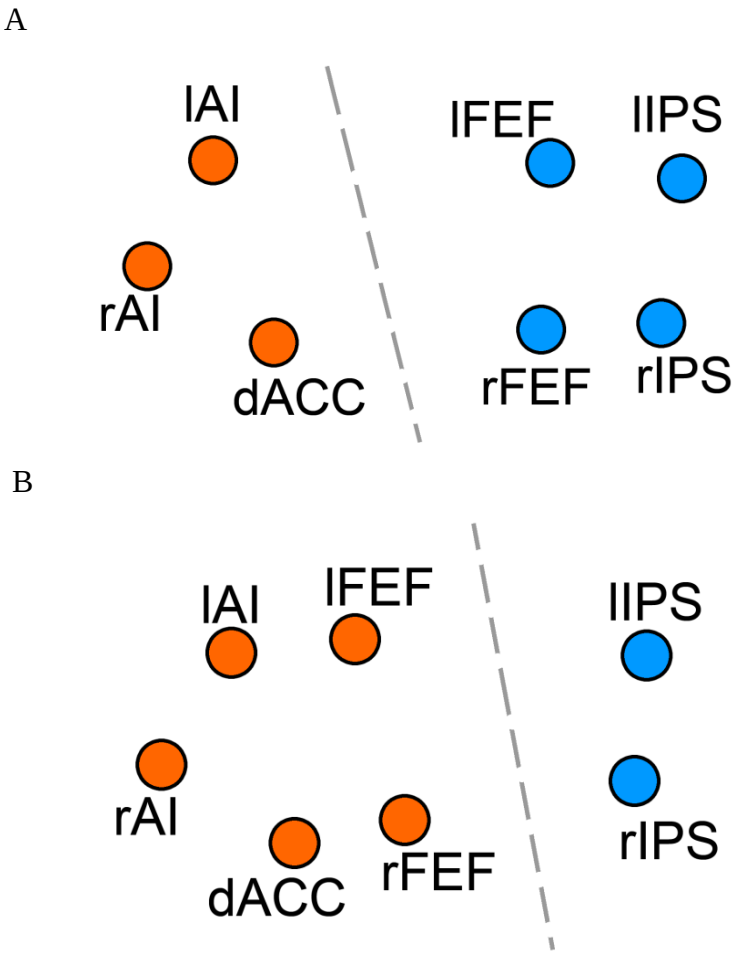

Figure 5-7. K-means clustering analysis. A: TI maps, treated as feature vectors, allowed the correct grouping of brain regions into the two known function networks: TCN (orange) and DAN (blue). B: CC maps, treated as feature vectors, made the incorrect assignment of rFEF and lFEF to TCN.

Table 5- 1. Center coordinates of task-activated regions of interest

ROI	t-value	p (FDR)	MNI coordinate (mm) x	y	z
dACC	14.64	<0. 0002	6	12	48
rAI	16.57	<0. 0002	36	27	6
lAI	14.11	<0. 0002	-30	21	0
rIPS	18.38	<0. 0002	42	-48	51
lIPS	12.90	<0. 0002	-30	-63	54
rFEF	10.68	<0. 0002	30	0	57
lFEF	9.63	<0. 0002	-30	-3	54

dACC: dorsal anterior cingulated cortex; AI: anterior insular; IPS: inferior parietal sulcus; FEF: frontal eyefield; p: significance level; MNI: Montreal Neurological Institute; r: right; l: left.

Table 5- 2**.** Center coordinates of regions of interest in DMN

ROI	t-value	p (FDR)	MNI coordinate (mm) x	y	z
PCC	10.51	<0.0002	3	-54	27
MPFC	27.35	<0.0002	-9	60	21
rIPL	9.63	<0.0002	48	-63	24
lIPL	13.78	<0.0002	-51	-69	27

PPC: posterior cingulate cortex; MPFC: medial prefrontal cortex; IPL: inferior parietal lobule; DMN: default mode network. Conventions are otherwise the same as Table 5-1.

CHAPTER 6
VISUAL INPUT INCREASES THE COUPLING BETWEEN VISUAL ALPHA OSCILLATIONS AND DEFAULT MODE ACTIVITY

6.1 Introduction

Field oscillations in the alpha range (8-12 Hz) are a prominent feature of human electroencephalogram (EEG) over the occipital-parietal cortex. The genesis and function of alpha has been the subject of intense study since the 1920s (Berger, 1929; Shaw, 2003; Lopes da Silva, 1991; Bollimunta et al. 2008; 2011). It is generally believed that for a given brain state (e.g., attention versus relaxed wakefulness), the magnitude of alpha is an inverse indicator of cortical excitability, with smaller alpha associated with improved visual processing. Goal-oriented increase of alpha, therefore, has been interpreted as reflecting a mechanism of active inhibition of task-irrelevant cortices (Klimesch, 1996; Jensen et al., 2002). In tasks demanding externally-oriented attention, alpha power, on average, is reduced over task-relevant cortices (Sauseng et al. 2005; Rajagovindan & Ding, 2011). Momentary increase of alpha power over these task-relevant cortices is indicative of decreased level of attention and worsened task performance (Macdonald et al. 2011). A recent study examining the neural signature of attention lapses has found increased alpha band oscillation up to 20 s prior to the occurrence of an error (O'Connell et al., 2009).

The level of BOLD activity in the default mode network (DMN), a key system mediating introspective processes such as mind wandering (Mason et al., 2007; Christoff et al., 2009), appears to exhibit behavior similar to that of alpha. It is suppressed or deactivated on average when subjects are actively engaged in demanding cognitive tasks (Buckner et al., 2008). Stronger deactivation of the DMN is associated with greater activation of the sensory cortices (Greicius and Menon, 2004). Attentional lapses, characterized by ineffective stimulus processing and

decreased task performance, are associated with momentarily insufficient deactivation of the DMN (Weissman et al. 2006; Eichele et al. 2008).

Based on these functional data, it seems reasonable to expect that alpha power and DMN activity be positively correlated, and this property should persist even in the absence of tasks. This hypothesis has been subjected to experimental test using the simultaneous EEG-fMRI technique. Despite repeated attempts (H. Laufs et al., 2003; Moosmann et al., 2003; Goldman et al., 2002; H Laufs et al. 2003; H Laufs et al., 2006), however, supporting evidence remains lacking. A closer examination of the literature suggests one possible reason, namely, resting-state data were often recorded with the eyes closed. Such data may not be ideally suited to model observations made under conditions of active visual processing. From a functional standpoint, positive alpha and DMN BOLD correlation, implying concurrent increase and decrease of alpha and DMN BOLD, may serve to gate out sensory input to protect introspective processes from external interference. This protection is only necessary in the presence of visual input. Moreover, the act of opening the eyes is known to reorganize brain activity; for example, it (1) suppresses alpha (Berger, 1929; Moosmann et al., 2003) and (2) increases functional connectivity within DMN (Yan et al., 2011).

In this study we sought to examine the relationship between occipital alpha oscillations and DMN activity by recording simultaneous EEG and fMRI in two types of resting-state sessions: a traditional eyes-closed session and a nontraditional eyes-open session. Group ICA was applied to the fMRI data to identify the regional components of the DMN. Alpha power fluctuations were extracted from visual EEG channels using short-time Fourier transforms and convolved with a canonical hemodynamic response function (HRF). The HRF-convolved alpha power time series were then correlated with the concurrent BOLD activity to assess their coupling.

6.2 Methods

6.2.1 Experimental procedure and data acquisition

Ten healthy college students with normal or corrected-to-normal vision participated in the study in exchange of course credit. The experimental protocol and data acquisition procedure were approved by the institutional review board of the University of Florida. Prior to participation informed consent was obtained from all participants.

The experiment consisted of two resting-state fMRI sessions each lasted 7 minutes. Participants were instructed to remain still, not to think any systematic thought, and keep their eyes closed during one session. During the other session, they were asked to open their eyes and fixate on a fixation cross presented at the center of an MR-compatible monitor, and the instructions were otherwise the same. The order of the two sessions was randomized across participants.

EEG acquisition: EEG data were recorded using a 32-channel MR-compatible EEG system (Brain Products GmbH). 31 sintered Ag/AgCl electrodes were placed according to the 10-20 system and one additional electrode was placed on the participant's upper back to monitor electrocardiograms (ECG) used subsequently to remove the cardioballistic artifact. The impedance from all scalp channels was kept below 10 kΩ during the entire recording session as recommended by the manufacturer. The online band-pass filter had the cutoff frequencies at 0.1 and 250 Hz. The filtered EEG signal was then sampled at 5 kHz and digitized to 16-bit digital signal. The digitized signal was then transferred to the recording computer via a fiber-optic cable. The EEG recording system was synchronized with the scanner's internal clock throughout the recording session. The synchronized recording technique along with a high sampling rate was essential to ensure the successful removal of the gradient artifact.

fMRI acquisition: Functional images were acquired on a 3-Tesla Philips Achieva whole-body MRI system (Philips Medical Systems, Netherlands) using a T2*-weighted echoplanar imaging (EPI) sequence [echo time (TE) = 30ms; repetition time (TR) = 1980ms; flip angle = 80°]. Two hundred and twelve (212) volumes of functional images were acquired during each experimental session, with each whole-brain volume consisting of 36 axial slices (field of view: 224 mm; matrix size: 64×64; slice thickness: 3.50mm; voxel size: 3.5×3.5×3.5mm). A T1-weighted high resolution structural image was obtained for each subject after the two resting-state sessions.

6.2.2 Data preprocessing

Dataset from two participants were excluded as they self-reported falling asleep during at least one of the sessions. The final dataset analyzed in this study contained 8 participants (4 females; mean age: 20.1±2.42).

EEG data: EEG data were contaminated by two sources of artifacts: gradient and cardioballistic. The gradient artifact was removed by subtracting an average artifact template from the EEG data as implemented in Brain Vision Analyzer 2.0 (Brain Products GmbH). The gradient artifact template was constructed by using a sliding-window approach which involved averaging the EEG signal across 41 consecutive volumes. The cardioballistic artifact was removed by an average artifact subtraction method proposed in (Allen et al. 1998). In this method, the R peaks were detected in the ECG recording in a semiautomatic way and then utilized to construct a delayed average artifact template over 21 consecutive heartbeat events. The cardioballistic artifact was then removed by subtracting the average artifact templates from the EEG data. After these two steps, the EEG data were then band-pass filtered between 0.5~50Hz, down-sampled to 250 Hz, and re-referenced to the average reference. The MR-corrected EEG data were then exported to EEGLAB (Delorme and Makeig, 2004) to correct for

eye-blinking, residual cardioballistic, and movement-related artifacts using SOBI (Second Order Blind Identification; Belouchrani et al., 1993). Recent work has shown that SOBI was effective in removing the cardioballistic artifact (Vanderperren et al., 2010), as well as in separating EEG data into interpretable components (Tang et al., 2005; Klemm et al., 2009).

fMRI data: fMRI data preprocessing was performed in SPM5 (http://www.fil.ion.ucl.ac.uk/spm/). The first 5 scans for each session were discarded in order to eliminate the transient effects. Preprocessing steps included slice timing, motion correction, normalization to the Montreal Neurological Institute (MNI) template and re-sampling of the functional images into a voxel size of 3×3×3 mm3 (Friston et al., 1995). Normalized images were spatial-smoothed by using an 8 mm FWHM (Full Width at Half Maximum) Gaussian core. Global scaling was then applied to remove the global signal from the BOLD time series. The BOLD time series were then high pass filtered with a cutoff frequency at 1/128 s.

6.2.3 Estimation of alpha power time series

The EEG data from three occipital channels: O1, O2, and Oz were selected. The average power spectra for eyes-closed or eyes-open sessions were obtained using the Welch's method. The alpha power time series were constructed for each subject by the following two steps. First, EEG signals were segmented into 500 ms non-overlapping epochs. Epochs that contained motion or muscle artifact were selected by visual inspection and replaced by linearly interpolating the alpha band power between epochs before and after the artifact period. Second, the EEG power spectrum for each single epoch was calculated using a nonparametric multitaper approach (Mitra and Pesaran, 1999), and the alpha band power was extracted by integrating the power spectrum between 8 and 12Hz. Following convolution with a canonical hemodynamic response function (HRF), downsampling to the same sampling frequency as the BOLD time series, and

normalization by 1) subtracting the mean and 2) dividing the mean-removed data by its standard deviation, we obtained the HRF-convolved alpha power time series.

6.2.4 Evaluation of functional relationship between alpha power and BOLD activity

To identify brain regions whose BOLD activities co-vary with EEG alpha power, we examined the temporal correlations between HRF-convolved alpha power time series and BOLD time series extracted from all voxels using the zero-lag cross correlation coefficient (Goldman et al., 2002; Fox et al., 2005; Mantini et al., 2007). Brain regions showing significant alpha-BOLD correlation at the group level was identified for eyes-open and eyes-closed conditions by a voxel-wise one-sample t-test on the Fisher transformed correlation coefficients from all subjects. To assess the systematic difference in alpha-BOLD correlation between the two resting-state conditions, we constructed a group-level contrast map by performing a paired t-test with experimental condition as a within-subjects factor.

As an alternative approach to construct the alpha-BOLD correlation map, HRF-convolved alpha power time series was introduced as a parametric regressor, modeling the modulatory effects of alpha on BOLD. Six additional regressors accounting for the six degrees of freedom of the rigid body movement were included as nuisance covariates in the general linear model (GLM). Regions showing significant alpha-BOLD correlation were identified within each subject by testing the appropriate coefficient in the linear regression model. Group-level maps were constructed by performing second-level analyses based on the statistical maps obtained from the within-subjects analyses.

6.2.5 Identification of resting state networks (RSNs) by ICA

To assess the spatial distribution of resting-state networks, independent component analysis (ICA) was applied to the BOLD time series using the GIFT toolbox (http://icatb.sourceforge.net/). The BOLD time series from all subjects and both eyes-open and

eyes-closed conditions were concatenated (number of time points: 207×8×2) before entering the GIFT toolbox. According to the Minimum Description Length (MDL) criteria twenty five aggregate independent components (ICs) were identified.

6.3 Result

6.3.1 EEG spectral analysis

Following the removal of gradient and cardioballistic artifacts, alpha oscillations are clearly revealed in both eyes-closed and eyes-open conditions in Figure 6-1A for a typical subject. At the group level, average power spectra from the three occipital channels are shown in Figure 1B, where the mean peak frequency is centered around 10 Hz (eyes-closed session: 9.38 ± 1.48 Hz; eyes-open session: 10.00 ± 0.78 Hz). The average alpha power under the eyes-open condition was significantly lower than that under the eyes-closed condition ($p < 0.05$), demonstrating the well-established phenomenon of "alpha blockade," initially described by Berger (Berger, 1929; Moosmann et al., 2003).

6.3.2 Alpha-BOLD correlation analysis

To demonstrate alpha power fluctuation, EEG data from a representative subject under the eyes-open condition was filtered between 8 and 12 Hz in Figure 6-2A, and the amplitude profile, referred to as alpha power time series, is superimposed. Over the 7 minute recording session, alpha power time series exhibits strong fluctuations, seen in Figure 6-2B. In Figure 6-2C, the HRF-convolved alpha power time series is plotted together with the simultaneously recorded BOLD time series from mPFC, a key hub of the DMN, where the zero-lag correlation coefficient between the two time series is 0.43 ($p<0.0001$). The positive correlation map between posterior alpha and BOLD activity is shown in Figure 6-3. With the eyes closed, no significant positive correlation was found between the HRF-convolved alpha power time series and BOLD activity

(Figure 6-3A), whereas upon eyes opening, the posterior alpha power became positively correlated with BOLD activity within posterior cingulate cortex (PCC, $p<0.005$ uncorrected) and medial prefrontal cortex (mPFC, $p<0.005$ uncorrected) (Figure 6-3B), both key hubs of the DMN (Buckner et al., 2008).

The negative correlation map is shown in Figure 6-3D, revealing a frontoparietal network, consistent with the finding of a previous study (Laufs et al., 2003a). It is interesting to note that the same network is found for both eyes-open and eyes-closed conditions. By using the GLM approach, the same negative correlated map is revealed by coefficient for the HRF-convolved alpha power time series under both conditions.

6.3.3 Eyes-closed versus eyes-open conditions

The difference map was derived from 2nd level paired t-test between eyes-closed and eyes-open conditions. Clusters showing significant differences in positive alpha-BOLD correlation are reported in Figure 3C. In addition to PCC and mPFC, additional areas within the DMN are revealed, including bilateral inferior parietal lobule (IPL) and left inferior temporal cortex (ITC). The coordinates of the above regions are listed in Table 1. As a comparison, the DMN obtained by applying the ICA algorithm to the resting-state fMRI data is shown in Figure 6-4. The similarity between Figure 6-3C and Figure 6-4 suggests that alpha power is preferentially coupled with DMN activity under the eyes-open condition.

6.4 Discussion

In this study we examined the correlation between EEG alpha power fluctuation and BOLD activity under both eyes-closed and eyes-open resting state conditions. Consistent with a previous report, the posterior alpha power is negatively correlated with BOLD activity in a frontoparietal network during both eyes-open and eyes-closed resting conditions (Laufs et al., 2003a). Positive alpha-BOLD correlation was not found for the eyes-closed condition but was

found in mPFC and PCC, two key nodes of the default mode network, for the eyes-open condition. Additional DMN areas were revealed when alpha-BOLD correlation maps of eyes-open condition are contrasted against the maps of eyes-closed condition.

Previous simultaneous EEG-fMRI studies examining the relationship between fluctuations in EEG power and resting state BOLD activity have found that major resting state networks in general are correlated with power fluctuations in multiple bands of EEG oscillations (Mantini et al., 2007). In particular, alpha power fluctuation was found to be negatively correlated with BOLD activities within a frontoparietal network (Laufs et al., 2003a, 2003b, 2006). Functional imaging studies show that higher alpha power and DMN activity precedes momentary lapses in attention (Weissman et al., 2006; Eichele et al., 2008; O'Connell et al., 2009), while the lower alpha power and DMN activity usually relate to higher attentional demand towards external cue and enhanced sensory processing (Foxe et al., 1998; McKiernan et al., 2003; Thut et al., 2006). Based on this observation, one may expect a positive correlation between alpha power and DMN activity. However, no direct relationship between the two under resting conditions has been reported to date. Noticing that only the eyes-closed condition is employed in typical fMRI-EEG resting-state studies, we reasoned that such a condition is not a good model for tasks involving active visual processing. By including the eyes-open condition, we report the first evidence of positive correlation between alpha power and DMN activity.

Strengthened alpha oscillation is indicative of inhibition of visual cortices (Klimesch, 1996; Klimesch et al., 2007). Empirical evidence in support of this theory includes 1) increased alpha oscillatory power during internal tasks such as mental imagery and working memory (Cooper et al., 2003; Sauseng et al., 2005), and 2) decreased alpha during external oriented visual attention (Worden et al., 2000; Thut et al., 2006; Rajagovindan and Ding, 2010). Increased alpha

over the occipital regions during internal tasks suppresses visual processing to protect internal processes from being disrupted by external sensory input; decreased occipital alpha during external attention tasks increases the excitability of visual cortex and facilitates sensory processing.

The default mode network is thought to reflect task-independent introspective processes (Buckner et al., 2008). Phenomena such as mind wandering have been associated with higher levels of activity within the default mode network, and contribute to attention lapses (Weissman et al., 2006; Mason et al., 2007; Eichele et al., 2008; Christoff et al., 2009). Using fMRI, a prior study has reported a negative correlation between DMN activity and the activation level in sensory cortices during a passive sensory stimulation task (Greicius and Menon, 2004).

Summarizing, during the more externally-oriented state, there is increased excitability in the sensory regions as indexed by decreased alpha power, and in the meantime DMN deactivates to facilitate task performance. During the DMN mediated internally-oriented state, higher DMN activity is accompanied by increased alpha power, which serves to protect internal information processing by gating out sensory input. Recent work suggests that in the resting state the brain spontaneously switches between a more externally-oriented state and a more internally-oriented state. Fransson (2005) reported that the PCC region is negatively correlated with regions that are usually involved in sensory processing and motor/movement planning, including bilateral premotor cortex, dorsolateral prefrontal cortex, supplementary motor cortex, inferior parietal lobe, occipital cortex, and the insula. These results are thought to reflect a basic survival technique that enables frequent interruption of introspective and self-referential processes to allow individuals to be aware of their surrounding environment and respond to possible appetitive or threatening events. Here, we further corroborated this argument by demonstrating

that cycles of suppressed DMN activity is coupled with decreased alpha power, indicating heightened sensory cortical excitability. Increased alpha power during episodes of increased DMN activity, on the other hand, may indicate a sensory gating mechanism that acts to block the external sensory information from interfering with the introspective processes (Kelly et al., 2006).

The absence of systematic association between alpha power and activity in default mode network under eyes-closed resting condition is intriguing. Because of it prior studies have generally failed to report any significant correlations between alpha power fluctuation and default mode network activity (Goldman et al., 2002; Laufs et al., 2003a, 2003b, 2006; Moosmann et al., 2003). A plausible explanation for the lack of alpha-DMN association might be that during eyes-closed resting, as no visual information is present, the gating mechanism described above is disengaged, and the brain might be engaged in an overall more introspective state compared to eyes-opening. Supporting this interpretation is the well-established "alpha blockade" phenomenon associated with opening of the eye (Berger, 1929). Recent simultaneous EEG-fMRI studies have also shown that the occipital alpha power variation across eyes-open and eyes-closed is negatively correlated with BOLD activity level within the visual cortex (Laufs et al., 2003a; Moosmann et al., 2003; Feige et al., 2005), signifying decreased visual cortical activity during eyes-closed compared to eyes-open conditions. The decreased visual cortical activity might allow more resources to be allocated to introspective processes, and render such processes less prone to be interrupted by external information. In addition, a recent study reported enhanced functional connectivity within the DMN during eyes-open resting state (Yan et al., 2009), implicating an enhanced competition of processing resources between internal and

external processes. The differential alpha-DMN coupling between eyes-closed and eyes-open resting conditions in our study in general agrees with the results reported in the prior study.

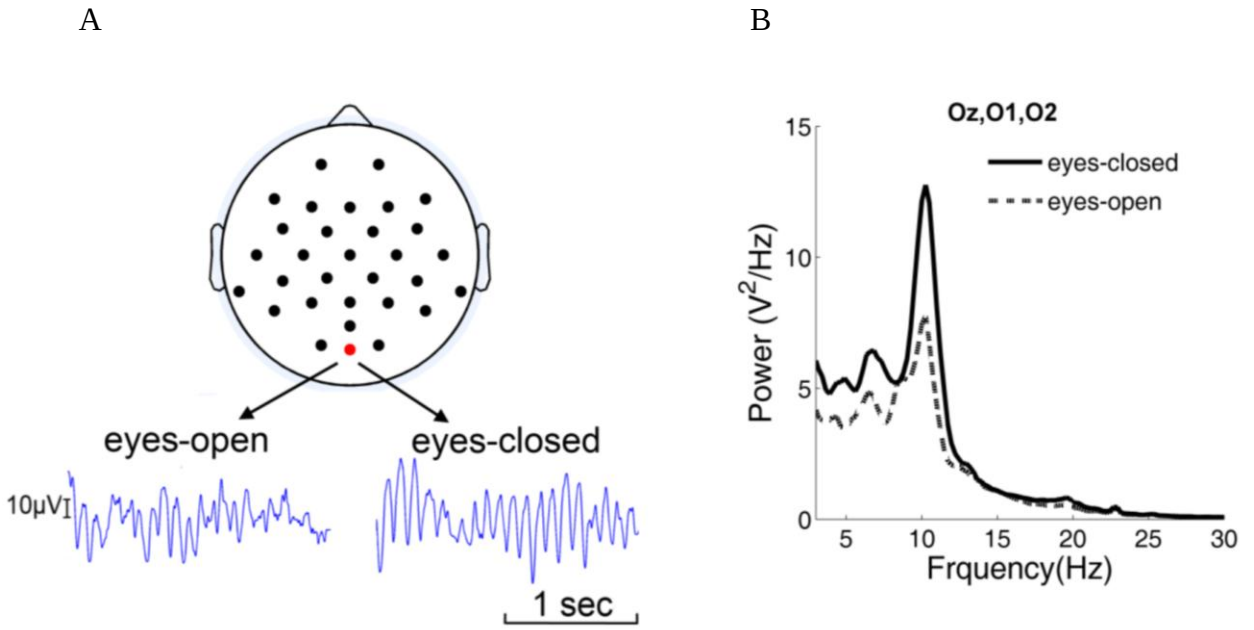

Figure 6-1. Alpha modulation by eyes-open condition. (A) EEG traces from a typical subject. (B) Power spectra from the three occipital channels averaged across subjects.

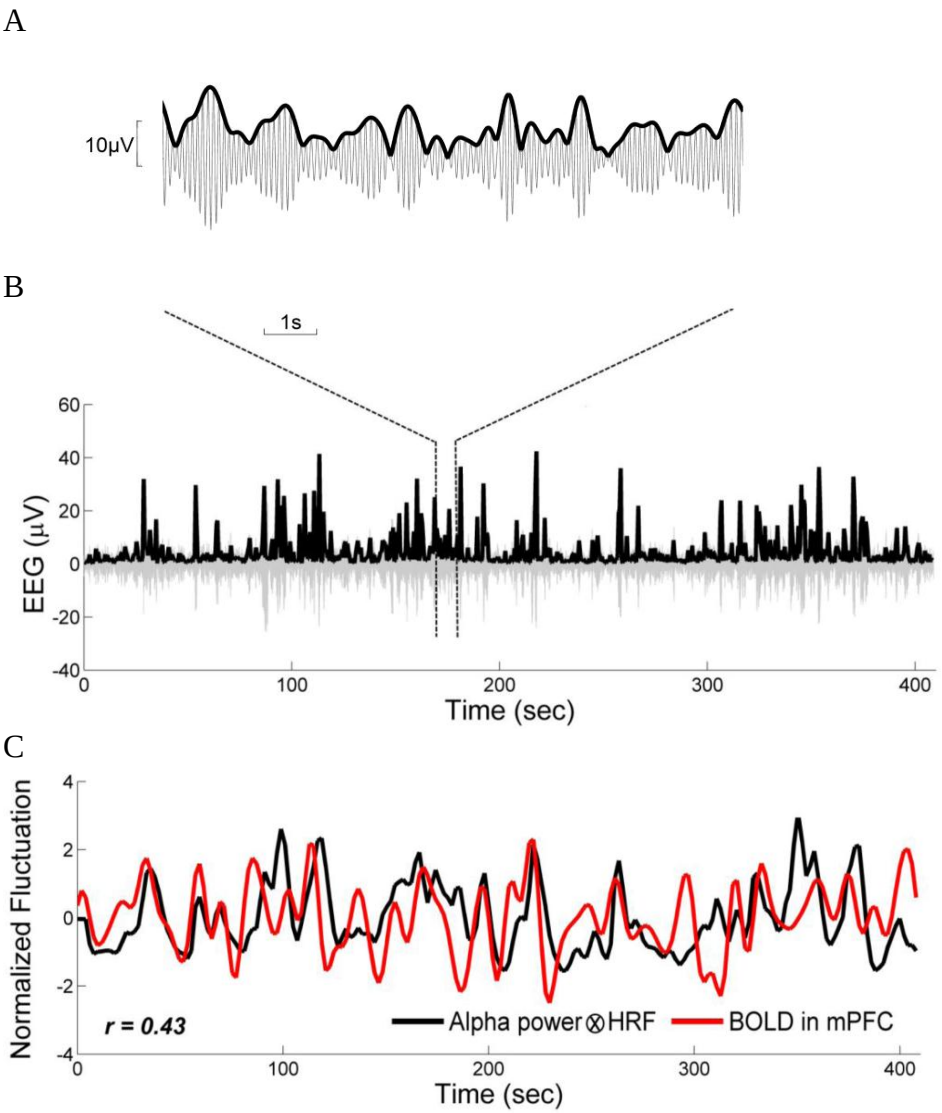

Figure 6-2. Alpha power time series and BOLD time series from a representative subject. (A) Alpha oscillations and its amplitude profile referred to the alpha power time series (eyes-open). (B) Alpha power time series over the entire 7-minute recording session (eyes-open). (C) HRF-convolved alpha power time series, obtained from the same alpha power time course in (B), plotted together with the simultaneously acquired BOLD time series from mPFC. The zero-lag correlation between the two time series is $r = 0.43$ ($p < 0.0001$).

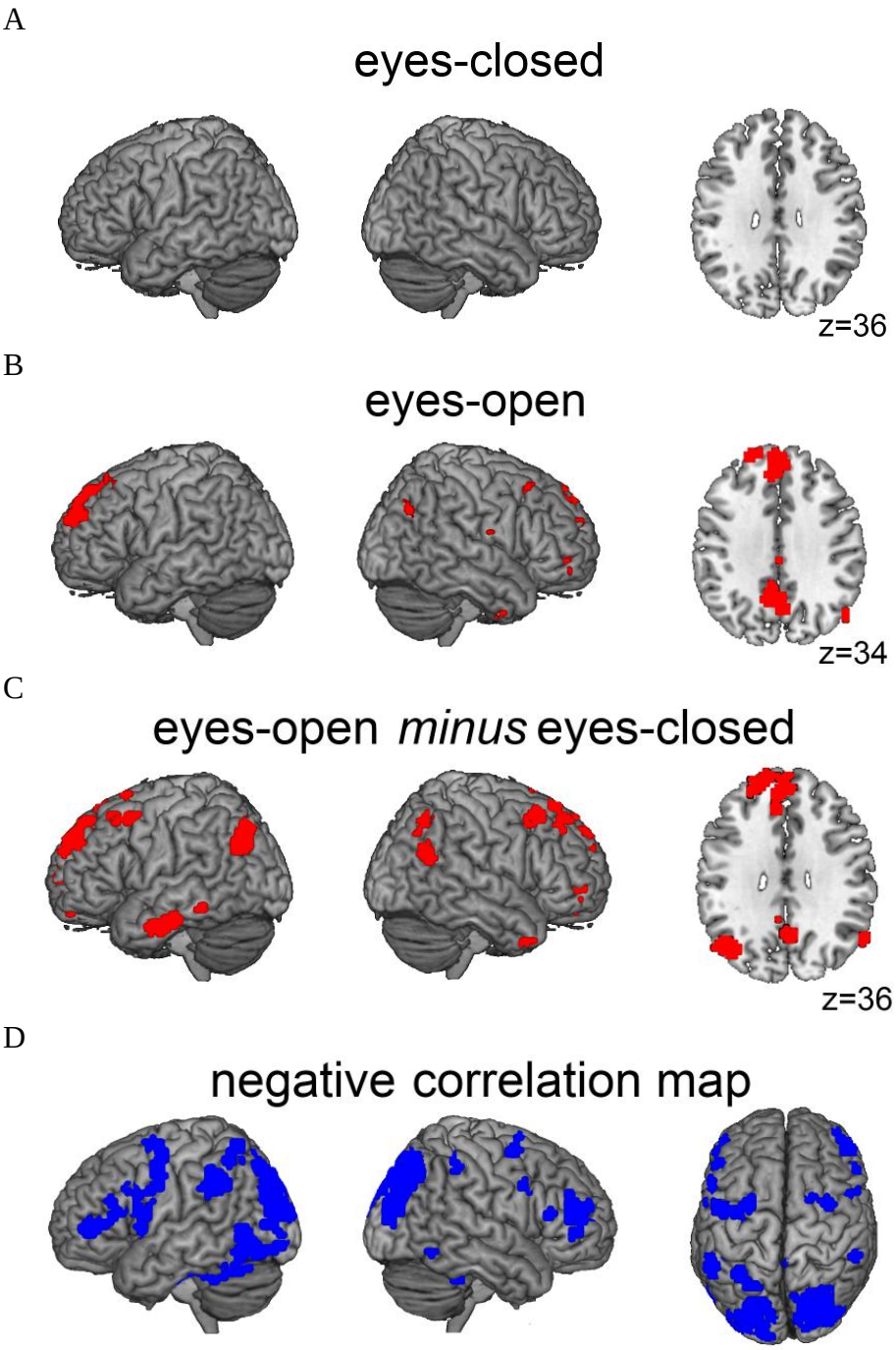

Figure 6-3. Alpha-BOLD correlation maps (red: positive correlation and blue: negative correlation). Positive correlation map for (A) eyes-closed condition ($t>3.47$, $p < 0.005$), and for (B) eyes-open condition ($t>3.47$, $p < 0.005$). (C) Eyes-open map minus eyes-closed map ($t>3.47$, $p < 0.005$). (D) Negative correlation map ($p<0.005$, eyes-open), and the map is similar for eyes-closed condition.

Table 6-1. Coordination of the ROIs in the DMN derived from the contrast map.

ROI name	Coordination (MNI, mm)	$P_{uncorrected}$(cluster level)	$P_{uncorrected}$(voxel level)
PCC	0,-60,39	0.004	0.002
ventral mPFC	-6,48,0	0.000	0.000
dorsal mPFC	15,36,60	0.000	0.000
left IPL	-48,-66,36	0.000	0.000
right IPL	51,-63,48	0.001	0.000
left ITC	-63,-6,-27	0.000	0.000

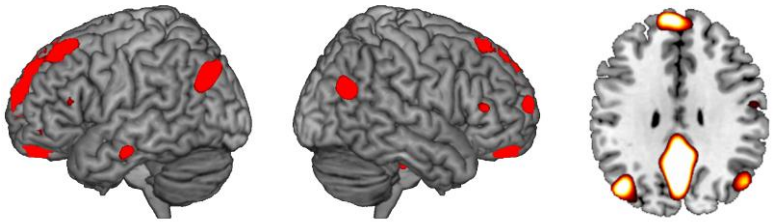

Figure 6-4. Spatial map of the DMN, comprised with PCC, mPFC, bilateral IPL and ITC, is derived from group ICA on resting state fMRI ($t>3.47$, $p < 0.005$ uncorrected). The coherent DMN regions identified in spatial map of the selected IC and the regions identified by the difference between eye-open and eye-closed alpha power correlation map (Figure 6-3C) are superimposed.

CHAPTER 7
CONCLUSION

The functional role of neuronal oscillations in visual stimulus or nociceptive input processing and higher-order cognitive processing such as attention and pain regulation was investigated along four cogent studies. The utilized imaging techniques cover a broad range of spatial resolution, from multiunit activity and local field potential to the whole brain functional MRI.

In the first study, we sought to identify the role of prestimulus ongoing oscillatory brain activity in inferotemporal (IT) cortex. Recent work reported the observation of alpha frequency oscillations (8 to 12 Hz) in several regions of macaque visual cortex including V2, V4 and IT cortex. While alpha-related physiology in V2 and V4 appears consistent with a role in attention-related suppression, in IT, alpha reactivity appears conflicted with such a role. We addressed this issue directly by analyzing laminar profiles of local field potentials and multiunit activities from the IT cortex of macaque monkeys during performance of an intermodal selective attention task (visual versus auditory). We found that (1) prior to visual stimulus onset (-200 ms to 0 ms), attention to visual input increased ongoing alpha power in IT relative to attention to auditory input, and (2) in contrast to the prevailing view of alpha inhibition, the increased ongoing alpha activity is accompanied by increased concurrent multiunit firing and facilitates visual stimulus processing. These results suggest that ongoing alpha oscillations in IT play a different functional role than that in the primary sensory cortex and may be part of the neuronal mechanism representing task-relevant information in IT.

In a following study, we assessed the temporal dynamic of a rhythmic clinical quality of pain, and investigated the electro-physiology biomarker for this rhythmic pathological process. We began by testing the vascular theory of the throbbing quality, which assume that the

sensation of throbbing pain arising directly from the activation of localized pain-sensory neurons by closely apposed blood vessels. We examined this presumption more closely by simultaneously recording the subjective report of the throbbing rhythm and the arterial pulse in subjects with throbbing dental pain – a prevalent condition whose pulsatile quality is widely regarded a primary sensation. Contrary to the generally accepted view, which would predict a direct correspondence between the two, we found that the throbbing rate (44 bpm ± 3 SEM) was much slower than the arterial pulsation rate (73 bpm ± 2 SEM, $p<0.001$), and that the two rhythms exhibited no underlying synchrony. Moreover, the beat-to-beat variation in arterial and throbbing events observed distinct fractal properties, indicating that the physiological mechanisms underlying these rhythmic events are distinct. Confirmation of the generality of this observation in other pain conditions would support an alternative hypothesis, that the throbbing quality is not a primary sensation but rather an emergent property, or perception, whose "pacemaker" lies within the central nervous system. As the initial study on the central representative of throbbing percept, we reported a patient with an unusual migrainous condition, whose isolated throbbing sensations, in the absence of pain or headache, presented the opportunity to gain further insights of the mechanisms underlying the throbbing quality. The electroencephalogram (EEG) has been shown by several investigators to be of utility in capturing the neurophysiological representations of pain in the brain, as well as the neurophysiological correlates of the migraine attack. The temporal resolution of the EEG is also well suited to representing a brain signature of the throbbing rhythm. As a further investigation, we report the results of the psychophysical characteristics of the throbbing rhythm, as well as its neurophysiological correlates by EEG from a patient with a persistent throbbing condition in association with migraine. Based on the psychophysical examination, a direct correspondence

between the throbbing quality and arterial pulsations in the periphery is unlikely, however, the overall alpha power increased with the subjective intensity of the throbbing quality. On closer examination we also found that the rhythm of the subjective throbbing experience was phase locked to the fluctuation of posterior alpha power, and the phase synchrony, or coherence, between the throbbing and alpha power increased with the intensity of the throbbing experience. This case illustrates a lack of evidence for the throbbing experience as a primary sensation of peripheral origin, and provides the consideration of an alternative possibility, that the throbbing quality is a perception whose origins derives from a CNS representation of pain.

As part of the third study, we introduce a new statistic way in computing resting-state functional connectivity and provide a thorough comparison to the conventional connectivity measurement. Prevailing methods for resting-state functional connectivity analysis do not take into account the time series structure in resting-state fMRI data. We propose to address this problem by introducing a method called total interdependence (TI). It was shown that, when combined with a random permutation approach, TI can reveal the degree of temporal dependence between BOLD signals that were not captured by the traditional zero-lag cross correlation (CC) method. Functionally, TI was able to more precisely identify the three constituent regions of the task control network, which were further validated by the task-state data recorded during the same experiment. Finally, we showed that TI performed better in a clustering analysis of network segregation and exhibited superior statistical sensitivity. The directional interaction between brain regions had been quantified under different experimental conditions, our result indicates that the slowly sampled fMRI recording does not only contain zero-lag synchrony but also effectively reflects the conductive delay between the interacting areas.

For the fourth and the final study, we found that, similar to what was observed in the active visual processing task, the posterior alpha power and the BOLD activity in default mode network concurrently fluctuate up and down under resting-state. High power of alpha oscillation was usually associated with lower excitability level, and is interpreted as active inhibition toward the external stimuli. The disengagement from the external event, on the other hand, is accompanied with higher activation in default mode network, which is prone to be more activated under the introspective mental processing. This positive correlation between the alpha power time series from occipital channels and the DMN activity was found only under eyes-open resting-state condition, but not under eyes-closed resting-state condition. Though the alpha amplitude reduction with eyes opening is a well-known phenomenon, the underlying mechanism is unknown. Still, other evidence indicates the change of network organization by eyes-open, such as increased anti-correlation between DMN and other task positive network, increased correlation between the activity in visual region and posterior alpha power. Hence, we infer that eyes-open is closely mimicking the baseline of visual processing task, and the intriguing coupling reflects a basic survival technique that enables frequent interruption of introspective and self-referential processes to allow individuals to be aware of their surrounding environment and respond to possible appetitive or threatening events; and this mechanism disengages without visual input.

It is shown in our studies and other previous studies that all cognitive functions depend on the oscillatory activity distributed across the brain. Throughout the four parts of our studies, we focused on neural oscillations and synchrony in order to address the mechanisms of executive processes and other cognitive processes. The results indicate that the rich temporal structure of brain signal enables objective measures of functional integrity of neuronal circuits and serves as

a biomarker of cognitive impairments brought by debilitating neurological and psychiatric disorders.

The progress along the four studies reveals the essential importance of utilizing multimodal imaging methods in neuroinformatic studies. As one example, not only the change in alpha power on average, but also the temporal dynamic of the alpha amplitude is informative to assess the change in brain state. Yet, the anatomic structure of the underlying modulator for the temporal dynamic is unknown. As another example, with invasive recording, the prominent power in alpha band is found serving distinct functional roles in different brain regions, while the noninvasive electrophysiology recording has limited spatial resolution to provide this information. A solution for this information loss is assembling the results from different imaging modalities, which provide complementary information. Hence, the current results derived from any imaging method still requires the further validation from other modalities.

REFERENCES

Aguirre GK, Zarahn E, D'Esposito M (1998) The Variability of human, BOLD hemodynamic responses. Neuroimage 8, 360–369.

Andersen P, Andersson SA (1968) Physiological basis of the Alpha Rhythm. New York: Appleton-Century-Crofts.

Anderson K, Rajagovindan R, Ghacibeh G, Meador KJ, Ding M (2011) Theta oscillations mediate interaction between prefrontal cortex and medial temporal lobe in human memory. Cerebral Cortex.

Ahn AH (2010) On the temporal relationship between throbbing migraine pain and arterial pulse. Headache 50(9): 1507-10.

Armstrong WF, Bach DS, Carey LM, Froehlich J, Lowell M, Kazerooni EA (1998) Clinical and echocardiographic findings in patients with suspected acute aortic dissection. Am Heart J. 136(6): 1051-60.

Arnold M, Cumurciuc R, Stapf C, Favrole P, Berthet K, Bousser MG (2006) Pain as the only symptom of cervical artery dissection. J Neurol Neurosurg Psychiatry 77:1021–1024.

Aslan FE, Badir A, Arli SK, Cakmakci H (2009) Patients' experience of pain after cardiac surgery. Contemp Nurse 34(1): 48-54.

Babiloni C, Brancucci A, Percio CD, Capotosto P, Arendt-Nielsen L, Chen ACN and Rossini PM (2006) Anticipatory Electroencephalography Alpha Rhythm Predicts Subjective Perception of Pain Intensity. The Journal of Pain 7, 709–717.

Backonja MM, Stacey B (2004) Neuropathic pain symptoms relative to overall pain rating. J Pain 5:491– 497.

Ballard K, Lane H, Hudelist G, Banerjee S, Wright J (2010) Can specific pain symptoms help in the diagnosis of endometriosis? A cohort study of women with chronic pelvic pain. Fertil Steril 94:20 –27.

Ballas SK, Delengowski A (1993) Pain measurement in hospitalized adults with sickle cell painful episodes. Ann Clin Lab Sci 23:358 –361.

Basbaum AI, Bautista DM, Scherrer G, Julius D (2009) Cellular and molecular mechanisms of pain. Cell 139:267–284.

Bastiaansen MCM, Brunia CHM (2001) Anticipatory attention: an event-related desynchronization approach. International Journal of Psychophysiology 43:91-107.

Bastiaansen MCM, Posthuma D, Groot PFC, de Geus EJC (2002) Event-related alpha and theta responses in a visuo-spatial working memory task. Clin Neurophysiol 113 (12), 1882-1893.

Beason-Held LL, Kraut MA, Resnick SM (2009) Stability of default-mode network activity in the aging brain. Brain Imaging Behav 3, 123–131.

Beckmann CF, DeLuca M, Devlin JT, Smith SM (2005) Investigations into resting-state connectivity using independent component analysis. Philos Trans R Soc Lond B Biol Sci 360, 1001–1013.

Berger RD, Akselrod S, Gordon D, Cohen RJ (1986) An efficient algorithm for spectral analysis of heart rate variability. IEEE Trans Biomed Eng 33:900 –904.

Birn RM, Diamond JB, Smith MA, Bandettini PA (2006) Separating respiratory-variation-related fluctuations from neuronal-activity-related fluctuations in fMRI. NeuroImage 31 (4): 1536-1548.

Bishop GH (1932) Cyclic change in the excitability of the optic pathway of the rabbit. Am J Physiol 130:213–224

Biswal B, Yetkin FZ, Haughton VM, Hyde JS (1995) Functional connectivity in the motor cortex of resting human brain using echo-planar MRI. Magn. Reson. Med. 34, 537–541.

Blumenfeld AM, Varon SF, Wilcox TK, Buse DC, Kawata AK, Manack A (2011) Disability,HRQoL and resource use among chronic and episodic migraineurs: results from the International Burden of Migraine Study (IBMS). Cephalalgia 31(3): 301-15.

Bollimunta A, Chen Y, Schroeder CE, Ding M (2008) Neuronal mechanisms of cortical alpha oscillations in awake-behaving macaques. Journal of Neuroscience 28(40):9976-9988.

Bollimunta A, Mo J, Schroeder CE, Ding M. (2011) Neuronal Mechanisms and Attentional Modulation of Corticothalamic Alpha Oscillations. J. Neurosci. 31, 4935–4943.

Botvinick MM, Cohen JD, Carter CS (2004) Conflict monitoring and anterior cingulate cortex: an update. Trends Cogn. Sci. 8, 539–546.

Brandt ME, Jansen BH (1991) The Relationship between prestimulus alpha-amplitude and visual evoked-potential pmplitude. Int J Neurosci 61:261-268

Bressler S, Seth AK (2011) Wiener-Granger causality: A well-established methodology. Neuroimage 58 (2), 323-329.

Brovelli A, Ding M, Ledberg A, Chen Y, Nakamura R, Bressler SL (2004) Beta oscillations in a large-scale sensorimotor cortical network: Directional influences revealed by Granger causality. Proc. Natl. Acad. Sci. 101, 9849-9854.

Buckner RL, Andrews-Hanna JR, Schacter DL (2008) The brain's default network: anatomy, function, and relevance to disease. Ann. N. Y. Acad. Sci. 1124, 1–38.

Buckner RL, Sepulcre J, Talukdar T, Krienen FM, Liu H, Hedden T, Andrews-Hanna JR, Sperling RA, Johnson KA (2009) Cortical hubs revealed by intrinsicfunctional connectivity: mapping, assessment of stability, and relation to Alzheimer's disease. J. Neurosci. 29, 1860–1873.

Burstein R, Cutrer MF, Yarnitsky D (2000) The development of cutaneous allodynia during a migraine attack clinical evidence for the sequential recruitment of spinal and supraspinal nociceptive neurons in migraine. Brain. 123 (8): 1703-9.

Buschman TJ, Miller EK (2007) Top-down versus bottom-up control of attention in the prefrontal and posterior parietal cortices. Science, 315, 1860-1862.

Canolty RT, Knight RT (2010) The functional role of cross-frequency coupling. Trends in Cognitive Sciences 14, 506–515.

Chao LL, Knight RT (1998) Contribution of human prefrontal cortex to delay performance. J Cogn Neurosci 10 (2), 167-177.

Chance FS, Abbott LF, Reyes AD (2002) Gain modulation from background synaptic input. Neuron 35:773-782.

Chang C, Glover GH (2010) Time-frequency dynamics of resting-state brain connectivity measured with fMRI. Neuroimage 50, 81–98.

Christoff K, Gordon AM, Smallwood J, Smith R, Schooler JW (2009) Experience sampling during fMRI reveals default network and executive system contributions to mind wandering. Proceedings of the National Academy of Sciences.

Church JA, Fair DA, Dosenbach NU, Cohen AL, Miezin FM, Petersen SE, Schlaggar BL (2009) Control networks in paediatric tourette syndrome show immature and anomalous patterns of functional connectivity. Brain 132, 225 -238.

Cohen AL, Fair DA, Dosenbach NUF, Miezin FM, Dierker D, Van Essen DC, Schlaggar BL, Petersen SE (2008) Defining functional areas in individual human brains using resting functional connectivity MRI. Neuroimage 41, 45–57.

Congedo M, John RE, De Ridder D, Prichep L (2010) Group independent component analysis of resting state EEG in large normative samples. Int J Psychophysiol *78*, 89–99.

Cooper NR, Croft RJ, Dominey SJJ, Burgess AP, Gruzelier HH (2003) Paradox lost? Exploring the role of alpha oscillations during externally vs. internally directed attention and the implications for idling and inhibition hypotheses. Int J Psychophysiol 47: 65-74.

Cooper NR, Burgess AP, Croft RJ, Gruzelier, JH (2006) Investigating evoked and induced electroencephalogram activity in task-related alpha power increases during an internally directed attention task. Neuroreport 17 (2), 205-208.

Corbetta M, Shulman GL (2002) Control of goal-directed and stimulus-driven attention in the brain. Nat. Rev. Neurosci. 3, 201–215.

Corbetta M, Patel G, Shulman GL (2008) The reorienting system of the human brain: from environment to theory of mind. Neuron 58, 306–324.

Craig AD (2009) How do you feel–now? The anterior insula and human awareness. Nat Rev Neurosci 10:59 –70.

Curtis CE, Sun FT, Miller LM, D'Esposito M (2005) Coherence between fMRI time-series distinguishes two spatial working memory networks. NeuroImage 26 (1), 177–183.

Damoiseaux JS, Rombouts SARB, Barkhof F, Scheltens P, Stam CJ, Smith SM, Beckmann CF, (2006) Consistent resting-state networks across healthy subjects.Proc. Natl. Acad. Sci. USA 103, 13848–13853.

Damoiseaux JS, Beckmann CF, Arigita EJS, Barkhof F, Scheltens P, Stam CJ, Smith SM, Rombouts SARB (2008) Reduced resting-state brain activity in the "default network" in normal aging. Cereb. Cortex 18 (8), 1856–1864.

Demanuele C, James CJ, Sonuga-Barke EJ (2007) Distinguishing low frequency oscillations within the 1/f spectral behaviour of electromagnetic brain signals.Behav Brain Funct. 10;3:62.

De Luca M, Beckmann CF, De SN, Matthews PM, Smith SM (2006) fMRI resting state networks define distinct modes of long-distance interactions in the human brain. Neuroimage 29, 1359–1367.

Dehghani M, Sharpe L, Nicholas MK (2003) Selective attention to pain-related information in chronic musculoskeletal pain patients. Pain 105, 37–46.

Dhamala M, Rangarajan G, Ding M (2008) Analyzing information flow in brain networks with nonparametric Granger causality. NeuroImage 41(2), 354-362.

van Dijk JG, Dorresteijn M, Haan J, Ferrari MD (1991) Visual evoked potentials and background EEG activity in migraine. Headache 31, 392–395.

van Dijk H, Nieuwenhuis, Jensen O (2010) Left temporal alpha band activity increases during working memory retention of pitches. Eur J Neurosci 31: 1701-1707.

Ding M, Bressler SL, Yang WM, Liang HL (2000) Short-window spectral analysis of cortical event-related potentials by adaptive multivariate autoregressive modeling: Data preprocessing, model validation, and variability assessment. Biol Cybern 83, 35-45.

Ding M, Chen Y, Bressler SL (2006) Granger causality: Basic theory and application to neuroscience. In Schelter. S., Winterhalder, N., Timmer, J., Handbook of Time Series Analysis. 437-460, Berlin (Germany): Wiley-VCH.

Dosenbach NU, Visscher KM, Palmer ED, Miezin FM, Wenger KK, Kang HC, Burgund ED, Grimes AL, Schlaggar BL, Petersen SE (2006) A core system for the implementation of task sets. Neuron 50, 799–812.

Dosenbach NU, Fair DA, Miezin FM, Cohen AL, Wenger KK, Dosenbach RAT, Fox MD, Snyder AZ, Vincent JL, Raichle ME, Schlaggar BL, Petersen SE (2007) Distinct brain networks for adaptive and stable task control in humans. Proc. Natl. Acad. Sci. U. S. A. 104, 11073–11078.

Driver J, Frith C (2000) Shifting baselines in attention research. Nat Rev Neurosci 1: 147-148.

Engel AK, Fries P, and Singer W (2001) Dynamic predictions: Oscillations and synchrony in top-down processing. Nat Rev Neurosci 2: 704-716.

Fries P (2005) A mechanism for cognitive dynamics: Neuronal communication through neuronal coherence. Trends in Cognitive Sciences 9:474-480.

Fisher NI (1995) Statistical analysis of circular data, pp 66–67. Cambridge, UK: Cambridge UP.

Foxe JJ, Simpson GV, Ahlfors SP (1998) Parieto-occipital similar to 10 Hz activity reflects anticipatory state of visual attention mechanisms. Neuroreport 9:3929-3933.

Fox MD, Snyder AZ, Vincent JL, Corbetta M, Van Essen DC, Raichle ME (2005) The human brain is intrinsically organized into dynamic, anticorrelated functional networks. Proc. Natl. Acad. Sci. U. S. A. 102, 9673–9678.

Fox MD, Corbetta M, Snyder AZ, Vincent JL, Raichle ME (2006) Spontaneous neuronal activity distinguishes human dorsal and ventral attention systems. Proc. Natl. Acad. Sci. USA 103, 10046–10051.

Fox MD, Raichle ME (2007) Spontaneous fluctuations in brain activity observed with functional magnetic resonance imaging. Nat. Rev. Neurosci. 8, 700–711.

Fox MD, Zhang D, Snyder AZ, Raichle ME (2009) The global signal and observed anticorrelated resting state brain networks. J Neurophysiology 101 (6): 3270-3283.

Friston KJ, Ashburner J, Frith CD, Poline JB, Heather JD, Frackowiak RSJ (1995) Spatial registration and normalization of images. Hum. Brain Mapp. 3, 165–189.

Fuster JM (2008) The Prefrontal Cortex, 4th Edition, Academic Press, New York.

Garofalo M, Nieus T, Massobrio P, Martinoia S (2009) Evaluation of the Performance of Information Theory-Based Methods and Cross-Correlation to Estimate the Functional Connectivity in Cortical Networks. PLos ONE 4 (8).

Gavrilescu M, Shaw ME, Stuart GW, Eckersley P, Svalbe ID, Egan GF (2002) Simulation of the effects of global normalization procedures in functional MRI. Neuroimage 17 (2): 532–542.

Gazzaniga MS, Ivry RB, Mangun GR (2009) The Cognitive Neurosciences, 4th Edition, The MIT Press.

Gelfand IM, Yaglom AM (1959) Calculation of the amount of information about a random function contained in another such function. Amer. Math. Soc. Transl. Ser. 2 (12), 99.

Geweke J (1982) Measurement of linear dependence and feedback between multiple time series. J. Am. Stat. Assoc. 77 (378), 304–313.

Gilbert SJ, Dumontheil I, Simons JS, Frith CD, Burgess PW (2007) Comment on "Wandering Minds: The Default Network and Stimulus-Independent Thought." Science *317*, 43.

Glover GH, Li T, Ress D (2000) Image-based method for retrospective correction of physiological motion effects in fMRI: RETROICOR. Magn Reson Med 44 (1): 162-167

Goadsby PJ (2009) The vascular theory of migraine: a great story wrecked by the facts. Brain 132:6 –7.

Go¨der R, Ha¨bler HJ, Ja¨nig W, Michaelis M (1993) Receptive properties of afferent nerve fibres associated with the rat saphenous vein. Neurosci Letter 164:175–178.

Goebel R, Roebroeck A, Kim DS, Formisano E (2003) Investigating directed cortical interactions in time-resolved fMRI data using vector autoregressive modeling and Granger causality mapping. Magn. Reson. Imaging. 21, 1251–1261.

Goldman RI, Stern JM, Engel J, Cohen MS (2002) Simultaneous EEG and fMRI of the alpha rhythm. Neuroreport *13*, 2487–2492.

Gomez-Ramirez M, Kelly SP, Molholm S, Sehatpour P, Schwartz TH, Foxe JJ (2011) Oscillatory sensory selection mechanisms during intersensory attention to rhythmic auditory and visual inputs: a human electrocorticographic investigation. J. Neurosci. 31, 18556–18567.

Gonçalves SI, de Munck JC, Pouwels PJW, Schoonhoven R, Kuijer JPA, Maurits NM, Hoogduin JM, Van Someren EJW, Heethaar RM, Lopes da Silva FH (2006) Correlating the alpha rhythm to BOLD using simultaneous EEG/fMRI: inter-subject variability. Neuroimage *30,* 203–213.

Graham JR, Wolff HG (1938) Mechanism of migraine headache and action of ergotamine tartrate. Arch Neurol Psychiatry 39:737–763.

Granger CWJ (1969) Investigating causal relations by econometric models and crossspectral methods. Econometrica 37 (3), 424–438.

Gregoriou GG, Gotts SJ, Zhou H, Desimone R (2009) High-frequency, long-range coupling between prefrontal and visual cortex during attention. Science 324:1207-1210.

Greicius MD, and Menon V (2004) Default-mode activity during a passive sensory task: uncoupled from deactivation but impacting activation. J Cogn Neurosci *16*, 1484–1492.

Grushka M, Sessle BJ (1984) Applicability of the McGill Pain Questionnaire to the differentiation of 'toothache' pain. Pain 19:49 –57.

Gusnard DA, Akbudak E, Shulman GL, Raichle ME (2001) Medial prefrontal cortex and self-referential mental activity: Relation to a default mode of brain function. Proceedings of the National Academy of Sciences *98*, 4259 –4264.

Hampson M, Driesen NR, Skudlarski P, Gore JC, Constable RT (2006) Brain Connectivity Related to Working Memory Performance. The Journal of Neuroscience *26*, 13338 – 13343.

Handwerker D, Ollinger J, D'Esposito M (2004) Variation of BOLD hemodynamic responses across subjects and brain regions and their effects on statistical analyses. NeuroImage 21, 1639–1651.

Hanslmayr S, Gross J, Klimesch W, Shapiro KL (2011) The role of alpha oscillations in temporal attention. Brain Res Rev *67*, 331–343.

Hansen N, Klein T, Magerl W, Treede RD (2007) Psychophysical evidence for long-term potentiation of C-fiber and Adelta-fiber pathways in humans by analysis of pain descriptors. J Neurophysiol. 97(3): 2559-63.

Hayden BY, Smith DV, Platt ML (2009) Electrophysiological correlates of default-mode processing in macaque posterior cingulate cortex. Proceedings of the National Academy of Sciences *106*, 5948 –5953.

He BJ, Snyder AZ, Vincent JL, Epstein A, Shulman GL, Corbetta M (2007) Breakdown of functional connectivity in frontoparietal networks underlies behavioral deficits in spatial neglect. Neuron 53, 905–918.

He Y, Wang L, Zang Y, Tian L, Zhang X, Li K, Jiang T (2007) Regional coherence changes in the early stages of Alzheimer's disease: a combined structural and resting-state functional MRI study. NeuroImage 35, 488–500.

Headache Classification Subcommittee of the International Headache Society (2004) The international classification of headache disorders, 2nd edition. Cephalalgia 24[Suppl 1]:9 – 160.

Hermanstyne TO, Markowitz K, Fan L, GoldMS (2008) Mechanotransducers in rat pulpal afferents. J Dent Res 87:834–838.

Herrmann CS, Munk MHJ, Engel AK (2004) Cognitive functions of gamma-band activity: memory match and utilization. Trends Cogn Sci 8:347-355

van den Heuvel MP, Hulshoff Pol HE (2010) Exploring the brain network: a review on resting-state fMRI functional connectivity. Eur. Neuropsychopharmacol. 20, 519–534.

Hlinka J, Palus M, Vejmelka M, Mantini D, Corbetta M (2011) Functional connectivity in resting-state fMRI: Is linear correlation sufficient? NeuroImage 54 (3), 2218-2225.

Ho N, Destexhe A (2000) Synaptic background activity enhances the responsiveness of neocortical pyramidal neurons. Journal of Neurophysiology 84:1488-1496.

Hopfinger JB, Buonocore MH, Mangun GR (2000) The neural mechanisms of top-down attentional control. Nat Neurosci 3: 284-291.

Hughes SW, Crunelli V (2005) Thalamic mechanisms of EEG alpha rhythms and their pathological implications. Neuroscientist, 11 (4), 357-72.

Isnard J, Magnin M, Jung J, Mauguie`re F, Garcia-Larrea L (2011) Does the insula tell our brain that we are in pain? Pain 152:946 –951.

Jensen MP, Gould EM, Victor TW, Gammaitoni AR, White RE, Galer BS (2010) The relationship of changes in pain quality to pain interference and sleep quality. J Pain 11(8): 782-8.

Jensen O, Gelfand J, Kounios J, Lisman JE (2002) Oscillations in the alpha band (9-12 Hz) increase with memory load during retention in a short-term memory task. Cereb Cortex 12 (8), 877-882.

Jensen O, Tesche CD (2002) Frontal theta activity in humans increases with memory load in a working memory task. European Journal of Neuroscience 15:1395-1399.

Jerbi K, Vidal JR, Ossandon T, Dalal SS, Jung J, Hoffmann D, Minotti L, Bertrand O, Kahane P, and Lachaux JP (2010) Exploring the Electrophysiological Correlates of the Default-Mode Network with Intracerebral EEG. Front Syst Neurosci *4*.

Jiao Q, Lu G, Zhang Z, Zhong Y, Wang Z, Guo Y, Li K, Ding M, Liu Y (2011) Granger causal influence predicts BOLD activity levels in the default mode network. Hum. Brain Mapp. 32, 154-161.

Jolles DD, van Buchem MA, Crone EA, Rombouts SA (2011) A comprehensive study of whole-brain functional connectivity in children and young adults. Cereb. Cortex 21 (2), 385 -391.

Jones SR, Pinto DJ, Kaper TJ, Kopell N (2000) Alpha-frequency rhythms desynchronize over long cortical distances: a modeling study. J Comput Neurosci 9:271-291.

Jonkman EJ, Lelieveld MHJ (1981) EEG computer analysis in patients with migraine. Electroencephalography and Clinical Neurophysiology 52, 652–655.

Junghöfer M, Schupp H, Stark R, Vaitl D (2005) Neuroimaging of emotion: empirical effects of proportional global signal scaling in fMRI data analysis. NeuroImage 25 (2): 520-526.

Kahana MJ, Sekuler R, Caplan JB, Kirschen M, Madsen JR (1999) Human theta oscillations exhibit task dependence during virtual maze navigation. Nature 399:781-784.

Kam JWY, Dao E, Farley J, Fitzpatrick K, Smallwood J, Schooler JW, and Handy TC (2012) Slow Fluctuations in Attentional Control of Sensory Cortex. Journal of Cognitive Neuroscience *23*, 460–470.

Kastner S, Pinsk MA, De Weerd P, Desimone R, and Ungerleider LG (1999) Increased activity in human visual cortex during directed attention in the absence of visual stimulation. Neuron 22: 751-761.

Kelly AM, Di Martino A, Uddin LQ, Shehzad Z, Gee DG, Reiss PT, Margulies DS, Castellanos FX, Milham MP (2009) Development of anterior cingulate functional connectivity from late childhood to early adulthood. Cereb. Cortex 19, 640–657.

Kelly SP, Lalor EC, Reilly RB, Foxe JJ (2006) Increases in alpha oscillatory power reflect an active retinotopic mechanism for distracter suppression during sustained visuo spatial attention. Journal of Neurophysiology 95:3844-3851.

Kelman L (2006) Pain characteristics of the acute migraine attack. Headache 46:942–953.

Kenet T, Bibitchkov D, Tsodyks M, Grinvald A, Arieli A (2003) Spontaneously emerging cortical representations of visual attributes. Nature 425, 954–956.

Kerns JG, Cohen JD, MacDonald AW, Cho RY, Stenger VA, Carter CS (2004) Anterior cingulate conflict monitoring and adjustments in control. Science 303, 1023–1026.

Klimesch W, Sauseng P, Hanslmayr S (2007) EEG alpha oscillations: The inhibition-timing hypothesis. Brain Res Rev 53:63-88.

Knight RT, Staines WR, Swick D, Chao LL (1999) Prefrontal cortex regulates inhibition and excitation in distributed neural networks. Acta Psychol 101:159-178.

Knyazev GG, Slobodskoj-Plusnin JY, Bocharov AV, and Pylkova LV (2011) The default mode network and EEG alpha oscillations: an independent component analysis. Brain Res *1402*, 67–79.

Kobayashi M, Musha T (1982) 1/f fluctuation of heartbeat period. IEEE Trans Biomed Eng 29:456–457.

Kolotylo CJ, Broome ME (2000) Predicting disability and quality of life in a community-based sample of women with migraine headache. Pain Manag Nurs 1:139 –151.

Komatsu T, Kimura T, Nishiwaki K, Fujiwara Y, Sawada K, Shimada Y (1997) Recovery of heart rate variability profile in patients after coronary artery surgery. Anesth Analg 85:713–718.

Kreiner M, Falace D, Michelis V, Okeson JP, Isberg A (2010) Quality difference in craniofacial pain of cardiac vs. dental origin. J Dent Res 89:965–969.

Kruggel F, von Cramon DY (1999) Temporal properties of the hemodynamic response in functional MRI. Hum. Brain Mapp. 8 (4), 259-271.

LaBerge D (1997) Attention, awareness, and the triangular circuit. Consciousness and Cognition 6:149-181.

LaBerge D (2005) Sustained attention and apical dendrite activity in recurrent circuits. Brain Res Rev 50 (1), 86-99.

Lakatos P, Karmos G, Mehta AD, Ulbert I, Schroeder CE (2008) Entrainment of neuronal oscillations as a mechanism of attentional selection. Science 320:110-113.

Lam DK, Schmidt BL (2011) Orofacial pain onset predicts transition to head and neck cancer. Pain 152:1206 –1209.

Lasko TA, Bhagwat JG, Zou KH, Ohno-Machado L (2005) The use of receiver operating characteristic curves in biomedical informatics. Journal of Biomedical Informatics, 38(5):404–415.

Laufs H, Kleinschmidt A, Beyerle A, Eger E, Salek-Haddadi A, Preibisch C, Krakow K (2003a) EEG-correlated fMRI of human alpha activity. Neuroimage 19, 1463–1476.

Laufs H, Krakow K, Sterzer P, Eger E, Beyerle A, Salek-Haddadi A, Kleinschmidt A (2003b) Electroencephalographic signatures of attentional and cognitive default modes in spontaneous brain activity fluctuations at rest. Proceedings of the National Academy of Sciences. 100, 11053 –11058.

Laufs H, Holt JL, Elfont R, Krams M, Paul JS, Krakow K, and Kleinschmidt A (2006) Where the BOLD signal goes when alpha EEG leaves. Neuroimage *31*, 1408–1418.

Leech R, Kamourieh S, Beckmann CF, and Sharp DJ (2011) Fractionating the Default Mode Network: Distinct Contributions of the Ventral and Dorsal Posterior Cingulate Cortex to Cognitive Control. The Journal of Neuroscience *31*, 3217 –3224.

Lee MC, Mouraux A, IannettiGD (2009) Characterizing the cortical activity through which pain emerges from nociception. J Neurosci 29:7909 –7916.

Leijon G, Boivie J, Johansson I (1989) Central post-stroke pain–neurological symptoms and pain characteristics. Pain 36:13–25.

Leopold DA, Murayama Y, Logothetis NK (2003) Very Slow Activity Fluctuations in Monkey Visual Cortex: Implications for Functional Brain Imaging. Cereb. Cortex 13, 422–433.

Levy D, Burstein R, Strassman AM (2005) Calcitonin gene-related peptide does not excite or sensitize meningeal nociceptors: implications for the pathophysiology of migraine. Ann Neurol 58:698 –705.

Lfeachor EC, Jarvis BW. Digital signal processing: A practical approach. Essex: Prentice Hall.

Lopes da Silva FH, van Lierop TH, Schrijer CF, van Leeuwen WS (1973) Organization of thalamic and cortical alpha rhythms: spectra and coherences. Electroencephalogr Clin Neurophysiol 35: 627–639.

Lowe MJ, Dzemidzic M, Lurito JT, Mathews VP, Phillips MD (2000) Correlations in low-frequency BOLD fluctuations reflect cortico-cortical connections. Neuroimage 12, 582–587.

Lund TE, Madsen KH, Sidaros K, Luo W, Nichols TE (2006) Non-white noise in fMRI: does modelling have an impact? NeuroImage 29 (1): 54-66.

Lütkepohl H (2005) New Introduction to Multiple Time Series Analysis, Springer, pp 695-697.

Lynall ME, Bassett DS, Kerwin R, McKenna PJ, Kitzbichler M, Bullmore E (2010) Functional connectivity and brain networks in schizophrenia. J. Neuroscience 30 (28), 9477–9487.

Ma Q (2010) Labeled lines meet and talk: population coding of somatic sensations. J Clin Invest 120:3773–3778.

MacDonald AW, Cohen JD, Stenger VA, Carter CS (2000) Dissociating the role of the dorsolateral prefrontal and anterior cingulate cortex in cognitive control. Science 288, 1835–1838.

Macdonald JSP, Mathan S, and Yeung N (2011) Trial-by-Trial Variations in Subjective Attentional State are Reflected in Ongoing Prestimulus EEG Alpha Oscillations. Front Psychol *2*.

Macey PM, Macey KE, Kumar R, Harper RM (2004) A method for the removal of global effects from fMRI time series. Neuroimage 22 (1): 360–366.

MacQueen JB (1967) Some methods for classification and analysis of multivariate observations. Proceedings of 5th Berkeley Symposium on Mathematical Statistics and Probability 1, 281-297, Berkeley, University of California Press.

Makeig S, Westerfield M, Jung TP, Enghoff S, Townsend J, Courchesne E, Sejnowski TJ (2002) Dynamic brain sources of visual evoked responses. Science 295: 690-694.

Malliani A, Pagani M (1976) Afferent sympathetic nerve fibres with aortic endings. J Physiol 263:157–169.

Mantini D, Perrucci MG, Del Gratta C, Romani GL, Corbetta M (2007) Electrophysiological signatures of resting state networks in the human brain. Proceedings of the National Academy of Sciences 104, 13170 –13175.

Mason MF, Norton MI, Van Horn JD, Wegner DM, Grafton ST, and Macrae CN (2007) Wandering Minds: The Default Network and Stimulus-Independent Thought. Science *315*, 393 –395.

Mathewson KE, Gratton G, Fabiani M, Beck DM, Ro T (2009) To See or Not to See: Prestimulus Phase Predicts Visual Awareness. J Neurosci The Journal of Neuroscience 29:2725-2732

Meck WH, Penney TB, Pouthas V (2008) Cortico-striatal representation of time in animals and humans. Curr Opin Neurobiol 18:145–152.

Mehta AD, Ulbert I, and Schroeder CE (2000a) Intermodal selective attention in monkeys. II: Physiological mechanisms of modulation. Cereb Cortex 10: 359-370.

Mehta SD, Ulbert I, and Schroeder CE (2000b) Intermodal selective attention in monkeys. I: Distribution and timing of effects across visual areas. Cereb Cortex 10: 343-358.

Melzack R (1987) The short-form McGill Pain Questionnaire. Pain 30:191–197.

Mennes M, Kelly C, Zuo XN, Di Martino A, Biswal B, Castellanos, F.X., and Milham, M.P., (2010) Interindividual differences in resting state functional connectivity predict task induced BOLD activity. Neuroimage 50 (4), 1690–1701.

McCormick DA, Shu YS, Hasenstaub A, Sanchez-Vives M, Badoual M, Bal T (2003) Persistent cortical activity: Mechanisms of generation and effects on neuronal excitability. Cerebral Cortex 13:1219-1231.

Miller EK and Desimone R (1994) Parallel neuronal mechanisms for short term memory. Science 263: 520-523.

Miller EK, Cohen JD (2000) The prefrontal cortex and cognitive control. Nat Rev Neurosci 1: 59-65.

Miltner WH, Braun C, Arnold M (1999) Coherence of gamma-band EEG activity as a basis for associative learning. Nature 397:917-924.

Mitra P, Bokil H (2007) Observed brain dynamics. New York: Oxford University Press.

Mitra PP, Pesaran B (1999) Analysis of dynamic brain imaging data. Biophys J 76: 691-708.

Montez T, Poil SS, Jones BF, Manshanden I, Verbunt JPA, van Dijk BW, Brussaard AB, van Ooyen A, Stam CJ, Scheltens P (2009) Altered temporal correlations in parietal alpha and prefrontal theta oscillations in early-stage Alzheimer disease. Proceedings of the National Academy of Sciences 106, 1614 –1619.

Moore T, Armstrong KM (2003) Selective gating of visual signals by microstimulation of frontal cortex. Nature 421 (6921): 370-373.

Moosmann M, Ritter P, Krastel I, Brink A, Thees S, Blankenburg F, Taskin B, Obrig H, and Villringer A (2003) Correlates of alpha rhythm in functional magnetic resonance imaging and near infrared spectroscopy. Neuroimage *20*, 145–158.

Naya Y, Yoshida M, Miyashita Y (2001) Backward spreading of memory-retrieval signal in the primate temporal cortex. Science 291 (5504): 661-664.

Nelson SM, Dosenbach NU, Cohen AL, Wheeler ME, Schlaggar BL, Petersen SE (2010) Role of the anterior insula in task-level control and focal attention. Brain Struct Funct 214 (5-6), 669-680.

Nishitani N, Hari R (2002) Viewing lip forms: cortical dynamics. Neuron 36 (6), 1211-1220.

O'Connell RG, Dockree PM, Robertson IH, Bellgrove MA, Foxe JJ, and Kelly SP (2009) Uncovering the Neural Signature of Lapsing Attention: Electrophysiological Signals Predict Errors up to 20 s before They Occur. J of Neurosci *29*, 8604 –8611.

Ofek H, Defrin R (2007) The characteristics of chronic central pain after traumatic brain injury. Pain 131:330 –340.

Olesen J, Burstein R, Ashina M, Tfelt-Hansen P (2009) Origin of pain in migraine: evidence for peripheral sensitisation. Lancet Neurol 8:679 – 690.

Ossandón T, Jerbi K, Vidal JR, Bayle DJ, Henaff MA, Jung J, Minotti L, Bertrand O, Kahane P, Lachaux JP (2011) Transient Suppression of Broadband Gamma Power in the Default-Mode Network Is Correlated with Task Complexity and Subject Performance. The J of Neurosci. *31*, 14521 –14530.

Palva S, Palva JM (2007) New vistas for alpha-frequency band oscillations. Trends Cogn Sci 30 (4): 150-158.

Pasternak T, Greenlee MW (2005) Working memory in primate sensory systems. Nature Reviews Neuroscience 6(2): 97-107.

Pfurtscheller G, da Silva FHL (1999) Event-related EEG/MEG synchronization and desynchronization: Basic principles. Clinical Neurophysiology 110:1842-1857.

Pfurtscheller G, Stancak A, Neuper C (1996) Event-related synchronization (ERS) in the alpha band - an electrophysiological correlate of cortical idling: a review. Int J Psychophysiol 24: 39-46.

Potter M, Kinsner W (2008) Instantaneous heart rate: should RR-intervals be resampled? Conf Proc IEEE Eng Med Biol Soc 2008:277–282.

Procyk E, Goldman-Rakic PS (2006) Modulation of dorsolateral prefrontal delay activity during self-organized behavior. Journal of Neuroscience 26(44): 11313-11323.

Raghavachari S, Lisman JE, Tully M, Madsen JR, Bromfield EB, Kahana MJ (2006) Theta oscillations in human cortex during a working-memory task: Evidence for local generators. J Neurophysiol 95 (3): 1630-1638

Raghavachari S, Kahana MJ, Rizzuto DS, Caplan JB, Kirschen MP, Bourgeois B, Madsen JR, Lisman JE (2001) Gating of human theta oscillations by a working memory task. Journal of Neuroscience 21:3175-3183.

Raichle ME, Mintun MA (2006) Brain work and brain imaging. Annu. Rev. Neurosci. 29, 449–476.

Rajagovindan R, Ding M (2008) Decomposing neural synchrony: toward an explanation for near-zero phase-lag in cortical oscillatory networks. PLoS ONE 3 (11), doi:10.1371/journal.pone.0003649.

Rajagovindan R, Ding M (2010) From prestimulus alpha oscillation to visual evoked response: An inverted U function and its attentional modulation. J Cogn Neurosci, in press.

Ray WJ, Cole HW (1985) EEG alpha-activity reflects attentional demands, and beta-activity reflects emotional and cognitive-processes. Science 228 (4700): 750-752.

Rempel-Clower NL, and Barbas H (2000) The laminar pattern of connections between prefrontal and anterior temporal cortices in the rhesus monkey is related to cortical structure and function. Cereb Cortex 10: 851-865.

Ritter P, Moosmann M, and Villringer A (2009) Rolandic alpha and beta EEG rhythms' strengths are inversely related to fMRI-BOLD signal in primary somatosensory and motor cortex. Hum Brain Mapp *30*, 1168–1187.

Roebroeck A, Formisano E, Goebel R (2005) Mapping directed influence over the brain using Granger causality and fMRI. Neuroimage 25, 230–242.

Romei V, Rihs T, Brodbeck V, Thut G (2008) Resting electroencephalogram alpha-power over posterior sites indexes baseline visual cortex excitability. Neuroreport 19:203-208.

Rosman HS, Patel S, Borzak S, Paone G, Retter K (1998) Quality of history taking in patients with aortic dissection. Chest 114:793–795.

Rozen TD (2010) Brief sharp stabs of head pain and giant cell arteritis. Headache 50:1516 – 1519.

Rossi AF, Bichot NP, Desimone R, Ungerleider LG (2007) Top-down attentional deficits in macaques with lesions of lateral prefrontal cortex. J Neurosci 27: 11306-11314.

Sadaghiani S, Scheeringa R, Lehongre K, Morillon B, Giraud AL, and Kleinschmidt A (2010) Intrinsic connectivity networks, alpha oscillations, and tonic alertness: a simultaneous electroencephalography/functional magnetic resonance imaging study. J. Neurosci *30*, 10243–10250.

Sarnthein J, Stern J, Aufenberg C, Rousson V, Jeanmonod D (2006) Increased EEG power and slowed dominant frequency in patients with neurogenic pain. Brain 129, 55–64.

Sauseng P, Klimesch W, Stadler W, Schabus M, Doppelmayr M, Hanslmayr S, Gruber WR, Birbaumer N (2005) A shift of visual spatial attention is selectively associated with human EEG alpha activity. Eur J Neurosci 22:2917-2926.

Schmolesky MT, Wang Y, Hanes DP, Thompson KG, Leutgeb S, Schall JD, Leventhal AG (1998) Signal timing across the macaque visual system. J. Neurophysiol. 79, 3272–3278.

Scheeringa R, Fries P, Petersson KM, Oostenveld R, Grothe I, Norris DG, Hagoort P, and Bastiaansen MCM (2011) Neuronal dynamics underlying high- and low-frequency EEG oscillations contribute independently to the human BOLD signal. Neuron *69*, 572–583.

Scher AI, Stewart WF, Liberman J, Lipton RB (1998) Prevalence of frequent headache in a population sample. Headache 38:497–506.

Schooler JW, Smallwood J, Christoff K, Handy TC, Reichle ED, and Sayette MA (2011) Meta-awareness, perceptual decoupling and the wandering mind. Trends in Cognitive Sciences.

Schroeder CE, Lakatos P (2009) Low-frequency neuronal oscillations as instruments of sensory selection. Trends in Neurosciences *32*, 9–18.

Seeley WW, Menon V, Schatzberg AF, Keller J, Glover GH, Kenna H, Reis AL, Greicius MD (2007) Dissociable intrinsic connectivity networks for salience processing and executive control. J Neurosci 27(9): 2349–2356.

Seymour RA, Charlton JE, Phillips ME (1983) An evaluation of dental pain using visual analogue scales and the McGill Pain Questionnaire. J Oral Maxillofac Surg 41:643– 648.

Shao S, Shen K, Yu K, Wilder-Smith EPV, Li X (2012) Frequency-domain EEG source analysis for acute tonic cold pain perception. Clinical Neurophysiology: Official Journal of the International Federation of Clinical Neurophysiology.

Shaw JC (2003) Brain's Alpha Rhythm and the Mind. Amsterdam: Elsevier.

Smit DJA, de Geus EJC, van de Nieuwenhuijzen ME, van Beijsterveldt CEM, van Baal GCM, Mansvelder HD, Boomsma DI, Linkenkaer-Hansen K (2011) Scale-Free Modulation of Resting-State Neuronal Oscillations Reflects Prolonged Brain Maturation in Humans. The Journal of Neuroscience 31, 13128 –13136.

Steriade M, Gloor P, Llinás RR, Lopes da Silva FH, Mesulam MM (1990) Basic mechanisms of cerebral rhythmic activities. Electroencephalography and Clinical Neurophysiology 76, 481–508.

Stern J, Jeanmonod D, and Sarnthein J (2006) Persistent EEG over activation in the cortical pain matrix of neurogenic pain patients. NeuroImage 31, 721–731.

Strassman AM, Levy D (2006) Response properties of dural nociceptors in relation to headache. J Neurophysiol 95:1298 –1306.

Strassman AM, Raymond SA, Burstein R (1996) Sensitization of meningeal sensory neurons and the origin of headaches. Nature 384:560 –564.

Steriade M, Gloor P, Llinas RR, Lopes da Silva FH, Mesulam MM (1990) Basic mechanisms of cerebral rhythmic activities. Electroencephalogr Clin Neurophysiol 76: 481-508.

Sridharan D, Levitin DJ, Menon V (2008) A critical role for the right fronto-insular cortex in switching between central-executive and default-mode networks. Proc. Natl. Acad. Sci. U. S. A. 105, 12569–12574.

Supekar K, Menon V, Rubin D, Musen M, Greicius MD (2008) Network analysis of intrinsic functional brain connectivity in Alzheimer's disease. PLoS Comput. Biol. 4, e1000100. doi:10.1371/journal.pcbi.1000100.

Tallon-Baudry C, Bertrand O (2005) Attention Modulates Gamma-band Oscillations Differently in the Human Lateral Occipital Cortex and Fusiform Gyrus. Cereb Cortex 15: 654-662.

Tass P, Rosenblum MG, Weule J, Kurths J, Pikovsky A, Volkmann J, Schnitzler A, Freund HJ (1998) Detection of n:mphase locking from noisy data: application to magnetoencephalography. Phys Rev Lett 81:3291–3294.

Thomson DJ (1982) Spectrum estimation and harmonic analysis. Proceedings of the IEEE 70:1055-1096.

Thut G, Nietzel A, Brandt SA, Pascual-Leone A (2006) alpha-Band electroencephalographic activity over occipital cortex indexes visuospatial attention bias and predicts visual target detection. J Neurosci 26: 9494-9502.

de Tommaso M, Sciruicchio V, Guido M, Sasanelli G, Specchio LM, Puca FM (1998) EEG spectral analysis in migraine without aura attacks. Cephalalgia 18, 324–328.

Rossi AF, Bichot NP, Desimone R, Ungerleider LG (2007) Top-down attentional deficits in macaques with lesions of lateral prefrontal cortex. J Neurosci 27: 11306-11314.

Van Essen DC, Anderson CH, Felleman DJ (1992) Information processing in the primate visual system: an integrated systems perspective. Science 255, 419–423.

Vertes RP (2005) Hippocampal theta rhythm: A tag for short-term memory. Hippocampus 15:923-935.

Vincent JL, Patel GH, Fox MD, Snyder AZ, Baker JT, Van Essen DC, Zempel JM, Snyder LH, Corbetta M, Raichle ME (2007) Intrinsic functional architecture in the anaesthetized monkey brain. Nature 447, 83–86.

Victor TW, Jensen MP, Gammaitoni AR, Gould EM, White RE, Galer BS (2008) The dimensions of pain quality: factor analysis of the Pain Quality Assessment Scale. Clin J Pain 24:550 –555.

Wallny T, Hess L, Seuser A, Zander D, Brackmann HH, Kraft CN (2001) Pain status of patients with severe haemophilic arthropathy. Haemophilia 7:453– 458.

Wasay M, Kojan S, Dai AI, Bobustuc G, Sheikh Z (2010) Headache in cerebral venous thrombosis: incidence, pattern and location in 200 consecutive patients. J Headache Pain 11:137–139.

Weiss S, Rappelsberger P (2000) Long-range EEG synchronization during word encoding correlates with successful memory performance. Cognitive Brain Research 9:299-312.

Weissman DH, Roberts KC, Visscher KM, Woldorff MG (2006) The neural bases of momentary lapses in attention. Nat Neurosci *9*, 971–978.

Wen X, Li Y, Liu Y, Ding M (2012) Causal Interactions in Attention Networks Predict Behavioral Performance. J Neuroscience.

Wise RG, Ide K, Poulin MJ, Tracey I (2004) Resting fluctuations in arterial carbon dioxide induce significant low frequency variations in BOLD signal. NeuroImage 21 (4): 1652-1664.

Worden MS, Foxe JJ, Wang N, Simpson GV (2000) Anticipatory biasing of visuospatial attention indexed by retinotopically specific alpha-band electroencephalography increases over occipital cortex. J Neurosci 20 (6): RC63

Yan C, Liu D, He Y, Zou Q, Zhu C, Zuo X, Long X, Zang Y (2009) Spontaneous brain activity in the default mode network is sensitive to different resting-state conditions with limited cognitive load. PLoS ONE 4 (5), e5743. doi:10.1371/journal.pone.0005743.

Zanto TP, Rubens MT, Thangavel A, Gazzaley A (2011) Causal role of the prefrontal cortex in top-down modulation of visual processing and working memory. Nat Neurosci. 14(5):656-61. Epub 2011 Mar 27.

Zarahn E, Aguirre GK, D'Esposito M (1997) Empirical analyses of BOLD fMRI statistics. I. Spatially unsmoothed data collected under null-hypothesis conditions. Neuroimage 5: 179–197.

Zuo X, Martino AD, Kelly C,Shehzad ZE, Gee DG, Klein DF, Castellanos X,Biswal B and Michael P (2010) The Oscillating Brain: Complex and Reliable Neuroimage. 49(2): 1432–1445.

BIOGRAPHICAL SKETCH

Jue Mo was born in 1984 in the city of Nanning, China. She grew up in the city of Dongguan, and graduated from Dongguan Secondary School in 2002. She earned the B.E. degree in biomedical engineering from the Zhejiang University, Hangzhou in 2007. In the same year Jue enrolled in the graduate program at the University of Florida. She joined the biomedical engineering department to pursue the Doctor of Philosophy degree in 2007. She conducted her doctoral studies in biomedical engineering specializing in neuroimaging, signal processing and cognitive neuroscience under the mentorship of Dr. Mingzhou Ding. Jue intends to pursue her research interests in functional biomarker investigation, and continue to explore other potential applications of neuroimaging in the clinical and commercial fields.